MICROCOPY RESOLUTION TEST CHART
NATIONAL BUREAU OF STANDARDS-1963-A

ADA 132418

WHITE LIGHT SIGNAL PROCESSING WITH THE APPLICATION TO SPREAD SPECTRUM COMMUNICATIONS

The Pennsylvania State University

Francis T. S. Yu

ROME AIR DEVELOPMENT CENTER
Air Force Systems Command
Griffiss Air Force Base, NY 13441
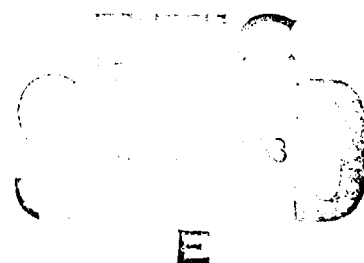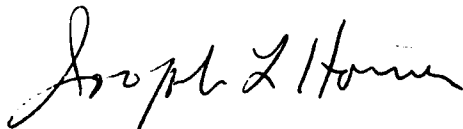
83 09 07 128

This report has been reviewed by the RADC Public Affairs Office (PA) and is releasable to the National Technical Information Service (NTIS). At NTIS it will be releasable to the general public, including foreign nations.

RADC-TR-83-119 has been reviewed and is approved for publication.

APPROVED: *[signature]*

JOSEPH L. HORNER
Project Engineer

APPROVED: *[signature]*

HAROLD ROTH
Director, Solid State Sciences Division

FOR THE COMMANDER: *[signature]*

JOHN P. HUSS
Acting Chief, Plans Office

REPORT DOCUMENTATION PAGE		READ INSTRUCTIONS BEFORE COMPLETING FORM
1. REPORT NUMBER RADC-TR-83-119	2. GOVT ACCESSION NO. AD -A132 418	3. RECIPIENT'S CATALOG NUMBER
4. TITLE (and Subtitle) WHITE-LIGHT OPTICAL SIGNAL PROCESSING WITH APPLICATION TO SPREAD SPECTRUM COMMUNICATION		5. TYPE OF REPORT & PERIOD COVERED Final Technical Report
		6. PERFORMING ORG. REPORT NUMBER N/A
7. AUTHOR(s) Francis T.S. Yu		8. CONTRACT OR GRANT NUMBER(s) F19628-81-K-0038
9. PERFORMING ORGANIZATION NAME AND ADDRESS The Pennsylvania State University Electrical Engineering Department University Park PA 16802		10. PROGRAM ELEMENT, PROJECT, TASK AREA & WORK UNIT NUMBERS 61101F LD1614C4
11. CONTROLLING OFFICE NAME AND ADDRESS Rome Air Development Center (ESO) Hanscom AFB MA 01731		12. REPORT DATE June 1983
		13. NUMBER OF PAGES 108
14. MONITORING AGENCY NAME & ADDRESS(if different from Controlling Office) Same		15. SECURITY CLASS. (of this report) UNCLASSIFIED
		15a. DECLASSIFICATION/DOWNGRADING SCHEDULE N/A

16. DISTRIBUTION STATEMENT (of this Report)

Approved for public release; distribution unlimited

17. DISTRIBUTION STATEMENT (of the abstract entered in Block 20, if different from Report)

Same

18. SUPPLEMENTARY NOTES

19. KEY WORDS (Continue on reverse side if necessary and identify by block number)
Optical correlators
white-light signal processing
pseudorandom code
PN code detection
spread spectrum communication

20. ABSTRACT (Continue on reverse side if necessary and identify by block number)
Spread spectrum communication requires several operational processes. First, the informational signal should be encoded by some pseudorandom (PN) code into a broad bandwidth signal (e.g., frequency hopping). The transmitted signal should have the capability of anti-jamming or interference during the transmission. Second, the transmitted signal, which is at high bandwidth, must be decoded at the receiving end to give rise to the low bandwidth informational signal. The decoding process requires a synchronous

DD FORM 1473 EDITION OF 1 NOV 65 IS OBSOLETE

pseudorandom (PN) reference code. Third, the informational signal may or may not be error correction coded and hence requires an appropriate decoding process.

In this study we investigate the utilization of a white-light or incoherent optical correlator for the signal decoding. There are several reasons for selecting the optical technique rather than electronic or digital counterpart, because the optical technique rather than electronic or digital counterpart, because the optical technique offers the following capabilities: 1. It is capable of handling very long code words; 2. It has a very large space-bandwidth product; 3. It has the ability of performing parallel processing; and 4. The compatibility with optical storage. The advantages of using white-light processing technique are: 1. It eliminates the coherent noise; 2. The incoherent system is economical and easy to maintain; 3. It is suitable for color signal decoding.

The coherence requirement of the white-light optical correlator for the spread spectrum decoding is analyzed. We have shown that the temporal coherence requirement is strongly dependent on the spatial frequency and the extension of the target (i.e., code word). The spatial coherence requirement however depends only on the extension of the code word.

The effect on noise performance of an incoherent optical correlator is also discussed. The output signal-to-noise (SNR) is evaluated by partial coherence theory. The sources of noise considered are the grain-noise and the phase-noise at the input and Fourier planes. Except for the grain-noise at the input plane, we have shown that the output SNR can be improved considerably by using a broadband light source. The overall SNR increases rapidly as the number of spectral band filters increases. This increase in SNR confirms this validity of noise-suppression under a white-light illumination.

We have also reported a polychromatic correlation detection technique. This technique offers true color correlation detection which is a step closer to actual human observation. The polychromatic correlation may also apply to decode wideband color coded pseudorandom signal.

Several experimental demonstrations of the incoherent optical correlator as applied to character recognition, pseudorandom code are provided. Comparison with the results obtained by the coherent system are also given. We note that the results obtained with the incoherent source provide a higher SNR. Several demonstrations for polychromatic correlation detection are also included.

Finally, the net effect of this study is to emphasize the truth of our assumption that the incoherent or white-light optical correlator can be an essential decoder for the application of spread spectrum signal decoding.

Table of Contents

List of Illustrations

List of Illustrations (cont'd)

List of Illustrations (cont'd)

List of Tables

I. Introduction

1.1 Air Force Goals and Needs

The U.S. Air Force needs to improve the space communication technique not only by increasing the bandwidth (e.g., spread spectrum or frequency hopping) of the transmitted signal but also needs to improve the security such that the transmitted signal is capable of against jamming, fading, doppler shifts, channel noise, multipath effects, etc.

The basic communication technique that we would like to investigate may center in the spread spectrum communication technique; particularly in the application of white-light optical signal processing to detect a wideband pseudo random code, which was originally transmitted with spread spectrum communication method.

There are several reasons for selecting the optical signal processing technique rather than their electronic or digital counterpart, because the optical technique has the following capabilities:

1. It is capable of handling very long code words;

2. It has a very large space-bandwidth product;

3. It has the capability of performing parallel information processing, and

4. The compatibility with optical storage techniques.

We would, however, use the white-light processing technique rather than the coherent optical counterpart, because of the following advantages:

1. It eliminates the coherent artifact noise that generally plagues the coherent optical system;

2. The white-light processing system is generally economical to operate and easy to maintain.

3. The white-light technique is very versatile and simpler to handle.

We emphasize again, the basic objective of this research is to improve the decoding (i.e., detection) capability in such a way that high signal-to-noise ratio of the correlation can be obtained.

1.2 Spread Spectrum Communication

Literally, spread spectrum communication is one in which the transmitted signal is spread over a wide frequency band. Usually the bandwidth is much larger than the base bandwidth of the informatio· signal. The most familiar example of spread spectrum modulation is the frequency or phase modulation. The bandwidth requirement of the transmitted signal is generally much higher than bandwidth of the information signal. Following are three general types of spread spectrum modulations[1]:

1. Direct Sequence – modulation of a carrier by a digital code sequence (i.e., PN code) whose bit rate is much higher than the bandwidth of the informational signal.

2. Frequency hoppings – carrier frequency shifting in discrete manner followed by a code sequence.

3. Chirp Modulation – the carrier frequency is swept over a wide band during a given pulse interval followed by a code sequence.

Nevertheless, a spread spectrum communication system must have transmitted bandwidth much greater than the information bandwidth. The art of spreading the transmitted bandwidth is to allow the communication system to deliver error-free information through a noisy environment with a proper decoding process.

One type of the spread spectrum communication that the U.S. Air Force is particularly interested in is the hybrid forms of frequency hopping and direct sequence modulation. The form of spread spectrum

signal usually required is a large space-bandwidth PN code to encode
and to decode the transmitted signal. It is this reason that we believed
the optical processing technique would be most applicable for a large
space-bandwidth signal. In the optical signal processing technique,
we shall deal with an incoherent optical correlator that is capable
of performing the task of correlating the PN code for the spread
spectrum signal decoding.

1.3 Report Outline

We deal primarily on an incoherent optical correlator as applied
to PN code correlation for spread spectrum signal decoding. Since
the optical correlation operation rely on complex amplitude operation,
the partial coherence requirement of bhe correlator should be
evaluated. The system noise performance is also a criti-al issue
for the incoherent optical signal correlator as applied to the
proposed research problem. We shall report in the following the analysis
of the white-light optical correlator, and the applications to complex
signal detection, pseudorandom code (i.e., PN code) correlation, poly-
chromatic signal detection and noise performances. Experimental
demonstrations are also provided.

II. Complex Signal Detection by Spectrally Broadband Source

2.1 System Analysis

We shall now describe a technique of complex spatial filtering to be
carried out by a spectrally incoherent light source, for example, a white
light source[2-4]. We place a diffraction grating behind an input-signal
transparency, $s(x,y)$, at the input plane P_1 of a white light optical pro-
cessor, as shown in Fig. 1. The resultant complex amplitude transmittance
of the input plane is then

$$s(x,y) \ T(x) = K \ s(x,y) \ [1 + \cos(p_o x)], \qquad (1)$$

4
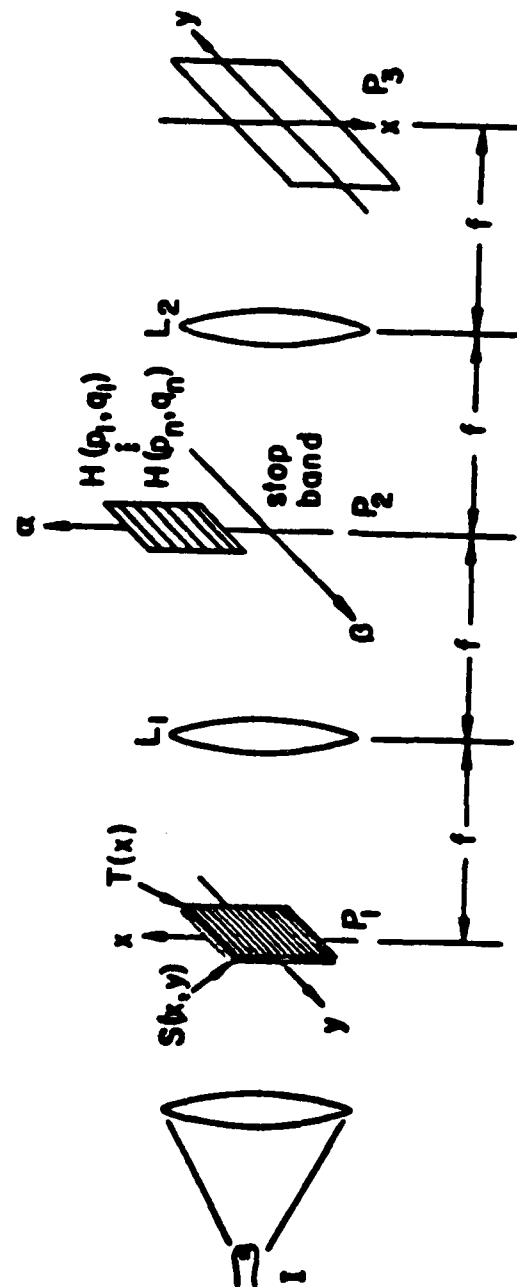
Figure 1   A white light optical correlator. I, white-
light point source; s(x,y), input signal trans-
parency; T(x), high efficient diffraction grating;
$H(p_n,q_n)$, complex spatial filters.

where $T(x)$ represents the diffraction grating, K is a proportionality constant, p_0 is the angular spatial frequency of the diffraction grating, and (x,y) is the spatial coordinate system. We note that, to obtain a high diffraction efficiency, a phase grating may be used.[4] Since the input plane is illuminated by collimated white light, the complex light distribution for a given wavelength λ at the back focal plane P_2 of the achromatic transform lens may be written

$$E(p,q;\lambda) = C\iint s(x,y) \ [1 + \cos(p_0 x)] \ \exp[-i(px + qy)] \ dxdy, \quad (2)$$

where the integral is over the spatial domain and spectral bandwidth of the light source, (p,q) denotes the angular spatial frequency coordinate system, and C is a complex constant. For simplicity of analysis, we dropped the proportionality constant and Eq. (2) is therefore

$$E(p,q;\lambda) = S(p,q) + S(p-p_0,q) + S(p+p_0,q), \quad (3)$$

where $s(p,q)$ is the Fourier spectrum of $s(x,y)$, $p = \frac{2\pi}{\lambda f}\alpha$ and $q = \frac{2\pi}{\lambda f}\beta$, (α,β) is the linear spatial coordinate system of (p,q) and f is the focal length of the achromatic transform lens. In terms of the spatial coordinates α and β, Eq. (3) can be written,

$$E(\alpha,\beta;\lambda) = C_1 S(\alpha,\beta) + C_2 S(\alpha - \frac{\lambda f}{2\pi} p_0, \beta) + C_3 S(\alpha + \frac{\lambda f}{2\pi} p_0, \beta). \quad (4)$$

From the above equation, we see that two first-order signal spectral bands (i.e., second and third terms) are dispersed into rainbow color Fourier spectrums along the α axis, and each spectrum is centerd at $\alpha = \pm(\lambda f/2\pi)p_0$.

In the analysis, we assume that a sequence of complex spatial filters of various λ_n are available, i.e.,

$$H(p_n,q_n) = K_1 + K_2 + K \ |S(p_n,q_n)| \ \cos[\beta_0 q_n + \Phi(p_n,q_n)],$$
$$n = 1,2,\ldots,N, \quad (5)$$

where $p_n = \frac{2\pi}{\lambda_n f}\alpha$, $q_n = \frac{2\pi}{\lambda_n f}\beta$, β_0 is the spatial frequency in the q_n direction, K's are the appropriate constants, and $S(p_n,q_n)$ is the complex signal spectrum of $s(x,y)$. We note that these complex spatial filters can be computer generated.[6]

If we place these complex spatial filters in the spatial frequency plane, each centered at $\alpha = (\lambda_n f/2\pi)p_0$, as shown in Fig. 2, then the complex light field behind the spatial-frequency plane is

$$E(p,q;\lambda) = S(p-p_0,q) \sum_{n-1}^{N} H(p_n-p_0,q_n), \tag{6}$$

The corresponding complex light distribution at the output plane P_3 of the processor is therefore,

$$g(x,y) = \sum_{n=1}^{N} \iiint S(p-p_0,q) \, H(p_n-p_0,q_n) \, \exp[i(p_n x+q_n y)]dp_n dq_n d\lambda, \tag{7}$$

where the integration is over the spatial domain and the wavelength spread of the filters. We assume that the signal spectrum is spatial frequency limited and the bandwidth of $H(p_n,q_n)$ is extended to this limit, i.e.,

$$H(p_n,q_n) = \begin{cases} H(p_n,q_n), & \alpha_1 \leq \alpha \leq \alpha_2 \\ 0, & \text{otherwise} \end{cases} \tag{8}$$

where $\alpha_1 = (\lambda_n f/2\pi)(p_0 + \Delta p)$, and $\alpha_2 = (\lambda_n f/2\pi)(p_0 - \Delta p)$ are the upper and the lower spatial limits of $H(p_n,q_n)$, and Δp is the bandwidth of the input signal. The limiting wavelengths of the dispersed spectrums at the upper and the lower edges of the filters are

$$\lambda_\ell = \lambda_n \frac{p_0+\Delta p}{p_0-\Delta p} , \text{ and } \lambda_h = \lambda_n \frac{p_0-\Delta p}{p_0+\Delta p}, \tag{9}$$

and the corresponding wavelength spread over the filters is therefore,

$$\Delta\lambda_n = \lambda_n \frac{4p_0\Delta p}{p_0^2-(\Delta p)^2}. \tag{10}$$

If the spatial frequency p_0 of the grating is high, then the wavelength spreads over the filters can be approximated,

$$\Delta\lambda_n \sim \frac{4\Delta p}{p_0}\lambda_n, \quad p_0 \gg \Delta p. \tag{11}$$

7

Figure 3   Sketch of output diffraction.
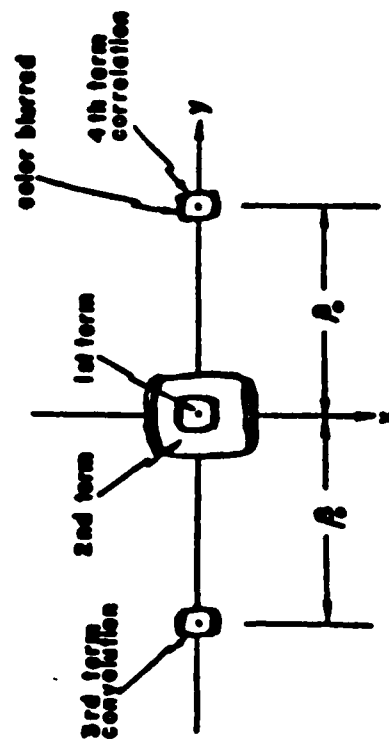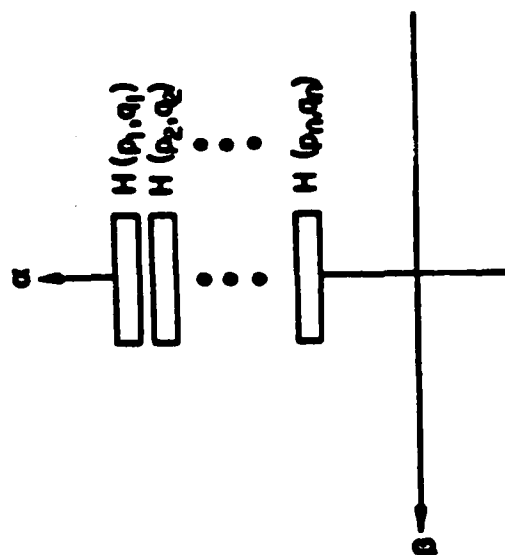
Figure 2   Sketch of multi-complex spatial filterings.

Since the complex spatial filterings take place in discrete Fourier spectral bands of the light source, the filtered signals are _mutually_ incoherent, therefore the output complex light distribution is

$$g(x,y) \sim \sum_{n=1}^{N} \Delta\lambda_n [s_n(x,y)e^{ip_o x} + s_n(x,y)e^{ip_o x} * s_n(x,y)e^{ip_o x} * s_n^*(x,y)e^{ip_o x}$$

$$+ s_n(x,y)e^{ip_o x} * s_n(x,y+\beta_o)e^{ip_o x} + s_n(x,y)e^{ip_o x} * s_n^*(-x,-y+\beta_o)e^{ip_o x}],$$

$$(12)$$

where * denotes the convolution operation and the superscript * denotes the complex conjugate. For simplicity, the proportionality constants K were dropped from the above equation. From Eq. (12) we see that the first and second terms represent the zero order terms, which are diffracted in the neighborhood at (0,0) in the output plane, and the third and fourth terms are the convolution and correlation terms, which are diffracted in the neighborhood of $(0,-\beta_o)$ and $(0,\beta_o)$ respectively, as shown in Fig. 3. Furthermore, we note that the diffracted output signal is formed by _incoherent_ addition of the discrete spectral bands, therefore the annoying coherent artifact noise can be avoided.

Let us now discuss the correlation term of Eq. (12), i.e.,

$$R(x,y) = \sum_{n=1}^{N} \iiint S(\alpha - \frac{\lambda f}{2\pi}p_o,\beta)S_n^*(\alpha - \frac{\lambda_n f}{2\pi}p_o,\beta)e^{-i\beta_o y} \exp[i\frac{2\pi}{\lambda_n f}(\alpha x + \beta y)]d\alpha d\beta d\lambda.$$

$$(13)$$

From this equation, we see that there is a _mismatch_ in location and in scaling of the incoming signal spectrum with respect to the filter function. In other words, if the spatial carrier frequency p_o of the diffraction grating is high, a narrower spread in the x direction of the correlation peak can be obtained. Thus the accuracy of the complex filtering in

the x direction is somewhat lower than that in the y direction. In other words this white light processing technique is effective only in one direction, and for some two-dimensional processing, this technique may pose some drawbacks. However, this technique offers no coherent artifact noise and it can be applied to various problems in optical information processing. We shall emphasize that, although the technique uses a _temporal_ incoherent source, the signal spectrum is displayed in partial coherence mode so that the signal can be processed in complex amplitude.

We would note that, the white-light or incoherent optical processing scheme is to apply in the detection of the pseudo random PN code in the spread spectrum communication system. A general matched filter as proposed by Caulfield[6] may be employed for this signal decoding. We shall also note that, besides this for the application to decode the pseudo random code for spread spectrum communication, there are several other areas of intense interest to the U.S. Government relying heavily on complex signal detection and hence stands to benefit from our proposed work. Those areas are radar, sonar, target recognition, etc.

III. Coherence Requirement

3.1 Basic Formulation

Recent investigations of Morris and George[7] have led to a relationship between the correlation intensity and the wavelength spread of the light source. Prior to their work, Watrasiewiez[8] had evaluated the effect of spatial coherence on the correlation intensity with a rectangular function. Here, we shall quantitatively evaluate the temporal and spatial coherence requirement of a partially coherent correlation detector, that we proposed in previous sections.

The partially coherent optical signal processor of Fig. 4 employs an extended broadband light source. For such an optical processor, let the source intensity distribution, which can be modulated by a source encoding mask[9], at source plane P_o be $\gamma(x_o, y_o)$. In complex signal detection, an input signal transparency of complex amplitude distribution $t(u,v)$ is inserted at the input plane P_1 of the optical processor. A matched spatial filter having an amplitude transmittance $H(x,y) = T^*(x,y)$ is inserted at the spatial frequency plane P_2, where $T(x,y)$ is the corresponding Fourier transform of the input signal $t(u,v)$ and $*$ denotes the complex conjugate from the theory of partial coherence[10,11], the output correlation intensity can be written as

$$I(u',v') = \iint_{\Delta S} \gamma(x_o, y_o) \int_{\Delta\lambda} s(\lambda)\, c(\lambda) \left| \iint_{-\infty}^{\infty} 1/\lambda^2 f^2\, T(x + x_o,\, y + y_o; \lambda) \right.$$

$$\left. H(x,y;\lambda_o) \exp[i\,\frac{2\pi}{\lambda f}\,(xu' + yv')]\, dxdy \right|^2 dx_o dy_o d\lambda, \tag{14}$$

where ΔS is the source size, $\Delta\lambda$ is the spectral bandwidth of the light source, $S(\lambda)$ is the relative spectral intensity of the source, $C(\lambda)$ is the relative spectral response sensitivity of the detector or recording material, λ_o is the central wavelength of the light source, and $H(x,y;\lambda_o)$ is the complex spatial filter at $\lambda = \lambda_o$.

3.2 Temporal Coherence Requirement

We shall now discuss the temporal coherence requirement of the light source. Let us assume we have a point source with a broad spectrum i.e., $\gamma(x_o, y_o) = \delta(x_o, y_o)$. For simplicity we let $S(\lambda)$ and $C(\lambda)$ be constant. The output intensity distribution of Eq. (14) becomes

$$I(u',v') = \int_{\lambda_o\, 0\, \Delta\lambda/2}^{\lambda_o\, +\, \Delta\lambda/2} |A(u',v';\lambda)|^2\, d\lambda, \tag{15}$$
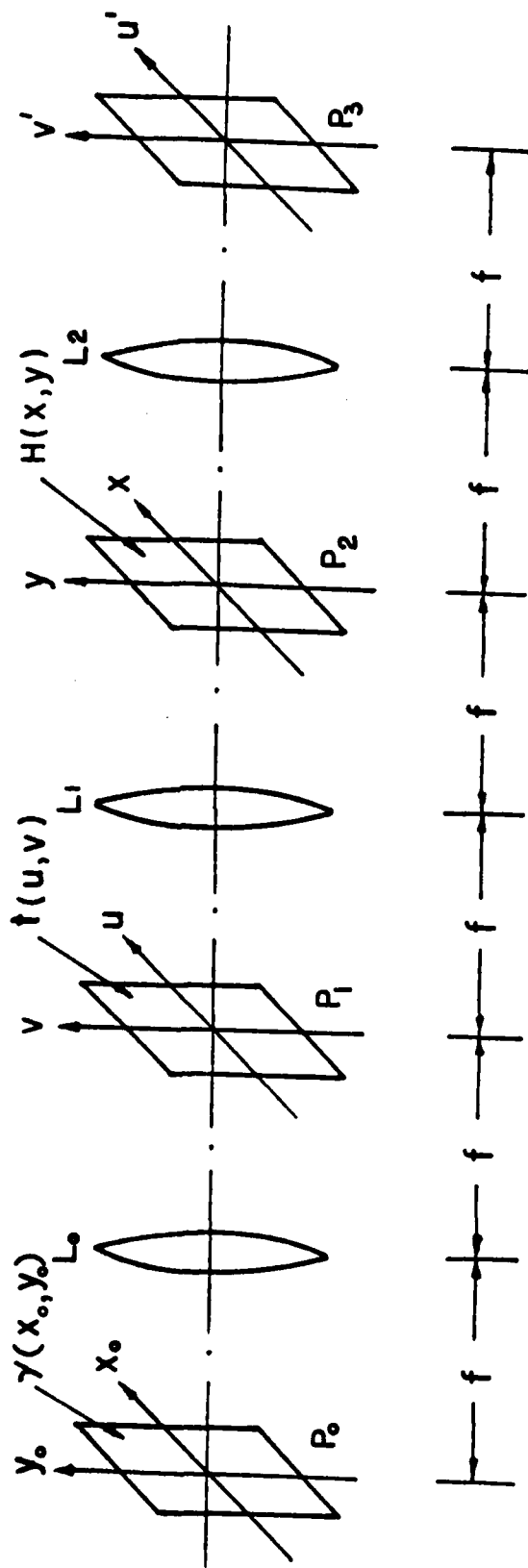
Figure 4   A partially coherent optical processor.

where

$$A(u',v';\lambda) = \int\int_{-\infty}^{\infty} T(f_x,f_y) \; T^*(f_x^o,f_y^o) \; \exp[i2\pi(f_x u' + f_y v')] \; df_x df_y,$$

$$\simeq \frac{\lambda_o}{\lambda} \; t(u',v') * t_o(u',v'), \tag{16}$$

where $f_x = x/\lambda f$, $f_y = y/\lambda f$, $f_x^o = x/\lambda_o f$, $f_y^o = y/\lambda_o f$, f is the focal length of the achromatic transform lens and * denotes the correlation operation.

As a special example to illustrate the temporal coherence requirement, let us consider a one-dimensional spatially Gaussian target, i.e.,

$$t(u) = e^{-a^2 u^2}, \tag{17}$$

where a is an arbitrary constant. The corresponding Fourier spectrum at the spatial frequency plane is

$$T(f_x) = \sqrt{\pi}/a \; \exp[-(\frac{\pi}{a} f_x)^2], \tag{18}$$

where $f_x = x/\lambda f$, and λ is the wavelength of the broadband source and f is the focal length of the transform lens. We now insert a matched filter for $\lambda = \lambda_o$ at the spatial frequency plane,

$$H(f_x^o) = T^*(f_x^o) = \sqrt{\pi}/a \; \exp[-(\pi/a \; f_x^o)^2]. \tag{19}$$

The output intensity distribution of Eq. (2) becomes,

$$I(u') = 2\pi/a^2 \int_{\lambda_o}^{\lambda_o + \Delta\lambda/2} \frac{\lambda_o^2}{\lambda^2 + \lambda_o^2} \; \exp[-2a^2 \; (\frac{\lambda_o^2}{\lambda^2 + \lambda_o^2})(u')^2]d\lambda. \tag{20}$$

From this equation, we see that the output intensity has again a Gaussian-like distribution. The correlation peak occurs at u = 0, i.e.,

$$I(0) = 2\lambda_o[\tan^{-1}(1 + \Delta\lambda/2\lambda_o) - \tan^{-1}(1)]. \tag{21}$$

Since the spatially Gaussian target essentially has low spatial frequency content, the normalized correlation peak (i.e., $I(0)/\Delta\lambda$) is relatively independent of the spectral bandwidth, as shown in Fig. 5.

To investigate the effect of spatial frequency on the temporal coherence requirement, we shall now assume that a one-dimensional
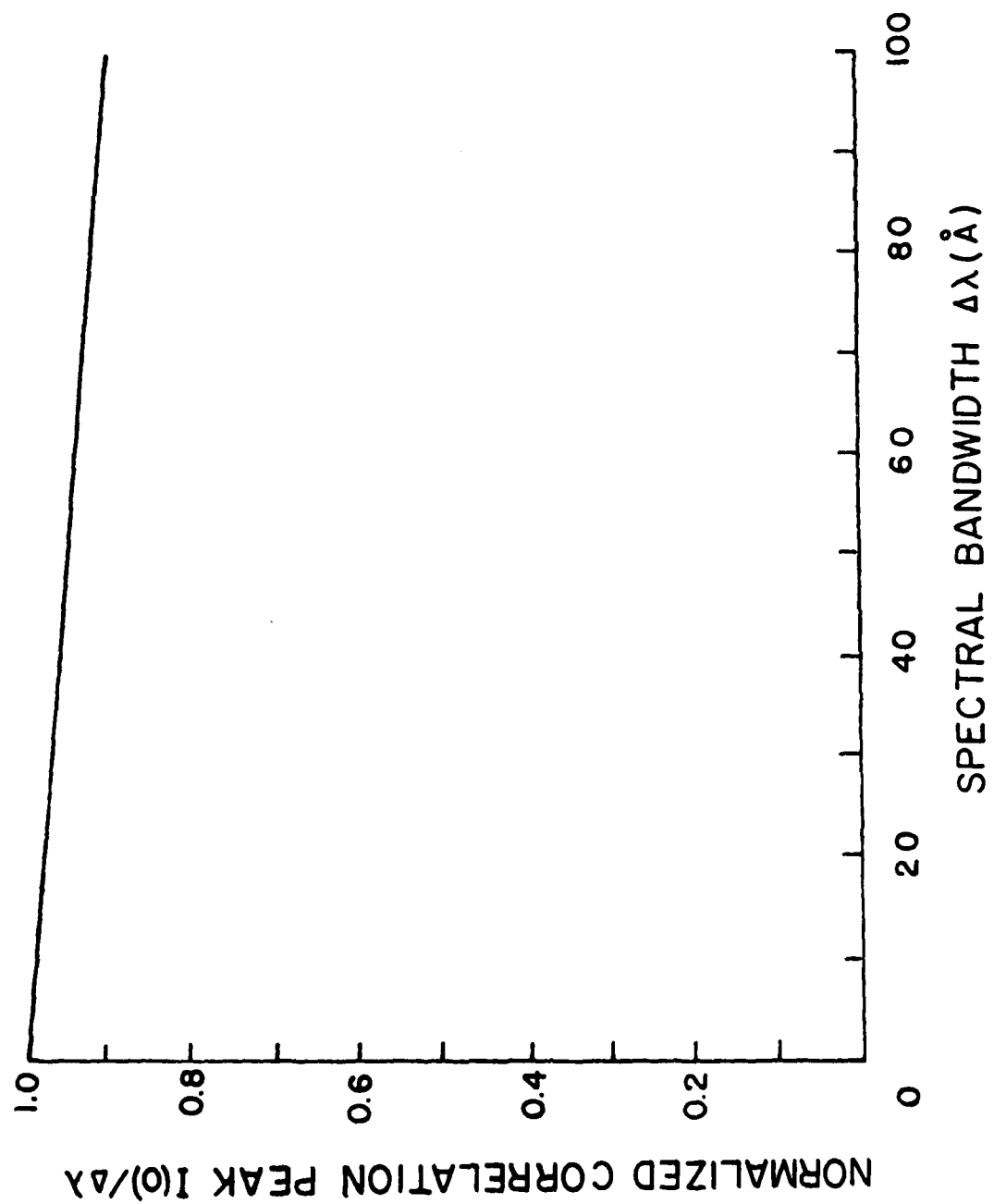
Figure 5. Normalized correlation peak as a function of some spectral bandwidth, for a Gaussian spatial signal.

sinusoidal function as the input object, i.e.,

$$t(u) = \text{rect}(\tfrac{u}{W}) \ [1 + \cos(2\pi q u)], \tag{22}$$

where q is the spatial frequency of the input sinusoid, and

$$\text{rect}(\tfrac{u}{W}) \overset{\Delta}{=} \begin{array}{l} 1, \ |u| \leq W/2, \\ 0, \ \text{otherwise}, \end{array} \tag{23}$$

where W is the spatial extension of the target. By substituting Eq. (22) into Eq. (16), we have

$$A(u';\lambda) = \lambda_o/\lambda \ \int_{-\infty}^{\infty} \text{rect} \ (\tfrac{\xi}{W}) \ [1 + \cos(2\pi q \xi)] \ \text{rect} \ (\tfrac{\xi - u'}{W_o}) \ \{1 +$$

$$\cos[2\pi q_o(\xi - u')]\} d\xi \ , \tag{24}$$

where $W_o = W\lambda/\lambda_o$, and $q_o = q\lambda/\lambda_o$. Thus at $u' = 0$, Eq. (24) becomes

$$A(W,q,\lambda) = \lambda_o/\lambda \ \{W + \frac{\sin(\pi W q_o)}{\pi q_o} + \frac{\sin(\pi W q)}{\pi q}$$

$$+ \frac{\sin[\pi W(q - q_o)]}{2\pi(q - q_o)} + \frac{\sin[\pi W(q + q_o)]}{2\pi(q + q_o)}\}. \tag{25}$$

The normalized correlation peak can be determined by the following equation:

$$\frac{I(0)}{\Delta\lambda} = \frac{1}{\Delta\lambda} \ \int_{\lambda_o - \Delta\lambda/2}^{\lambda_o + \Delta\lambda/2} A^2(w,q;\lambda) d\lambda \tag{26}$$

Figure 6 shows the variation of the normalized correlation peak as a function of the spectral bandwidth of the light source, for different spatial frequencies of target (i.e., input object) signal. From this figure we see that the normalized correlation peak monotonically decreases as the spectral bandwidth of light source increases. We also see that the normalized correlation peak drops rather rapidly as the spatial frequency of target increases.
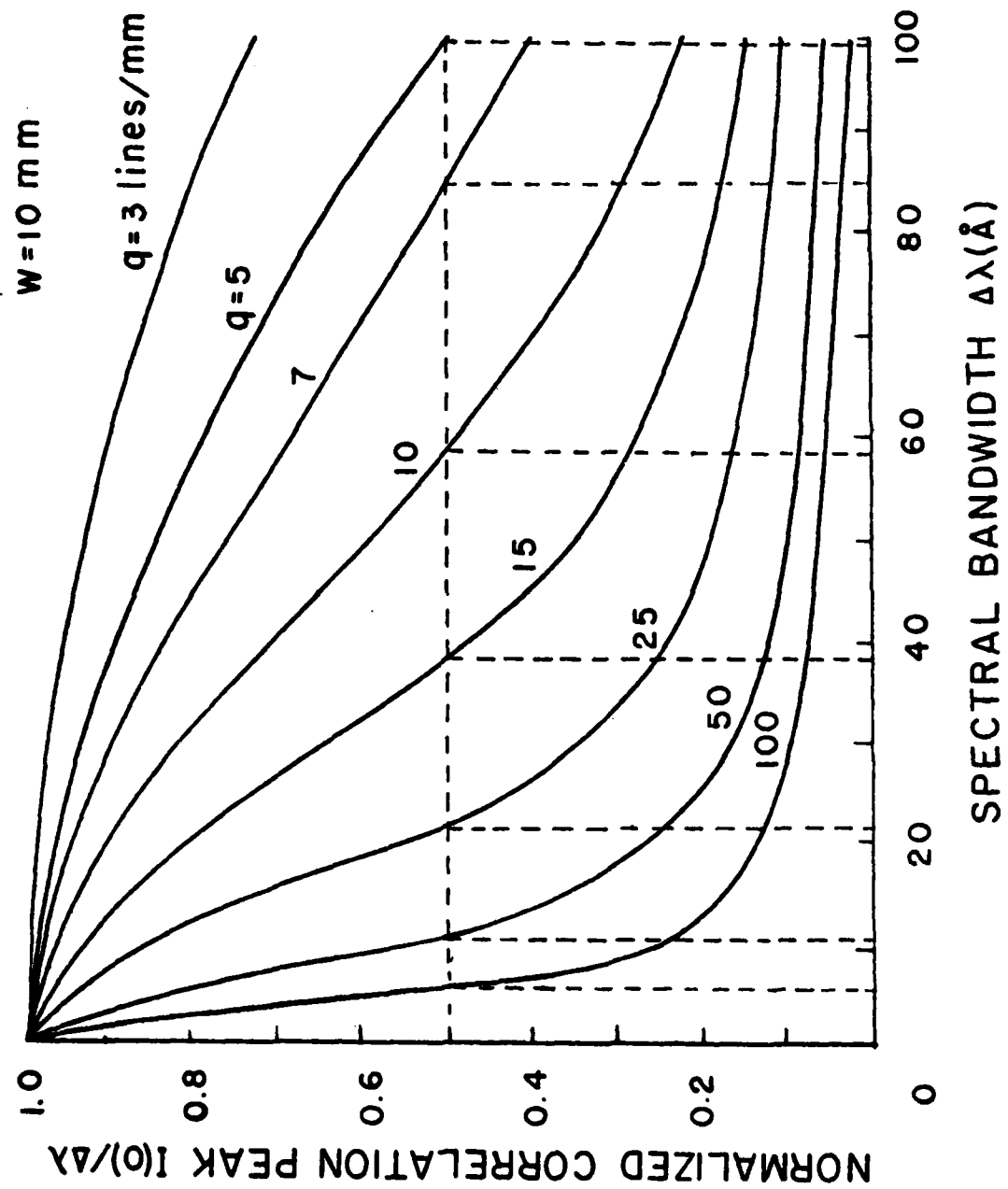
Figure 6. Normalized correlation peak as a function of source spectral bandwidth, for various input spatial frequencies.

On the other hand, Figure 7 shows the variation of the normalized correlation peak as a function of the spatial bandwidth $\Delta\lambda$, for various target extension W. Again we see that the normalized correlation peak decreases monotonically as $\Delta\lambda$ increases. And the normalized peak decreases very rapidly as the target extension W increases. Thus from Figs. 6 and 7, we see that the normalized correlation peak strongly depends on the spatial frequency and the extension of the target.

Using the half power point (i.e., 50%) as a criterion of the normalized correlation peak, we can determine the spectral width $\Delta\lambda$ requirement (i.e., temporal coherence requirement). The results are shown in Tables 1 and 2.

From these tables, we see that for relatively small and lower spatial frequency target, a relatively broader spatial bandwidth of the light source can be used. In other words the higher the spatial frequency of the target or the larger the extension of the detecting signal is, the higher the temporal coherence requirement (i.e., narrower spectral bandwidth) of the light source is needed. Furthermore, from Tables 1 and 2, a plot of the space bandwidth product (i.e., Wq) as a function of the required spectral bandwidth of the light source is shown in Fig. 8. From this figure, we see that the space bandwidth product exponentially decreases as the spatial bandwidth of the light source increases. Thus, for a large space bandwidth product, an extremely high temporal coherent light source is required.

3.3 Spatial Coherence Requirement

We shall now discuss the spatial coherence requirement of the light source for the correlation detection. For simplicity, we assume that the light source $\gamma(x_o, y_o)$ is one-dimensional extended monochromatic source, i.e.,
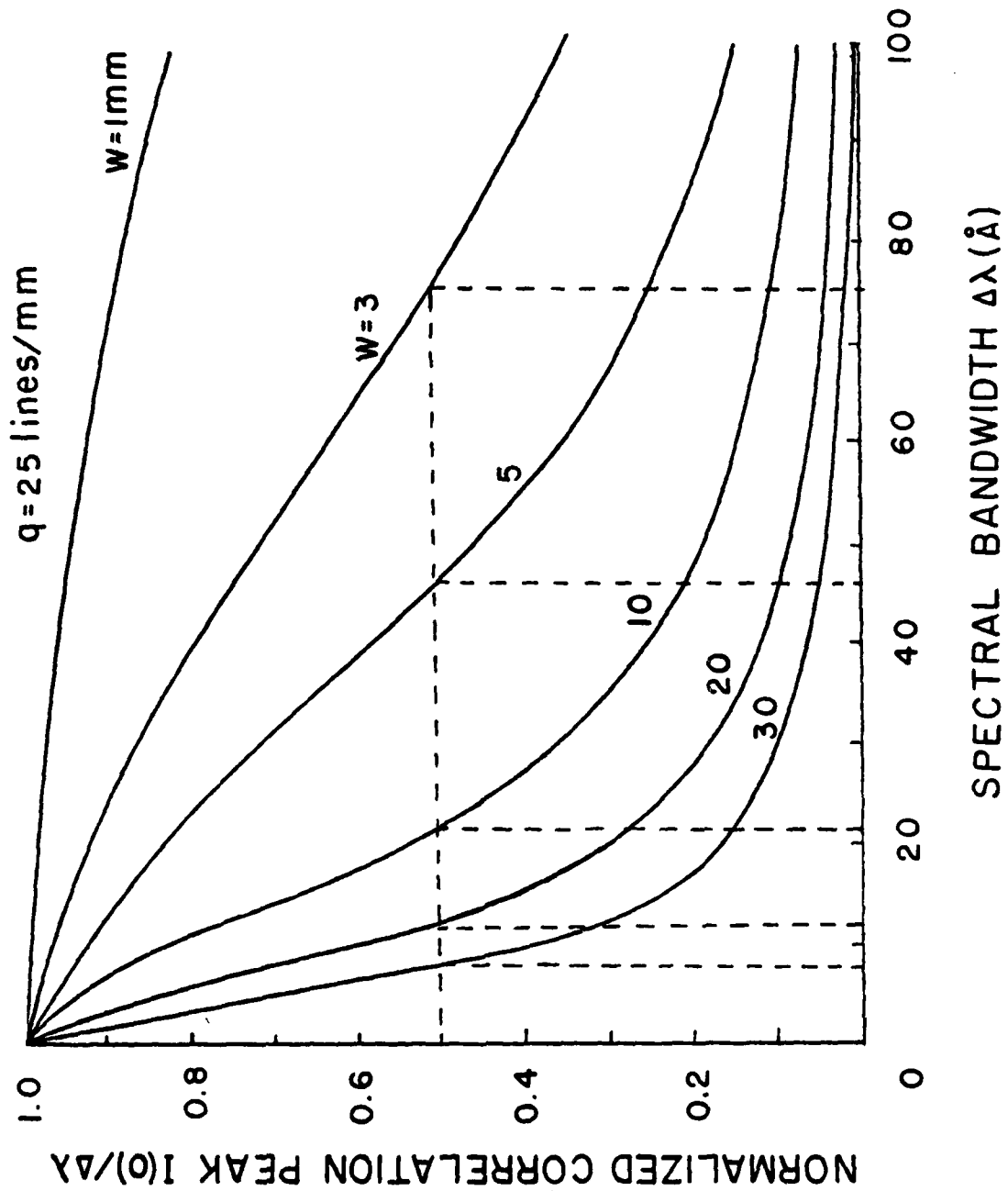
Figure 7.   Normalized correlation peak as a function source
spectral bandwidth, for different target extensions.
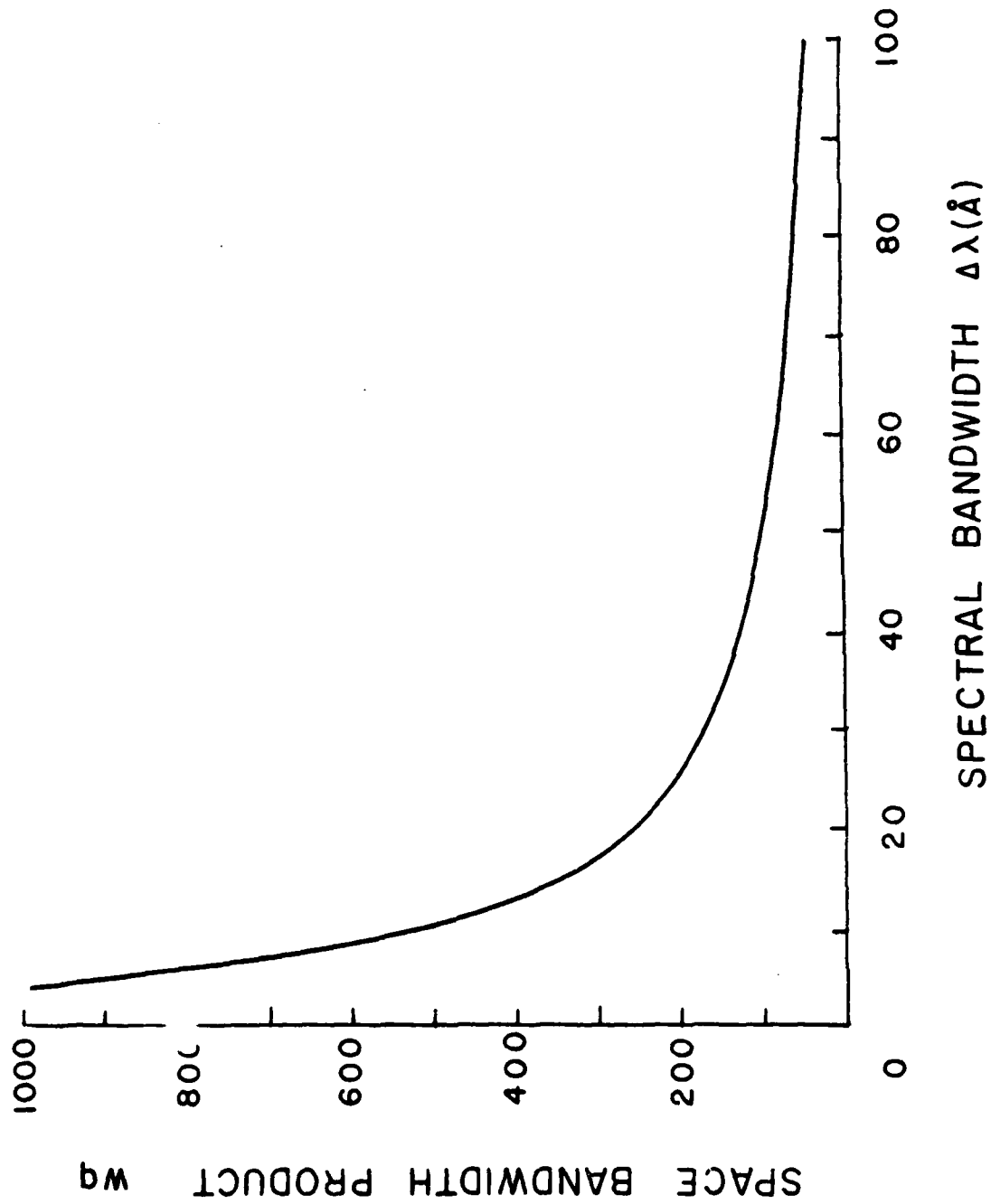
Figure 8. Space bandwidth product as a function of the required spectral bandwidth of the light source.

Table 1. Temporal Coherence Requirement as a Function of Spatial Frequency q, where W = 10 mm and λ_o = 5461Å.

q(lines/mm)	1	3	5	7	10	25	50	100
$\Delta\lambda$(Å)	540	180	99	85	58	22	11	6

Table 2. Temporal Coherence Requirement as a Function of the extension of target W, where q = 25 lines/mm and λ_o = 5461Å.

W(mm)	1	2	3	5	10	20	30	60
$\Delta\lambda$ (Å)	220	99	75	46	22	11	8	4.7

$$\gamma(x_o, y_o) = \text{rect}\left(\frac{x_o}{\Delta S}\right) f(y_o) \tag{27}$$

where

$$\text{rect}\left(\frac{x_o}{\Delta S}\right) \triangleq \left\{ \begin{array}{l} 1, \ |x_o| \leq \Delta S/2, \\ \\ 0, \ \text{ohterwise}, \end{array} \right. \tag{28}$$

and Δ is the size of the extended source. Similarly, the output plane

intensity distribution can be shown as

$$I(u') = \int_{-\Delta S/2}^{\Delta S/2} \text{rect}\left(\frac{x_o}{\Delta S}\right) A^2(u'; x_o) dx_o = 2 \int_0^{\Delta S/2} A^2(u'; x_o) dx_o, \tag{29}$$

where

$$A(u'; x_o) = \int_{-\infty}^{\infty} t^*(\xi) \ t(\xi - u') \exp[i 2\pi f_{x_o} \xi] d\xi, \tag{30}$$

and $\ f_{x_o} = \dfrac{x_o}{\lambda_o f}$.

We shall again consider a spatially Gaussian target of Eq. (17),

where we obtain

$$A(u'; x_o) = \frac{1}{a} \ \frac{\pi}{2} \ \exp\left[-\left(\frac{\pi}{a\sqrt{2}} f_{x_o}\right)^2\right] \exp\left[-\frac{a^2}{2}(u')^2\right] \tag{31}$$

The corresponding output intensity distribution can be shown as

$$I(u') = \frac{\pi}{a^2} \exp[-a^2 (u')^2] \int_0^{\Delta S/2} \exp\left[-\left(\frac{\pi}{a} f_{x_o}\right)^2\right] dx_o. \tag{32}$$

Since the integral is independent of u', it can be shown that the output

intensity, like before, has a Gaussian-like distribution. To determine

the correlation peak, we shall let $u' = 0$, i.e.,

$$I(0) = \frac{\pi}{a^2} \int_0^{\Delta S/2} \exp\left[-\left(\frac{\pi}{a} f_{x_o}\right)^2\right] dx_o. \tag{33}$$

It is evident from the equation that $I(0)$ depends on the size of

the extended monochromatic source ΔS. Figure 9 shows the normalized

correlation peak $I(0)/\Delta S$ of the Gaussian target. We see that the cor-

relation peak drops quickly with the increasing size of the source.
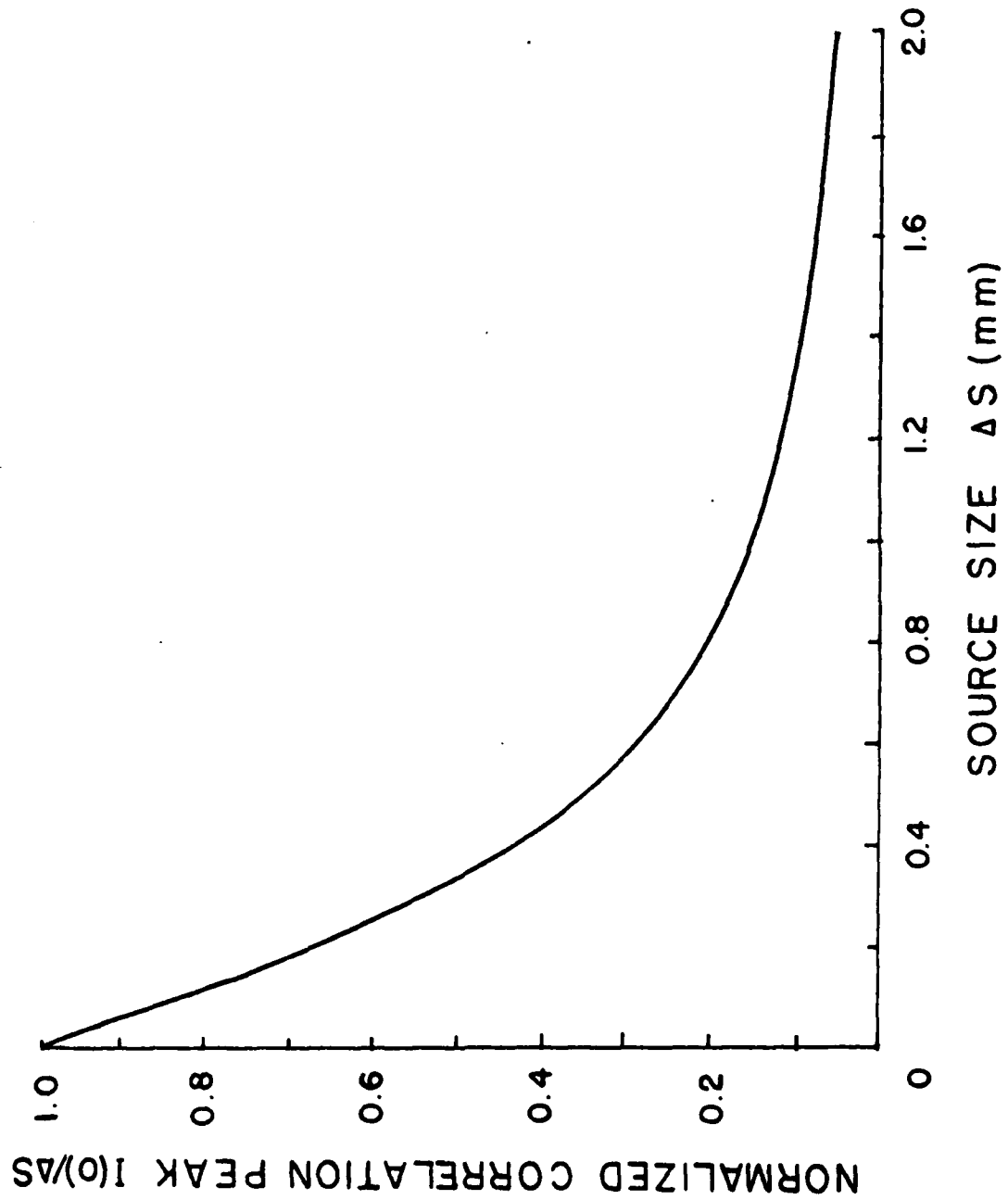
Figure 9. Normalized correlation peak as a function of source size, for a Gaussian spatial signal.

We shall now consider the effect of spatial frequency in the correlation peak. Again we use a spatially limited sinusoidal grating of Eq. (22) as the input signal. For simplicity of notation we let $q = x_o/(\lambda_o f)$ and $g = \pi/(\lambda_o f)$, Eq. (33) becomes

$$I(0) = 2 \int_0^{\Delta S/2} (0;x_o)dx_o, \qquad (34)$$

where

$$A(0,x_o) = \frac{\sin(gWx_o)}{gx_o} + \frac{\sin[W(gx_o-\pi q)]}{(gx_o - \pi q)} + \frac{\sin[W(gx_o+\pi q)]}{(gx_o + \pi q)}$$

$$+ \frac{1}{(gx_o+2\pi q)} \left[\sin(Wgx_o)\cos^2(\pi Wq) + \frac{q\sin[W(gx_o-2\pi q)]}{(gx_o - 2\pi q)}\right.$$

$$\left. + \frac{\pi q\sin(Wgx_o)}{gx_o}\right] \qquad (35)$$

q is the spatial frequency and W is the spatial extension of the target. Since q is not related to x_o, the spatial coherence requirement is evidently independent of the spatial frequency of the input object, as expected. However the spatial coherence strongly depends on the extension of the target, as can be seen in Fig. 10. From this figure, we see that, the normalized correlation peak monotonically decreases with increasing source size. The rate of the decrease rapidly increases for larger extension of the target. Again by using the half power point criterion, the spatial coherence requirement for various values of the target extension are tabulated in Table 3. The table shows the spatial coherence requirement (i.e., source size requirement) increases rapidly as the target extension increases.

In concluding this section, we have developed equations for the coherence requirements of correlation detection for partially coherent optical processing. We have also calculated numerical estimates for
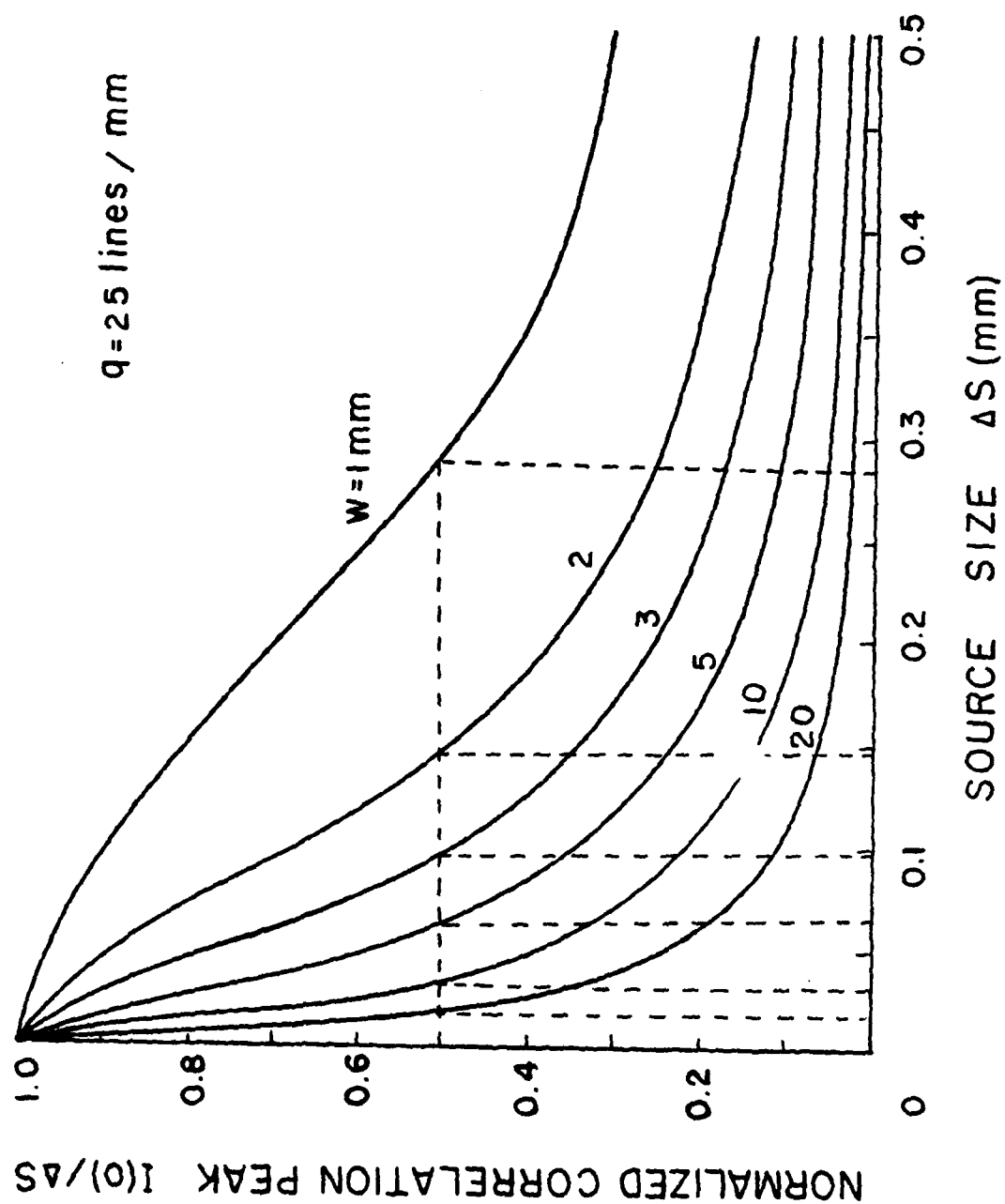
Figure 10.   Normalized correlation peak as a function of source size, for different target extensions.

Table 3. Spatial Coherence Requirement as a Function of the Extension of Target, where $\lambda_o = 5461\text{Å}$.

W(mm)	1	2	3	5	10	20	50
ΔS(mm)	0.28	0.14	0.09	0.07	0.03	0.015	0.006

these requirements using half power criterion for some special cases.
We have shown that the temporal coherence requirement strongly
depends on the spatial frequency and the extension (i.e., space
bandwidth product) of the target signal to be detected. However,
the spatial coherence requirement depends only upon the extension
of the target. We have also shown the coherence requirement for
a spatially Gaussian signal, as a special case. For this case, the
normalized correlation peak is relatively independent of the spectral
bandwidth of the light source, but it decreases rapidly as the
source size increases.

IV. Noise Performance

4.1 Problem Formulation

The noise performance of an achromatic coherent optical system
was reported by Leith and Roth[12]. They approached the analysis through
the introduction of the concept of a three-dimensional transfer function
to describe the noise-suppression properties of the system. They showed
that such a system produces considerable noise-suppression if the system
is illuminated by a broad-spectrum light source. Both signal-dependent
and signal-independent noise were considered. In each case, they showed
that the achromatic coherent system behaves much like an incoherent
imaging system.

Here, we shall analyze the noise performance for a white-light optical
signal processor[1-3] (or a partially coherent optical processor), as proposed
in Fig. 11. We shall derive the output signal-to-noise as a means of
measurement for the noise performance of the system. The noise sources that
we shall discuss are primarily due to grain-noise and plane-noise at the
input and Fourier planes. The development of the output signal irradiance
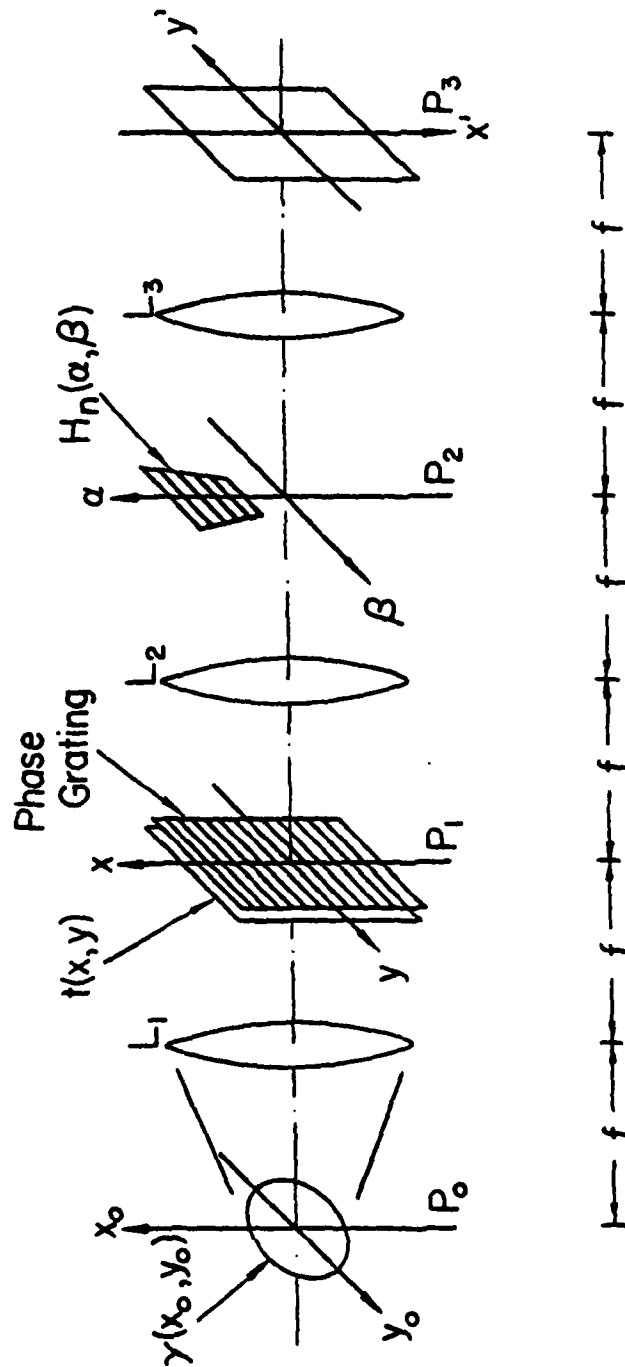
Figure 11. A white-light optical signal processor. $\gamma(x_o, y_o)$, source intensity distribution; $t(x,y)$, input object; $H_n(\alpha,\beta)$, spectral band filter; P_o source plane, P_1, input plane, P_2, fourier plane; P_3, output plane; L, achromatic lens.

and noise fluctuation are primarily based upon the partial coherence

theory of Wolf[10,13]. Since output noise fluctuation is dependent on

the degree of coherence illumination, we shall quantitatively analyze

the effect of noise-suppression due to temporally and spatially partial

coherent illumination. In this section, we shall, however, analyze

the noise performance due only to the temporally coherent illumination.

The noise effect due to spatially coherent illumination will be

followed by a subsequent report.

We shall now evaluate the noise performance of the proposed white-

light optical signal processor, as described in Fig. 11. We shall first

investigate the statistical nature of intensity distribution at the

output plane. In order to do so, we shall evaluate the output light intensity

distribution due to the nth narrow spectral band spatial filter, such as[13]

$$I_n(x',y') = \int_{\lambda_{\ell n}}^{\lambda_{hn}} \iint_{-\infty}^{\infty} \Upsilon(x_o,y_o;\lambda)S(\lambda)C(\lambda) \left| \iint_{-\infty}^{\infty} S(x_o+\alpha-\lambda f\nu_o, y_o+\beta) \right.$$

$$\left. H_n(\alpha,\beta)\exp\left\{-i\frac{2\pi}{\lambda f}(x'\alpha+y'\beta)\right\} d\alpha\, d\beta \right|^2 dx_o\, dy_o\, d\lambda,$$

(36)

where $\Upsilon(x_o,y_o)$ is intensity distribution of the white-light source,

$S(\lambda)$ and $C(\lambda)$ are the relative spectral intensity of the light source

and the relative spectral response sensitivity of the detector, respec-

tively; $\lambda_{\ell n}$ and λ_{hn} are the longest and the shortest limiting wavelenths

of the nth spectral band filter, $S(x_o + \alpha - \lambda f\nu_o, y_o + \beta)$ represents

the Fourier spectrum of the input signal $s(x,y)$ due to wavelength

λ, ν_o in the spatial frequency of the phase grating, $H_n(\alpha,\beta)$ is the

nth spectral band spatial filter and f is the focal length of the

achromatic Fourier transform lens.

The overall intensity distribution for the entire spatial band of the light source would be,

$$
I(x', y') = \sum_{n=1}^{N} I_n(x', y')
$$

$$
= \sum_{n=1}^{N} \int_{\lambda_{\ell n}}^{\lambda_{h n}} \iint \gamma(x_o, y_o; \lambda) S(\lambda) C(\lambda) \Big| \iint_{-\infty}^{\infty} S(x_o + \alpha - \lambda f \nu_o, y_o + \beta)
$$

$$
H_n(\alpha, \beta) \exp\left\{ -i \frac{2\pi}{\lambda f} (x'\alpha + y'\beta) \right\} d\alpha d\beta \Big|^2 dx_o dy_o d\lambda,
$$

$$
\tag{37}
$$

where N is the total number of the narrow spectral band filters.

The overall output signal-to-noise ratio (SNR) of the white-light processor can be written as

$$
SNR = \frac{1}{N} \sum_{n=1}^{N} SNR_n,
\tag{38}
$$

where SNR_n represents the output signal-to-noise ratio due to the nth spectral band spatial filter.

We shall now consider a spectrally broadband point source (i.e., a temporal incoherent source) for illumination. The spatial intensity distribution of the light source can be described by a δ-function [i.e., $\gamma(x_o, y_o) = \delta(x_o, y_o)$]. For simplicity, we assume that $C(\lambda)$ and $S(\lambda)$ are constant over the spectral width of the light source. Thus Eq.(37) can be written as

$$
I_n(x', y') = \int_{\lambda_{\ell n}}^{\lambda_{h n}} \Big| \iint_{-\infty}^{\infty} S(\alpha - \lambda f \nu_o, \beta) H_n(\alpha, \beta) \exp\left[-i \frac{2\pi}{\lambda f} (\alpha x' + \beta y') \right] d\alpha d\beta \Big|^2 d\lambda,
$$

$$
\tag{39}
$$

where the subscript n represents the nth output irradiance due to nth spectral filter $H_n(\alpha, \beta)$ and the proportionality constant is disregarded for convenience. In analysis, we let the input signal be a one dimensional object of y variable [i.e., $s(y)$]. The phase grating at the input plane is perpendicular to y direction, which can be described as $\exp(i2\pi\nu_o x)$. The corresponding Fourier smeared spectra are also one-variable function in the β-direction and they are smeared into rainbow color in the α-direction. Let us denote that the width of the nth

narrow spectral band filter be Δx_n. If this filter is placed in the appropriate spectral band of the smeared Fourier spectra, the corresponding spectral bandwidth $\Delta\lambda_n$ is obviously determined by the spatial width $\Delta\alpha_n$ of the filter, which can be approximated by the following equation;

$$\Delta\lambda_n = (\lambda_{hn} - \lambda_{\ell n}) = \Delta\alpha_n / \nu_0 f \qquad (40)$$

By fixing the spatial width $\Delta\alpha_n$ of the filter, the redundancy of the filtered signal would be proportional to the spectral bandwidth $\Delta\lambda_n$ of the filter. In other words, the broader the spectral bandwidth $\Delta\lambda_n$, the higher the redundancy of the filtered signal is expected. From Eq.(40), it is evident that either a lower spatial frequency ν_0 of phase grating or shorter focal length f of the transform lens should be used to improve the output SNR at the output plane. However decreasing the grating spatial frequency ν_0 also reduces the number of spectral band filters in the Fourier plane. Thus it would also reduce the processing capability. Although the output SNR would decrease as ν_0 increases, however larger the ν_0 is used also implies that a larger number of spectral band filters can be utilized in the Fourier plane. Thus the overall output SNR would be increased due to the addition of the mutually incoherent filtered signals, from each spectral band filters $H_n(\beta)$.

It may be known that the output intensity fluctuation is primarily due to the statistical nature of the phase and the amplitude noise fluctuations. We shall now define the output SNR as an ensemble average of the image intensity $I_n(y)$ divided by the square root of its variance σ_{In}, that is

$$SNR_n(y') = E[I_n(y')] / \sigma_{In} \qquad , \qquad (41)$$

where

$$\sigma_{I_n} = \left\{ E[I_n^2(y)] - [E[I_n(y)]]^2 \right\}^{1/2} . \tag{42}$$

Again we note that a one dimensional notation is used, since the input signal is assumed to be one-dimensional. In order to describe the output SNR explicitly due to the effect of partially coherent illumination, we shall define a normalized signal-to-noise ratio SNR, such as,

$$\overline{SNR_n(y')} \triangleq \frac{SNR_n(y') \quad \text{for partially coherent illumination}}{SNR_n(y') \quad \text{for coherent illumination}}, \tag{43}$$

which is equal to the SNR of the partially coherent case divided by the coherent case, where the subscript n denotes the nth spectral band filtering.

We stress that the spatial average of Eq. (43) shall be used for estimating the SNR over the entire output image plane, for example:

(a) For a continuous representation, the output normalized SNR is,

$$\overline{SNR_n} = \frac{1}{L} \int_{-L/2}^{L/2} \overline{SNR_n(y')} \, dy' , \tag{44}$$

where L is the size (i.e., the length) of the output image, and

(b) For a discrete representation,

$$\overline{SNR_n} = \frac{1}{M} \sum_{m=1}^{M} \overline{SNR_n(y'_m)} , \tag{45}$$

where M represents the total number of sampling points. From these definitions it is reasonable to assume that the $\overline{SNR}_n$ is equal to unity for a strictly coherent illumination and $\overline{SNR}_n$ increases as the degree of coherence decreases.

Since $\overline{SNR}_n$ is defined for nth spectral band filter, the overall output normalized signal-to-noise ratio can be written as

$$\overline{SNR} = \frac{1}{N} \sum_{n=1}^{N} \overline{SNR}_n \quad , \tag{46}$$

where N is the total number the spectral band filters in the Fourier plane, which can be estimated by,

$$N \stackrel{\Delta}{=} \frac{\Delta\lambda}{\Delta\lambda_n} \simeq \frac{\Delta\lambda \, \nu_0}{4\lambda_0 \, \Delta\nu_\alpha} \quad , \quad \text{for} \quad \nu_0 >> \Delta\nu_\alpha \tag{47}$$

$\Delta\lambda$ and λ_0 are the spectral bandwidth and the mean wavelength of the light source (e.g., white-light source), respectively, ν_0 is the spatial frequency of the phase grating, and $\Delta\nu_\alpha$ is the spatial frequency bandwidth of the input object, in α direction.

We stress that, Eqs. (39) to (46) shall be used for the evaluation of the noise performance of a white-light optical signal processor.

Prior going into the evaluation of the SNR, we shall specify the statistical properties of the phase noise and film-grain noise, respectively. Let us now adopt an overlapping grain mode [14] to describe the granularity of the recording medium. For simplicity of evaluation, we would make the following assumptions:

(a) The film-grains are rectangular in shape and the center of these rectangle grains fall randomly over the recording plate, as shown in Fig. 12.

(b) The distribution of the grains (i.e., the choice of where the center of a rectangle falls) is assumed to be independently distributed.

and (c) The distribution of the grain, over the recording plate, is Poisson distributed, i.e.,

$$G_N(m) = \frac{N!}{m! \, (N-m)!} \, P^N (1-P)^{N-m} \quad , \tag{48}$$

The mean value and the second-order moment (correlation function) are:

$$E[G(y)] = C_A \quad , \tag{49}$$
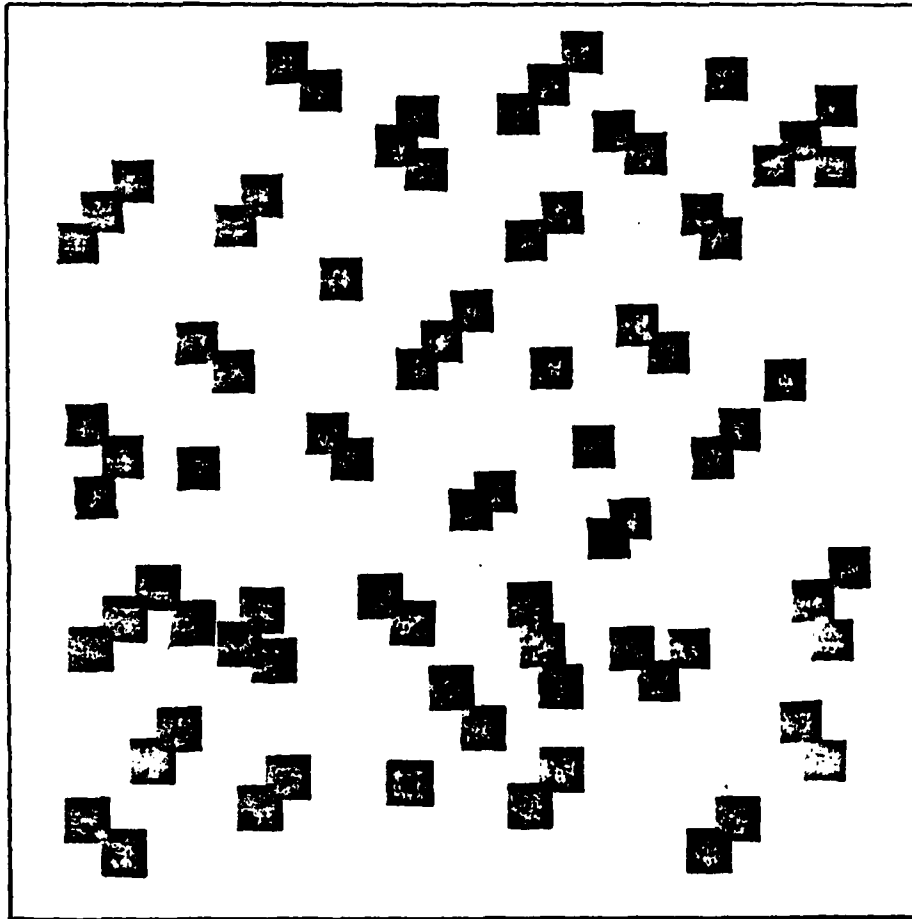
Figure 12.   Overlapping model of film granularity.

and

$$E[G(y_1)G(y_2)] = C_A^2 \exp[2.3 D R(|y_1 - y_2|/\ell)] \, , \qquad (50)$$

respectively, where D is the photographic density, ℓ is correlation distance and

$$R\left(\frac{|y_1 - y_2|}{\ell}\right) \overset{\Delta}{=} \begin{cases} 1 - |y_1 - y_2|/\ell \, , & \text{for } |y_1 - y_2| < \ell \\ \\ 0 & , \text{ otherwise } \, , \end{cases} \qquad (51)$$

where the function $R(|y_1 - y_2|/\ell)$ is shown in Fig.13.

Although the film granularity is generally a nonstationary Markow Chain [16], for simplicity, we assume that the grain-noise is a stationary process.

As for the phase-noise, the phase fluctuation $\phi(y)$ is primarily due to the thickness variation and the refractive index fluctuations of the emulsion. For simplicity, we would make the following assumptions:

(a) $\phi(y)$ is a stationary random function of the coordinates, the probability distribution of $\phi(y)$ is identical throughout the entire recording medium.

(b) It is reasonable to assume that $\phi(y)$ has zero mean i.e., $E[\phi(y)] = 0$, since the phase fluctuation can be regarded as a bipolar function.

(c) The autocorrelation function of $\phi(y)$ is dependent only on the difference in distance $|y_1 - y_2|$ since $\phi(y)$ is assumed to be a stationary process. We note that the autocorrelation function has various functional forms; for example [13], the Gaussian form representation;

$$E[\phi(y_1)\phi(y_2)] = \sigma^2 \exp[-(y_1 - y_2)^2/d^2] \, , \qquad (52)$$
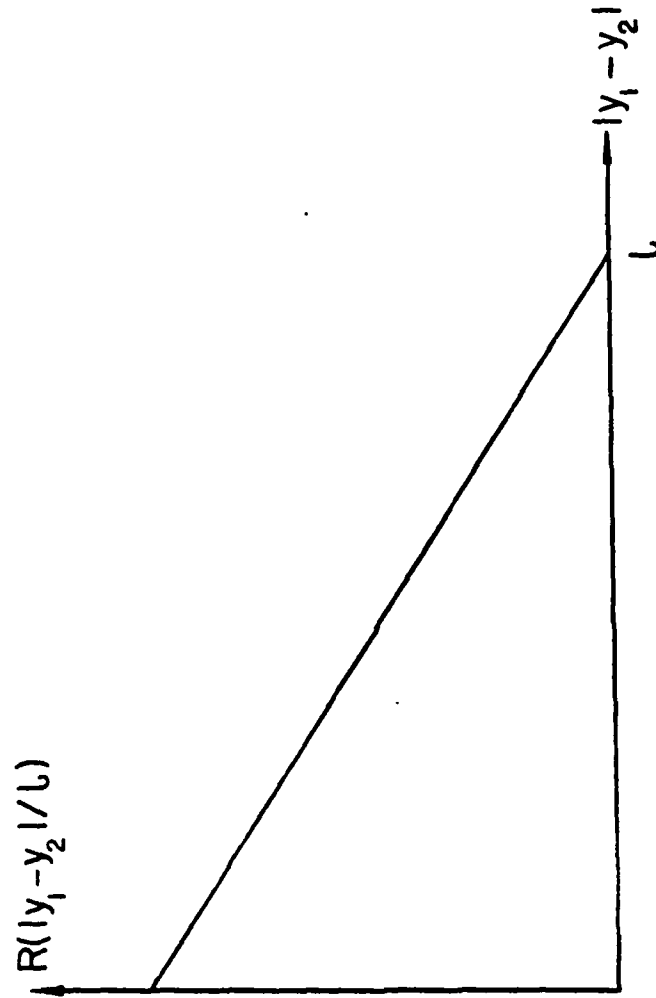
Figure 13. Variation of $R(|y_1 - y_2|/\ell)$ as a function of $|y_1 - y_2|$.

and the exponential form representation;

$$E\left[\phi(y_1)\phi(y_2)\right] = \sigma^2 \exp\left[-|y_1-y_2|/d\right] , \qquad (53)$$

where σ^2 is the variance of $\phi(y)$, and the quantity d is called the scale size of the irregularities and can be regarded as the size of an average blob, in the emulsion. However d is best known as the correlation distance. For simplicity, we shall however use the exponential form for evaluating the output SNR.

4.2 Effect of Noise at Input Plane

We shall now evaluate the noise performance of the proposed white-light optical signal processor due to input plane. Let us consider the output intensity distribution due to nth spectral band filter of Eq. (37). By Perseval's Theorem, the output intensity distribution, in a one-dimensional form, can be written as

$$I_n(y') = \int_{\lambda_{\ell n}}^{\lambda_{hn}} \left| \frac{1}{f\lambda} t(y') * \int\int_{-\infty}^{\infty} H_n(\beta)\exp\left(-i\frac{2\pi}{\lambda f}\beta y'\right)d\beta \right|^2 d\lambda , \quad (54)$$

where the subscript n denotes the nth spectral band filter, * denotes the convolution operation and t(y') represents the one-dimensional input signal with complex noise. The complex noise is due to the random thickness fluctuation of phase distribution $\phi(y)$ and the granularity G(y) of the input transparency. We note that the phase-noise and the grain-noise can be regarded as multiplicative and additive type noise, respectively. The overall input signal can be written as,

$$t(y) = s(y)\exp\left[iK\phi(y)\right] + G(y) , \qquad (55)$$

where $k = 2\pi/\lambda$, and s(y) is a one-dimensional signal.

To evaluate the output SNR, we let the input signal s(y) be a sinusoidal grating with a spatial frequency ν. Thus Eq. (55) becomes,

$$t(y) = (1 + \sin 2\pi \nu y) \exp[i K \phi(y)] + G(y) \quad . \tag{56}$$

We shall now investigate the effect due to phase-noise and film-grain noise independently in the following:

4.2.1 Phase-Noise

To investigate the effect due to phase-noise at the input plane, we simply let the film-grain noise be zero and assume that the nth spectral band filter $H_n(\beta)$ be bandlimited, i.e.,

$$H_n(\beta) = \text{rect}\left(\frac{\beta}{2\lambda f \nu}\right) \quad . \tag{57}$$

By substituting Eq. (57) into Eq. (54) we have

$$I_n(y') = \int_{\lambda_{\ell n}}^{\lambda_{hn}} \left| \int_{-\infty}^{\infty} (1 + \sin 2\pi \nu y) \exp[i K \phi(y)] \frac{\sin 2\pi \nu (y'-y)}{\pi (y'-y)} dy \right|^2 d\lambda \quad . \tag{58}$$

If we take the ensemble average, Eq. (58) becomes

$$E[I(y')] = \int_{\lambda_{\ell n}}^{\lambda_{hn}} \int\int_{-\infty}^{\infty} (1 + \sin 2\pi \nu y)(1 + \sin 2\pi \nu \bar{y}) \frac{\sin 2\pi \nu (y'-y)}{\pi (y'-y)}$$

$$\times \frac{\sin 2\pi \nu (y'-\bar{y})}{\pi (y'-y)} E[\exp[i K[\phi(y) - \phi(\bar{y})]]] dy d\bar{y} d\lambda \quad . \tag{59}$$

We shall evaluate Eq. (56), with the following assumptions:

(a) $k \phi(y) < 1$, a weak phase-noise, and

(b) higher-order moments of $\phi(y)$ are much smaller than the second-order moment.

With reference to the Taylor series, the ensemble of the exponential term can be written as:

$$E\left[\exp\left\{iK\left[\phi(y_1)-\phi(y_2)\right]\right\}\right]$$

$$= 1+iKE\left[\phi(y_1)-\phi(y_2)\right]+\frac{1}{2}(iK)^2 E\left\{\left[\phi(y_1)-\phi(y_2)\right]^2\right\}\cdots,$$

(60)

By utilizing the exponential form representation of Eq.   and the assumption of $E[\phi(y)] = 0$, Eq. (57) is reduced to

$$E\left[\exp\left\{iK\left[\phi(y)-\phi(\bar{y})\right]\right\}\right] = 1-K^2\sigma^2+K^2\sigma^2 \exp(-|y-\bar{y}|/d).$$ (61)

By substituting Eq. (61) into Eq. (59), we have

$$E\left[I_n(y')\right] = I_1^2(y')\int_{\lambda_{\ell n}}^{\lambda_{hn}}\left(1-\frac{4\pi^2\sigma^2}{\lambda^2}\right)d\lambda + I_2(y')I_3(y')\int_{\lambda_{\ell n}}^{\lambda_{hn}}\frac{4\pi^2\sigma^2}{\nu_0 f\lambda}d\lambda$$

$$= (\lambda_{hn}-\lambda_{\ell n})I_1^2(y')+\frac{4\pi^2\sigma^2(\lambda_{hn}-\lambda_{\ell n})}{\lambda_{hn}\lambda_{\ell n}}\left[I_1^2(y')-I_2(y')I_3(y')\right]$$

$$= \Delta\lambda\,I_1^2(y') - \frac{4\pi^2\sigma^2}{\lambda_{\ell n}(\lambda_{\ell n}+\Delta\lambda)}\left[I_1^2(y')-I_2(y')I_3(y')\right].$$

(62)

where

$$I(y') \stackrel{\Delta}{=} \int_{-\infty}^{\infty}(1+\sin 2\pi\nu y)\frac{\sin 2\pi\nu(y'-y)}{\pi(y'-y)}dy ,$$ (62a)

$$I_2(y') \stackrel{\Delta}{=} \int_{-\infty}^{\infty}(1+\sin 2\pi\nu y)\frac{\sin 2\pi\nu(y'-y)}{\pi(y'-y)}\exp(y/d)dy ,$$ (62b)

and

$$I_3(y') \stackrel{\Delta}{=} \int_{-\infty}^{\infty}(1+\sin 2\pi\nu y)\frac{\sin 2\pi\nu(y'-y)}{\pi(y'-y)}\exp(-y/d)dy .$$ (62c)

The ensemble of the square irradiance can be obtained by the following

integral equation:

$$E[I_n^2(y')] = E\left[\left\{\int_{\lambda_{\ell n}}^{\lambda_{hn}}\iint_{-\infty}^{\infty}(1+\sin 2\pi\nu y)(1+\sin 2\pi\nu\bar{y})\frac{\sin 2\pi\nu(y'-y)}{\pi(y'-y)}\right.\right.$$

$$\left.\times\frac{\sin 2\pi\nu(y'-\bar{y})}{\pi(y'-y)}\exp\{iK[\phi(y)-\phi(\bar{y})]\}dyd\bar{y}d\lambda\right\}^2\right]$$

$$=\iint_{\lambda_{\ell n}}^{\lambda_{hn}}d\lambda_1 d\lambda_2\iiiint_{-\infty}^{\infty}(1+\sin 2\pi\nu y_1)(1+\sin 2\pi\nu\bar{y}_1)(1+\sin 2\pi\nu y_2)$$

$$\times(1+\sin 2\pi\nu\bar{y}_2)\frac{\sin 2\pi\nu(y'-y_1)}{\pi(y'-y_1)}\frac{\sin 2\pi\nu(y'-\bar{y}_1)}{\pi(y'-y_1)}$$

$$\times\frac{\sin 2\pi\nu(y'-y_2)}{\pi(y'-y_2)}\frac{\sin 2\pi\nu(y'-\bar{y}_2)}{\pi(y'-\bar{y}_2)}E[\exp\{iK_1[\phi(y_1)-\phi(\bar{y}_1)]$$

$$+iK_2[\phi(y_2)-\phi(\bar{y}_1)]\}dy_1 d\bar{y}_1 dy_2 d\bar{y}_2 \qquad (63)$$

Similarly, the following equations can also be obtained for either

the weak phase-noise or the small higher order moments assumptions,

such as

$$E[\exp\{iK_1[\phi(y_1)-\phi(\bar{y}_1)]+iK_2[\phi(y_2)-\phi(\bar{y}_2)]\}]$$

$$= 1-(K_1^2+K_2^2)\sigma^2-K_1^2 E[\phi(y_1)\phi(y_2)]-K_2^2 E[\phi(\bar{y}_1)\phi(\bar{y}_2)]$$

$$+K_1 K_2 E[\phi(y_1)\phi(\bar{y}_1)]-E[\phi(y_1)\phi(\bar{y}_2)]$$

$$-E[\phi(y_2)\phi(\bar{y}_1)]+E[\phi(y_2)\phi(\bar{y}_2)] \qquad (64)$$

By substituting Eqs. (64) and (50) into Eq. (63) and using the symmetrical properties of the integral function about the variables (y_1, y_2) and $(\bar{y}_1, \bar{y}_2)$, we obtain the following result:

$$E[I_n^2(y')] = \int\limits_{\lambda_{\ell n}}^{\lambda_{hn}}\int I_1^4(y') - \frac{4\pi^2\sigma^2}{\lambda^2} I_1^2(y')[I_1^2(y') - I_2(y')I_3(y')]$$

$$\times \left(\frac{1}{\lambda_1^2} - \frac{1}{\lambda_2^2} \right) d\lambda_1 d\lambda_2$$

$$= (\lambda_{hn} - \lambda_{\ell n})^2 I_1^4(y') - 8\pi^2\sigma^2 \frac{(\lambda_{hn} - \lambda_{\ell n})^2}{\lambda_{hn} - \lambda_{\ell n}} I_1^2(y') \quad (65)$$

$$\times [I_1^2(y') - I_2(y')I_3(y')].$$

where I_1 to I_3 are defined in Eq. (62). With reference to the definition of SNR_n of Eq. (41), the signal-to-noise-ratio due to the nth spectral band filter would be

$$SNR_n^{(1)}(y') = \frac{E[I_n(y')]}{\{E[I^2(y')] - (E[I(y')])^2\}^{1/2}}$$

$$= \frac{(1 + \frac{\Delta\lambda_n}{\lambda_{\ell n}})I_1^2(y') - \frac{4\pi^2\sigma^2}{\lambda_{\ell n}^2}[I_1^2(y') - I_2(y')I_3(y')]}{\left| \frac{4\pi^2\sigma^2}{\lambda_{\ell n}^2}[I_1^2(y') - I_2(y')I_3(y')] \right|},$$

$$(66)$$

where the superscript (1) represents the output SNR due to the phase-noise at the input plane and $\Delta\lambda_n = \lambda_{hn} - \lambda_{\ell n}$ is the spectral bandwidth of $H_n(\beta)$. With reference to the definition of Eq. (45), the output normalized SNR_n can be obtained, such as

$$\overline{SNR}_n^{(1)} = \frac{1}{M}\sum_{m=1}^{M}\left\{1 + \frac{\Delta\lambda_n/\lambda_{\ell n} I_1^2(y'_m)}{\left| 1 - 4\pi^2\sigma^2/\lambda_{\ell n}^2 (I_1^2(y'_m) - I_2(y'_m)I_3(y'_m)) \right|}\right\}. \quad (67)$$

We note that the normalized output signal-to-noise ratio $\overline{SNR}_n^{(1)}$ due to nth spectral band filter shall be used to evaluate the input phase-noise performance as a function of $\Delta\lambda_n$ (i.e., the temporally partial coherence effect) of the proposed white-light optical signal processor of Fig.11. We shall first investigate the behavior of $\overline{SNR}_n^{(1)}$ as a function of spectral width $\Delta\lambda_n$, for various values of normalized spatial frequency Ω, i.e.,

$$\Omega \overset{\Delta}{=} \frac{\nu}{\nu_c} \ ,$$

where ν is the spatial frequency of the input object and ν_c is the cut-off spatial frequency of the optical processor. Plots of the $\overline{SNR}_n^{(1)}$ as a function of $\Delta\lambda_n$, for various values of Ω are given in Fig.14. From this figure, we notice that, the higher the spatial frequency of the input object the higher the $\overline{SNR}_n^{(1)}$ for broader bandwidth $\Delta\lambda_n$ (i.e., broader band temporally partial coherent illumination). In other words, the $\overline{SNR}_n^{(1)}$ would not noticably improve for low spatial frequency object, for phase-noise effect at the input plane. Nevertheless, the situation would be quite different, as we will show in a moment, for multi-spectral band filterings as depicted in Fig.11.

Let us now investigate the $\overline{SNR}_n^{(1)}$ as a function of $\Delta\lambda_n$ due to $\lambda_{\ell n}$ (i.e., shortest wavelength limit of the nth spectral band filter). Figure15 shows a set of plots of $\overline{SNR}_n^{(1)}$ as a function of the spectral bandwidth $\Delta\lambda_n$, for various values of $\lambda_{\ell n}$. From this figure, we see that, the $\overline{SNR}_n^{(1)}$ increases as the spectral bandwidth $\Delta\lambda_n$ increases. For a shorter wavelength limit $\lambda_{\ell n}$, the $\overline{SNR}_n^{(1)}$ shows a noticable improvement for wider spectral bandwidth $\Delta\lambda_n$ of this filter. In other words, the overall phase-noise improvement is more noticeable for short wavelengths.
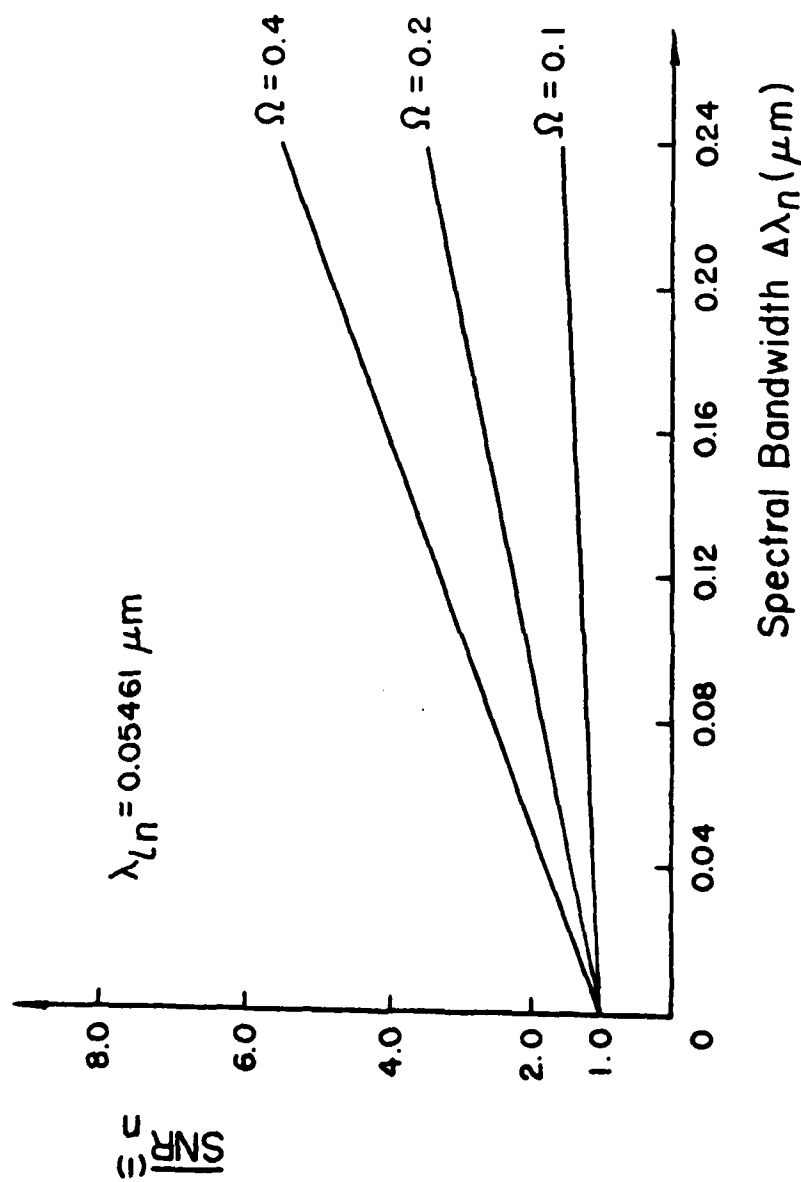
Figure 14.   Plots of normalized signal-to-noise ratio $\overline{SNR}$ (1),
due to phase-noise at input plane, as a function
of spectral bandwidth $\Delta\lambda_n$, for various normalized
spatial frequency Ω.

Figure 15. Plots of normalized signal-to-noise ratio $\overline{SNR}_n^{(1)}$, due to phase-noise at input plane, as a function of spectral bandwidth $\Delta\lambda_n$, for various of the shortest wavelength limit $\Delta\ell_n$ of the spectral band filter $H_n(\beta)$.

We shall now investigate the effect of overall phase-noise performance of the proposed white-light optical processor utilizing multispectral beam filterings. With reference to Fig. 11, the overall output signal-to-noise ratio of the processor would be the sum of the mutually incoherent narrow spectral band SNR_n. Thus the overall output normalized signal-to-noise ratio, due to phase-noise at input plane, can be written as

$$\overline{SNR}^{(1)} = \frac{1}{N}\sum_{n=1}^{N} \overline{SNR}_n^{(1)}$$

$$= \frac{1}{N}\frac{1}{M}\sum_{n=1}^{N}\sum_{m=1}^{M}\left\{1 + \frac{\Delta\lambda_n/\lambda_{\ell n}\, I_1^2(y'_m)}{\left|1 - 4\pi^2\sigma^2/\lambda_{\ell n}^2\left[I_1^2(y'_m) - I_2(y'_m)I_3(y'_m)\right]\right|}\right\}. \quad (68)$$

A plot of the overall $\overline{SNR}^{(1)}$ as a function of the number of spectral band filters N is given in Fig. 16. For this figure, we see that, the overall $\overline{SNR}^{(1)}$ increases rapidly (approximately exponential increasing) as the number of spectral band filters increases. This effect is quite noticeable for broad spectral band filtering as in contrast with the narrow spectral band filters [17]. Thus we conclude that, the broad-band white-light optical signal processor does improve the phase-noise performance at the output plane, as in contrast with a coherent processor.

4.2.2 Grain-Noise

Let us now evaluate the effect of the noise performance due to film-grain noise at the input plane. We note that, by varying the wavelength of the light source, it is generally noticeable to make a distinction between the grain-noise and the object, since the photographic grains will not alter by different wavelength illumination. In other words, a temporally partial coherence illumination can not reduce the effect of film-grain noise at the input plane. Nevertheless, we shall quantitatively evaluate this effect in the following:
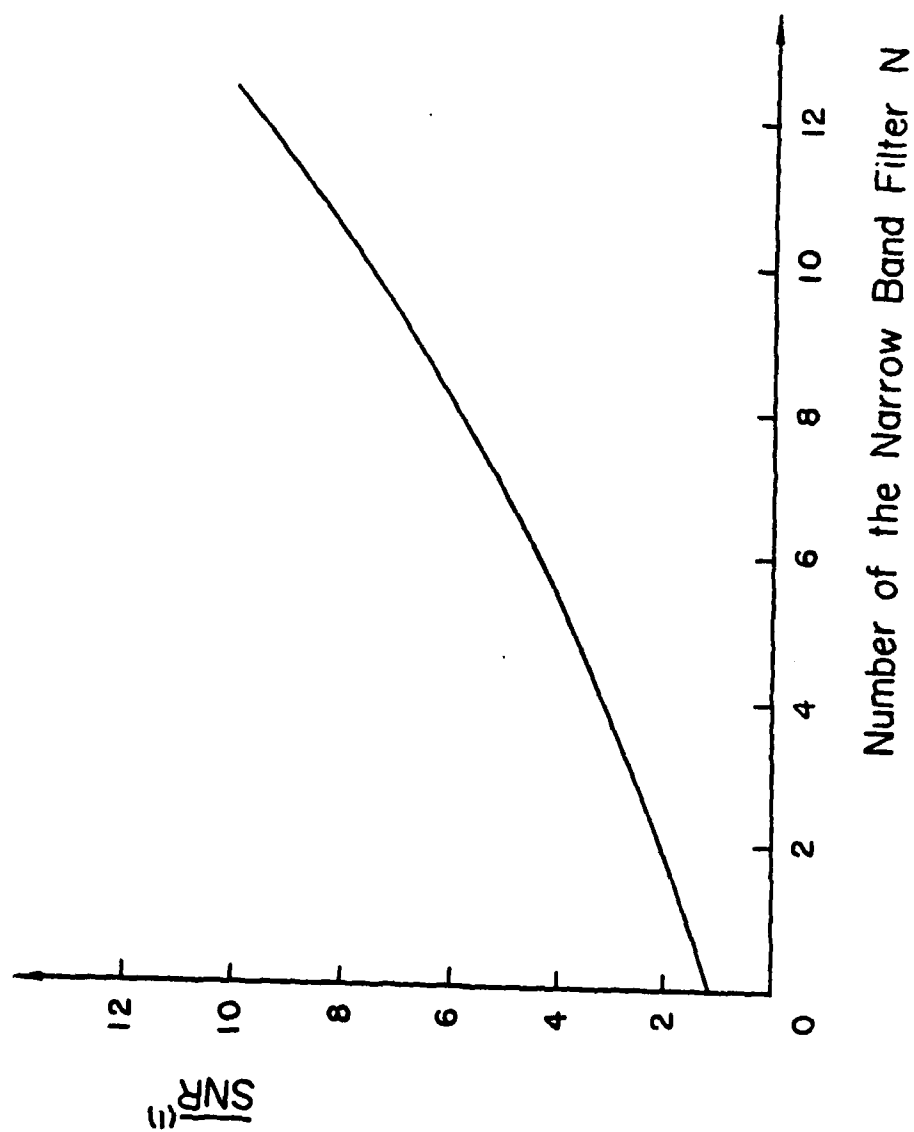
Figure 16.   Plots of the overall normalized signal-to-noise ratio $\overline{SNR}(1)$ as a function of the number of the spectral band filters in the Fourier plane.

As similar to the phase-noise evaluation, the output intensity distribution can be obtained by the following equation:

$$I_n(y') = \int_{\lambda_{en}}^{\lambda_{hn}} \left| \int_{-\infty}^{\infty} [1 + \sin 2\pi \nu y + G(y)] \frac{\sin 2\pi \nu (y'-y)}{\pi(y'-y)} dy \right|^2 d\lambda \ , \qquad (69)$$

where $G(y)$ represents the additive grain noise, and $[1 + \sin 2\pi \nu_y]$ is the input signal function. By taking the ensemble average of the above equation, we have

$$E[I_n(y')] = \int_{\lambda_{en}}^{\lambda_{hn}} \left\{ \iint_{-\infty}^{\infty} [(1 + \sin 2\pi \nu y)(1 + \sin 2\pi \nu \bar{y}) + (1 + \sin 2\pi \nu y) \right.$$

$$\times E[G(\bar{y})] + (1 + \sin 2\pi \nu \bar{y})E[G(y)] + E[G(y)G(\bar{y})]$$

$$\left. \times \frac{\sin 2\pi \nu(y'-y)}{\pi(y'-y)} \frac{\sin 2\pi \nu(y'-\bar{y})}{\pi(y-\bar{y})} dy d\bar{y} \right\} d\lambda . \qquad (70)$$

With reference to the definition of Eq. (50), we see that $E[G(y) \ G(\bar{y})]$ is discontinuous at $|y-\bar{y}| > \ell$. The integrant of Eq. (70) is not easy to evaluate.

To simplify the operation, we approximate $E[G(y) \ G(\bar{y})]$ by a continuous function, as shown below,

$$E[G(y)G(\bar{y})] = C_A^2 \left\{ [\exp(2.3D) - 1]\exp(-|y-\bar{y}|/a) + 1 \right\}, \qquad (71)$$

where $C_A = E[G(y)]$, and $a = 1/\{2.3 + \ln[\exp(2.3D)-1]\}$ is a continuous function.

To justify the approximation of Eq. (71), a plot of Eq. (71) as compared with variation of Eq. (50) is shown in Fig. 17. From this figure, we see that only small amounts of deviation is introduced by Eq. (71) as compared with the variation of Eq. (50). Thus the
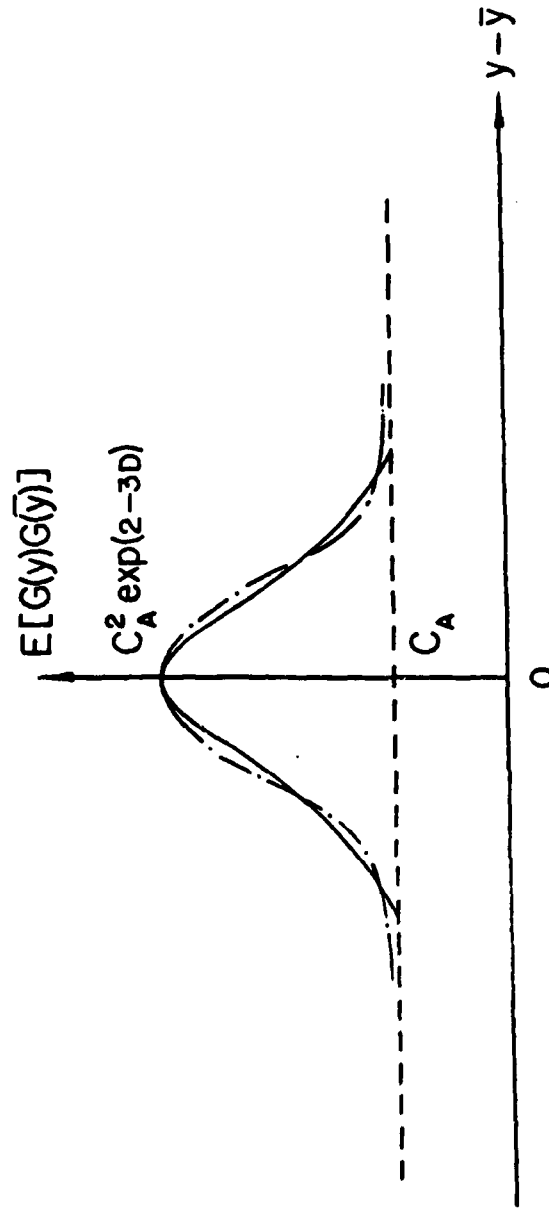
Figure 17.   Approximation for the autocorrelation function of the film-grain noise, continuous curve is for $C_A^2 \exp\{2-3DR(|y-\bar{y}|/\ell)\}$ and the dash dot curve is for $C_A^2\{[\exp(2-3D)-1]\exp(-|y-\bar{y}|/a)+1\}$.

approximated function of Eq. (71) would not expect to introduce significant errors in the subsequent evaluation.

Now by substituting Eq. (71) into Eq. (70), and using the same approach as Eq.(63), the ensemble average of the output irradiance $I_n(y')$, due to the nth spectral band filter, can be shown as

$$E[I_n(y')] = I_1^2(y') + 2C_A I_0(y') + C_A^2 [exp(2.3D) - 1] I_4(y') I_5(y') + C_A^2 I_0^2(y') , \qquad (72)$$

where

$$I_0(y') \overset{\Delta}{=} \int_{-\infty}^{\infty} \frac{\sin 2\pi\nu(y'-y)}{\pi(y'-y)} dy , \qquad (72a)$$

$$I_4(y') \overset{\Delta}{=} \int_{-\infty}^{\infty} \frac{\sin 2\pi\nu(y'-y)}{\pi(y'-y)} exp(-y/a) dy , \qquad (72b)$$

$$I_5(y') \overset{\Delta}{=} \int_{-\infty}^{\infty} \frac{\sin 2\pi\nu(y'-y)}{\pi(y'-y)} exp(y/a) dy . \qquad (72c)$$

and $I_1(y')$ is given in Eq. (62a). Similarly, the formula for the covariance can be derived in the following:

$$E[I_n^2(y')] = \int\int_{\lambda_{\ell n}}^{\lambda_{\ell n}} d\lambda_1 d\lambda_2 \iiiint_{-\infty}^{\infty} \{(1 + \sin 2\pi\nu y_1)(1 + \sin 2\pi\nu \tilde{y}_1)$$

$$\times (1 + \sin 2\pi\nu y_2)(1 + \sin 2\pi\nu \bar{y}_2) + 4(1 + \sin 2\pi\nu y_1)$$

$$\times (1 + \sin 2\pi\nu \bar{y}_1)(1 + \sin 2\pi\nu \bar{y}_2) E[G(y_1)]$$

$$+ 6(1 + \sin 2\pi\nu y_1)(1 + \sin 2\pi\nu \bar{y}_1) E[G(y_1) G(\bar{y}_1)]\}$$

$$\times dy_1 d\bar{y}_1 dy_2 d\bar{y}_2 , \qquad (73)$$

where we have utilized the symmetry property of the integral function with respect to the variables $(y_1, \bar{y}_1)$ and $(y_2, \bar{y}_2)$. We also assume that the higher-order moments of the random function $G(y)$ are much smaller as compared with the second-order moment (autocorrelation) function. Furthermore, by substituting Eq. (71) into Eq. (73), we obtain

$$E[I_n^2(y')] = I_1^4(y') + 4C_A I_1^3(y') I_0(y') + 6C_A^2 [\exp(2.3D) - 1]$$
$$\times I_1^2(y') I_4(y') I_5(y') + 6C_A^2 I_1^2(y') I_0^2(y') \ , \qquad (74)$$

where $C_A \triangleq E[G(y)]$.

With reference to Eqs. (41) to (45), the output normalized SNR, due to the input grain-noise can be written as

$$\overline{SNR}_n^{(2)} = \frac{1}{M} \sum_{m=1}^{M} \left\{ I_1^2(y_m') + 2C_A I_0(y_m') I_1(y_m') + C_A^2 [I_0^2(y_m') + C_A^2 [I_0^2(y_m')] \right.$$
$$+ (\exp(2.3D) - 1) I_4(y_m') I_5(y_m')] \Big\} / C_A \Big\{ 4 [\exp(2.3D)$$
$$-1] I_1^2(y_m') I_4(y_m') I_5(y_m') - 4C_A I_0(y_m') I_1(y_m') [I_0^2(y_m')$$
$$+ [\exp(2.3D) - 1] I_4(y_m') I_5(y_m')] - C_A^2 [I_0^2(y_m') +$$
$$(\exp(2.3D) - 1) I_4(y_m') I_5(y_m')]^2 \Big\}^{1/2} \ , \qquad (75)$$

where the superscript (2) denotes the SNR due to the input grain-noise.

We note that if $C_A \ll 1$, then Eq. (75) reduces to

$$\overline{SNR}_n^{(2)} = \frac{1}{M} \sum_{n=1}^{M} \frac{I_1(y_m')}{2C_A \{ [\exp(2.3D) - 1] I_4(y_m') I_5(y_m') \}^{1/2}} \qquad (76)$$

From the above equation, it is evident that the $\overline{SNR}_n^{(1)}$ is independent of the spectral bandwidth $\Delta\lambda_n$ (i.e., the degree of temporal coherence).

In other words, the effect of the grain-noise performance (due to the
input grain-noise) can not be improved by using a temporally partial
coherent or simply temporally incoherent illumination, as expected.
We note that this behavior is quite different from that as encountered
with the input phase-noise case, as described previously. There are,
however, several interesting behaviors that can be infered from the
result of Eq. (76). For example, the $\overline{SNR}_n^{(2)}$ is dependent on the mean
value C_A of the input grain-noise. The value of $\overline{SNR}_n^{(2)}$ decreases
(approximately exponentially) quite rapidly as the mean value C_A
increases, as shown in Fig. 18. However the $\overline{SNR}_n^{(2)}$ is independent
of the spectral bandwidth $\Delta\lambda_n$ of the processing filter, as shown in
Fig. 19. From this figure, we see that, the overall signal-to-noise
(i.e., $\overline{SNR}^{(2)}$) should be independent of the number of the spectral
band filters used in Fourier plane. In other words, the input grain-noise
is considered as a part of input object, which can not be eliminated by
temporally partial coherent or incoherent illumination.

4.3 Effect of Noise at the Fourier Plane

We shall now describe the effect of noise at the Fourier plane. Since
photographic plates are usually used to synthesize the optical spatial
filters for signal processing, the phase fluctuations and granularity of
the spatial filters have significant effect on noise performance of the
optical processor. Although the setup-noise[18] is primarily due to
scattering and reflections from the optical components of the optical
processing system, however we assume that all of the optical components
are sufficiently far from the input plane, as compared to the focal
depth of the optical system. It is therefore reasonable to assume that
all the setup-noise sources are concentrated in the Fourier plane. If
the optical components are of high quality, the resulting setup-noise
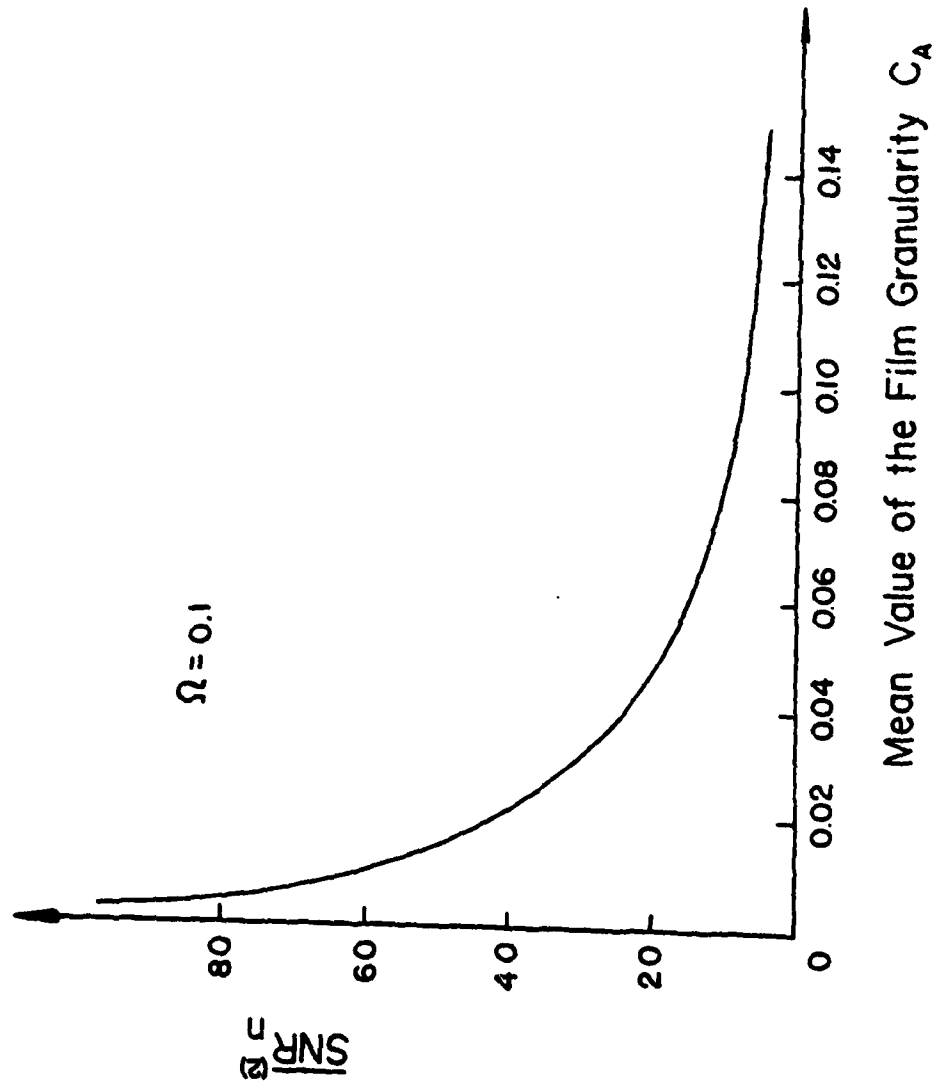
Figure 18. Plot of normalized *signal-to-noise ratio* $\overline{SNR}_n$ (2), due to grain-noise at the input plane, as a function of the mean value C_A of the *film* granularity.
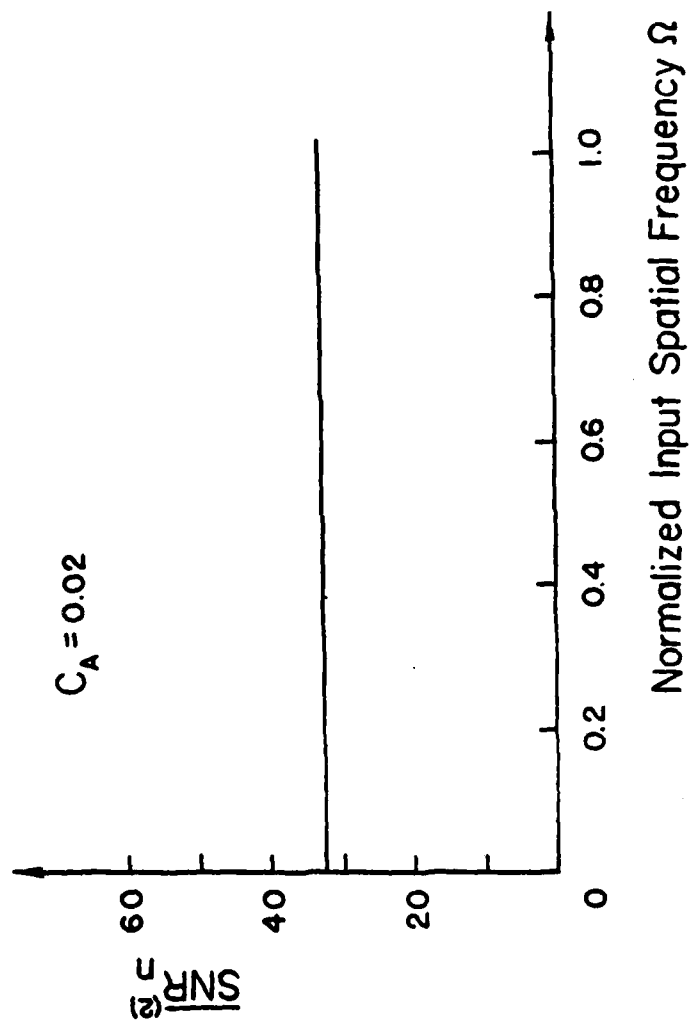
Figure 19. Plots of $\overline{SNR}_n^{(2)}$ as a function of normalized input spatial frequency Ω.

is generally very small as compared with the phase and the grain-noise of the photographic emulsion. Thus, the phase and grain-noise of the nth spectral band filter $H_n(\beta)$ may be written as,

$$H_n(\beta) = \left[\exp(iK\phi(\beta)) + G(\beta)\right] \text{rect}\left(\frac{\beta}{\nu\lambda f}\right) , \qquad (77)$$

where $\phi(\beta)$ and $G(\beta)$ are the respective random phase and grain-noise distributions, the rectangular function represents the size of the spatial filter in the β-direction, which is limited by the spatial frequency of the input signal, ν. Again, for simplicity, we would use a one-dimensional notation for the noise analysis.

We shall now analyze the effect of the noise performance, due to the random phase $\phi(\beta)$ and grain-noise, respectively, $G(\beta)$ at the output plane of the proposed white-light optical processor in the following:

4.3.1 Phase-Noise

Again we utilize a sinusoidal grating, as input signal, superimposed with a phase grating at the input plane. The resultant amplitude transmittance is

$$t(x,y) = (1 + \cos 2\pi\nu y) \exp(i2\pi\nu_0 x) , \qquad (78)$$

The corresponding Fourier spectrum at the spatial frequency plane can be written as

$$S(\alpha - \nu_0 f\lambda, \beta) = \delta(\alpha - \nu_0 f\lambda)\left[\delta(\beta) + \frac{1}{2}\delta(\beta - \nu f\lambda) + \frac{1}{2}\delta(\beta + \nu f\lambda)\right] . \qquad (79)$$

With reference to Eq. (39) the ensemble average of the output intensity due to the nth spectral band filter would be

$$E[I_n(y')] = \int\limits_{\lambda_{en}}^{\lambda_{en}} \iiiint\limits_{-\infty}^{\infty} \delta(\alpha_1 - \nu_0 f \lambda)[\delta(\beta_1) + \frac{1}{2}\delta(\beta_1 - \nu f \lambda)$$

$$+ \frac{1}{2}\delta(\beta_1 + \nu f \lambda)]\,\delta(\alpha_2 - \nu_0 f \lambda)[\delta(\beta_2)$$

$$+ \frac{1}{2}\delta(\beta_2 - \nu f \lambda) + \frac{1}{2}\delta(\beta_2 + \nu f \lambda)]$$

$$\times \text{rect}\left(\frac{\beta_1}{\nu f \lambda}\right)\text{rect}\left(\frac{\beta_2}{\nu f \lambda}\right)E[\exp\{iK[\phi(\beta_1)$$

$$- \phi(\beta_2)]\}]\exp\{-iK\frac{2\pi}{\lambda f}[(\alpha_1 - \alpha_2)x + (\beta_1 - \beta_2)y]\}$$

$$\times d\alpha_1 d\alpha_2 d\beta_1 d\beta_2 d\lambda \quad . \tag{80}$$

From the result of Eq. (61) Eq. (80) can be written as

$$E[I_n(y')] = \Delta\lambda_n(1 + \cos 2\pi\nu y')^2 - 4\pi^2\sigma^2\left\{4\left[\frac{1}{\lambda_{en}(\lambda_{en} + \Delta\lambda_n)}\right.\right.$$

$$- 4K_2(\Delta\lambda_n)]\cos 2\pi\nu y' + \left[\frac{1}{\lambda_{hn}(\lambda_{hn} + \Delta\lambda_n)}\right.$$

$$- 4K_1(\Delta\lambda_n)]\} \cos 4\pi\nu y' \quad , \tag{81}$$

where

$$K_1(\Delta\lambda_n) \overset{\Delta}{=} \int\limits_{\lambda_{en}}^{\lambda_{hn}} \frac{1}{\lambda^2}\exp(-\lambda f \nu / d)\,d\lambda$$

$$= \frac{\lambda_{hn}\exp(-\lambda_{hn}f\nu/d) - \lambda_{en}\exp(-\lambda_{en}f\nu/d)}{\lambda_{hn}\lambda_{en}}$$

$$= \frac{f\nu}{d}[E_i(-\lambda_{hn}f\nu/d) - E_i(-\lambda_{en}f\nu/d)] \quad , \tag{81a}$$

$$K_2(\Delta\lambda_n) \overset{\Delta}{=} \int\limits_{\lambda_{en}}^{\lambda_{hn}} \frac{1}{\lambda^2}\exp(-\lambda f \nu / 2d)\,d\lambda$$

$$= \frac{\lambda_{hn}\exp(-\lambda_{hn}f\nu/2d) - \lambda_{en}\exp(-\lambda_{en}f\nu/2d)}{\lambda_{hn}\lambda_{en}}$$

$$- \frac{f\nu}{2d}[E_i(-\lambda_{hn}f\nu/2d) - E_i(-\lambda_{en}f\nu/2d)] \quad , \tag{81b}$$

and

$$E_i(t) \overset{\Delta}{=} \int\limits_{-\infty}^{y} \frac{1}{y}\exp(y)\,dy \quad . \tag{81c}$$

Similarly, the ensemble average of $I_n^2(y')$ can be evaluated in the following:

$$E[I_n^2(y')] = \int_{\lambda_{\ell n}}^{\lambda_{An}} \iiint_{-\infty}^{\infty} [\delta(\beta_1) + \frac{1}{2}\delta(\beta_1 - \nu f \lambda_1) + \frac{1}{2}\delta(\beta_1 + \nu f \lambda_1)]$$

$$\times [\delta(\beta_2) + \frac{1}{2}\delta(\beta_2 - \nu f \lambda_1) + \frac{1}{2}\delta(\beta_2 + \nu f \lambda_1)]$$

$$\times [\delta(\bar{\beta}_1) + \frac{1}{2}\delta(\bar{\beta}_1 - \nu f \lambda_2) + \frac{1}{2}\delta(\bar{\beta}_1 + \nu f \lambda_2)]$$

$$\times [\delta(\bar{\beta}_2) + \frac{1}{2}\delta(\bar{\beta}_2 - \nu f \lambda_2) + \frac{1}{2}\delta(\bar{\beta}_2 + \nu f \lambda_2)]$$

$$\times \{1 - (K_1^2 + K_2^2)\sigma^2 + K_1^2 E[\phi(\beta_1)\phi(\beta_2)]$$

$$+ K_1 K_2 [E[\phi(\beta_1)\phi(\bar{\beta}_1)] + E[\phi(\beta_1)\phi(\bar{\beta}_2)]$$

$$+ E[\phi(\beta_2)\phi(\bar{\beta}_1)] - E[\phi(\beta_2)\phi(\beta_2)]$$

$$+ K_2^2 E[\phi(\bar{\beta}_1)\phi(\bar{\beta}_2)] \, \text{rect}\left(\frac{\beta_1}{\nu f \lambda_1}\right)$$

$$\times \text{rect}\left(\frac{\bar{\beta}_1}{\nu f \lambda_1}\right) \text{rect}\left(\frac{\beta_2}{\nu f \lambda_2}\right) \text{rect}\left(\frac{\bar{\beta}_2}{\nu f \lambda_2}\right)$$

$$\times \exp\{-i\frac{2\pi}{\lambda_1 f}(\beta_1 - \beta_2)y - i\frac{2\pi}{\lambda_2 f}(\bar{\beta}_1 - \bar{\beta}_2)y'\}$$

$$\times d\beta_1 d\beta_2 d\bar{\beta}_1 d\bar{\beta}_2 \, d\lambda_1 d\lambda_2 \ . \tag{82}$$

By substituting the exponential form representation of Eq. (53)   i.e.,

$E[\phi(\beta_1)\phi(\beta_2)] = \sigma^2 \exp[-|\beta_1 - \beta_2|/d]$ in Eq. (82), we have,

$$E[I_n^2(y')] = \Delta\lambda_n^2 \left[1 - \frac{4\pi^2\sigma^2}{\lambda_{\ell n}(\lambda_{\ell n} + \Delta\lambda_n)}\right](1 + \cos 2\pi\nu y')^2$$

$$+ 4\pi^2\sigma^2 \Delta\lambda_n (1 + \cos 2\pi\nu y')^2 \left[\frac{3\Delta\lambda_n}{\lambda_{\ell n}(\lambda_{\ell n} + \Delta\lambda_n)}\right.$$

$$+ K_5(\Delta\lambda_n)\cos 2\pi\nu y' + K_6(\Delta\lambda_n)\cos 4\pi\nu y']$$

$$+ 4\pi^2\sigma^2 K_3(\Delta\lambda_n)[K_4(\Delta\lambda_n) - K_3(\Delta\lambda_n)]$$

$$\times (1 - \cos 4\pi\nu y')(1 + \cos 2\pi\nu y')^2 \ , \tag{83}$$

where

$$K_3(\Delta\lambda_n) \triangleq \int_{\lambda_{\ell n}}^{\lambda_{hn}} \frac{1}{\lambda} \exp(-\lambda f\nu/2d)\,d\lambda = E_i(-\lambda_{hn}f\nu/2d) - E_i(-\lambda_{\ell n}f\nu/2d), \tag{83a}$$

$$K_4(\Delta\lambda_n) \triangleq \int_{\lambda_{\ell n}}^{\lambda_{hn}} \frac{1}{\lambda} \exp(f\lambda\nu/2d)\,d\lambda = E_i(\lambda_{hn}f\nu/2d) - E_i(\lambda_{\ell n}f\nu/2d), \tag{83b}$$

$$K_5(\Delta\lambda_n) \triangleq 2K_2(\Delta\lambda_n) - \frac{4d}{f\nu\lambda_{\ell n}\lambda_{hn}}[\exp(-\lambda_{hn}f\nu/2d)$$
$$- \exp(-\lambda_{\ell n}f\nu/2d)], \tag{83c}$$

and

$$K_6(\Delta\lambda_n) \triangleq K_1(\Delta\lambda_n)/2 - \frac{d}{f\nu\lambda_{\ell n}\lambda_{hn}}[\exp(-\lambda_{hn}f\nu/d)$$
$$- \exp(-\lambda_{\ell n}f\nu/d)]. \tag{83d}$$

With reference to the definitions of Eqs. (41) and (42), the output SNR_n, due to nth spectral band filter, under a broadband temporally partial coherent illumination is

$$SNR_n^{(3)} = \Delta\lambda_n \left\{ (1+\cos 2\pi\nu y)^2 - 4\pi^2\sigma^2 \left[4\left(\frac{1}{\lambda_{\ell n}(\lambda_{\ell n}+\Delta\lambda_n)} - 4K_2(\Delta\lambda_n)\right)\right.\right.$$
$$\left.\left. \times \cos 2\nu\pi y + \frac{1}{\lambda_{\ell n}(\lambda_{\ell n}+\Delta\lambda_n)} - 4K_1(\Delta\lambda_n))\cos 4\pi\nu y \right] \right\} /$$
$$\left\{ 4\pi^2\sigma^2(1+\cos 2\pi\nu y)^2 \left[K_3(\Delta\lambda_n)(K_4(\Delta\lambda_n) - K_5(\Delta\lambda_n))/\Delta\lambda_n \right.\right.$$
$$+ (K_5(\Delta\lambda_n) - 4K_2(\Delta\lambda_n) + \frac{4\Delta\lambda_n}{\lambda_{\ell n}(\lambda_{\ell n}+\Delta\lambda_n)}) \cos 2\pi\nu y'$$
$$+ \left[K_6(\Delta\lambda_n) - K_1(\Delta\lambda_n) - \frac{\Delta\lambda_n}{\lambda_{\ell n}(\lambda_{\ell n}+\Delta\lambda_n)} - K_3(\Delta\lambda_n) \right.$$
$$\left.\left. \times [K_4(\Delta\lambda_n) - K_3(\Delta\lambda_n)]/\Delta\lambda_n \right] \cos 4\pi\nu y' \right] \right\}^{1/2}, \tag{84}$$

where the superscripts (3) represents the effect due to phase-noise at the Fourier plane. Futhermore, we note that

$$\lim_{\Delta\lambda_n \to 0} K_1(\Delta\lambda_n)/\Delta\lambda_n = \frac{1}{\lambda_{\ell n}}\left(\frac{1}{\lambda_{\ell n}} - \frac{f\nu}{d}\right) , \tag{84a}$$

$$\lim_{\Delta\lambda_n \to 0} K_2(\Delta\lambda_n)/\Delta\lambda_n = \frac{1}{\lambda_{\ell n}}\left(\frac{1}{\lambda_{\ell n}} - \frac{f\nu}{2d}\right) \tag{84b}$$

$$\lim_{\Delta\lambda_n \to 0} K_3(\Delta\lambda_n)/\Delta\lambda_n = \frac{1}{\lambda_{\ell n}} - \frac{f\nu}{2d} , \tag{84c}$$

$$\lim_{\Delta\lambda_n \to 0} K_4(\Delta\lambda_n)/\Delta\lambda_n = \frac{1}{\lambda_{\ell n}} + \frac{f\nu}{2d} , \tag{84d}$$

$$\lim_{\Delta\lambda_n \to 0} K_5(\Delta\lambda_n)/\Delta\lambda_n = \frac{1}{\lambda_{\ell n}}\left(\frac{2}{\lambda_{\ell n}} - \frac{f\nu}{d}\right) + \frac{2}{\lambda_{\ell n}^2}\exp(-\lambda_{\ell n}f\nu/2d) , \tag{84e}$$

and

$$\lim_{\Delta\lambda_n \to 0} K_6(\Delta\lambda_n)/\Delta\lambda_n = \frac{1}{2\lambda_{\ell n}}\left(\frac{1}{\lambda_{\ell n}} - \frac{f\nu}{d}\right) + \frac{1}{\lambda_{\ell n}^2}\exp(-\lambda_{\ell n}f\nu/d) . \tag{84f}$$

Thus, the SNR_n for strict temporally coherent illumination would be

$$SNR_n^{(3)}(y')_{coherent} = \lim_{\Delta\lambda_n \to 0} SNR_n^{(3)}(y')$$

$$= \left\{(1+\cos 2\pi\nu y')^2 - 4\pi^2\sigma^2\left[\frac{4}{\lambda_{\ell n}^2}\cos 2\pi\nu y' + \frac{1}{\lambda_{\ell n}^2}\cos 4\pi\nu y'\right]\right\}/$$

$$\left\{4\pi^2\sigma^2(1+\cos 2\pi\nu y')^2\left[\left(\frac{1}{\lambda_{\ell n}} - \frac{\nu f}{2d}\right)\frac{f\nu}{d} + \left(\frac{2}{\lambda_{\ell n}} + \frac{\nu f}{\lambda_{\ell n}d}\right)\right.\right.$$

$$+ \frac{2}{\lambda_{\ell n}^2}\exp(-\lambda_{\ell n}f\nu/2d)\right)\cos 2\pi\nu y' + \left(\left(\frac{1}{\lambda_{\ell n}} - \frac{f\nu}{2d} + \frac{1}{2\lambda_{\ell n}^2}\right.\right.$$

$$+ \frac{f\nu}{2\lambda_{\ell n}d} + \frac{1}{\lambda_{\ell n}^2}\exp(-\lambda_{\ell n}f\nu/d)\right)\cos 4\pi\nu y'\left]\right\}^{1/2} . \tag{85}$$

Finally, the normalized output SNR, due to nth spectral band filter, can

be shown by the following definition:

$$\overline{SNR}_n^{(3)} = \frac{1}{M}\sum_{m=1}^{M} SNR_n^{(3)}(y'_m)/SNR_n^{(3)}(y'_m)_{coherent} . \tag{86}$$

Since conclusive results are rather difficult to deduce from Eqs. (85)

and (86) we would convert these equations in more amenable forms, for

which are suitable for numerical computation. Let us confine the

normalized spatial frequency of the input object transparency in a

region, that the following condition holds:

$$\Omega < \frac{d}{f\lambda\nu_c} \quad , \tag{87}$$

where d is the correlation distance, f is the focal length of transform

lens, λ is the wavelength of illumination, and ν_c is cutoff spatial

frequency of optical system.

We note that the correlation length d of the phase fluctuation

can be assumed equal to the minimum resolution distance of the optical

processor. Equation (85) is essentially representing a low spatial

frequency signal, since the ratio of $d/(f\lambda\nu_c)$ is generally true for the

proposed white-light optical signal processor. Thus we shall use the

condition of Eq. (87) [i.e., $\Omega < d/(f\lambda\nu_c)$] to describe the noise

performance due to phase-noise at Fourier plane. By the

imposition of Eq. (87) Eq. (86) can be written in the following form,

which is more suitable for numerical computation:

$$\overline{SNR}_n^{(3)} = \frac{1}{M}\sum_{m=1}^{M}\Bigg[\big((1+\cos 2\pi\nu y_m')^2 - \frac{4\pi^2\sigma^2 f}{d}\,\frac{\ell n\,(1+\Delta\lambda n/\lambda_{\ell n})}{\Delta\lambda n}$$

$$\times (\cos 2\pi\nu y_m' + \cos 4\pi\nu y_m')\big](1-3\cos 2\pi\nu y_m'$$

$$-2\cos 4\pi\nu y_m')\Big/\Big\{\big[(1+\cos 2\pi\nu y_m')^2 - \frac{4\pi^2\sigma^2 f\nu}{\lambda_{\ell n} d}$$

$$\times (2\cos 2\pi\nu y_m' + \cos 4\pi\nu y_m')\big]\big[(1+\cos 2\pi\nu y_m')$$

$$\times \frac{\lambda_{\ell n}\,\ell n(1+\Delta\lambda n/\lambda_{\ell n})}{\Delta\lambda n} + (2\cos 2\pi\nu y_m'$$

$$+\cos 4\pi\nu y_m')\,\frac{2\lambda_{\ell n}+\Delta\lambda n}{\lambda_{\ell n}+\Delta\lambda n}\Big]\Big\} \quad . \tag{88}$$

From the description of Eq. (88), and note that the term $[\ell n(1 + \Delta\lambda/\lambda_{\ell n}]/\Delta\lambda_n$

is a monotonically decreasing function of $\Delta\lambda_n$, we see that, the broader

the spectral bandwidth $\Delta\lambda_n$, the higher the $\overline{SNR}_n^{(3)}$ can be obtained.

Since $\Delta\lambda_n$ is inversely proportional to the spatial frequency ν_o of the

phase grating, a higher $\overline{SNR}_n^{(3)}$ could also be obtained by using a lower

ν_o. However the number of spectral band filters also reduces, for a lower ν_o. We should emphasize that, the larger the number of spectral band filters used, the higher the overall output $\overline{SNR}^{(3)}$ can be obtained, although $\overline{SNR}_n^{(3)}$ decreases somewhat for higher ν_o. In otherwords, the filtered signals, from each of the spectral band filters, would be incoherently superimposed at the output plane. Thus the effect due to the phase-noise from the spectral filters $H_n(\beta)$ would be substantially supressed due to the incoherent addition. Thus, the overall output $\overline{SNR}^{(3)}$, due to phase-noise at the Fourier plane, can be written as

$$\overline{SNR}^{(3)} = \frac{1}{N} \sum_{n=1}^{N} \overline{SNR}_n^{(3)} \quad . \tag{89}$$

We note that, by replacing $\Delta\lambda_n$ by $\Delta\lambda$ in Eq. (89), we have

$$\overline{SNR}^{(3)} \simeq \overline{SNR}_n^{(3)} \Big|_{\Delta\lambda_n \to \Delta\lambda} \tag{90}$$

where $\Delta\lambda = N\Delta\lambda_n$, the entire spectral band of the white-light source. We also note that this results is quite consistent with the experimental results for broadband deblurring with a white-light source[17].

In order to get some more feelings on the effects due to signal spatial frequency on the $\overline{SNR}_n^{(3)}$, we let $\Delta\lambda_n$ go to infinity, i.e.,

$$\lim_{\Delta\lambda_n \to \infty} \frac{\ln(1 + \Delta\lambda_n/\lambda_{en})}{\Delta\lambda_n} = 0, \quad \lim_{\Delta\lambda_n \to \infty} \frac{2\lambda_{en} + \Delta\lambda_n}{\lambda_{en} + \Delta\lambda_n} = 1 \quad . \tag{91}$$

Thus Eq. (88) reduces to the following form

$$\overline{SNR}_n^{(3)} = \frac{1}{M} \sum_{m=1}^{M} \left\{ (1 + \cos 2\pi\nu y_m')(1 + 5\cos 2\pi\nu y_m' + 2\cos 4\pi\nu y_m') \right\} /$$

$$\left\{ \left[(1 + \cos 2\pi\nu y_m')^2 - \frac{4\pi^2\sigma^2 f}{\lambda_{en} d} (2\cos 2\pi\nu y_m' \right. \right.$$

$$\left. \left. + \cos 4\pi\nu y_m') \right] (2\cos 2\pi\nu y_m' + \cos 4\pi\nu y_m') \right\}, \quad \text{for } \Delta\lambda_n \to \infty \tag{92}$$

Thus, we see that, for relatively low Ω, the $\overline{SNR}_n^{(3)}$ increases as the

spatial frequency of the signal increases. In other words, a significant

improvement of $\overline{SNR}_n^{(3)}$ can be obtained for higher spatial frequency signal.

However, the higher the spatial frequency requires a larger size of spectral

band filter [i.e., $\Delta H_n(\beta)$]. For temporally partial coherent illumination,

the noise at the output plane would also be increased, compared with a

lower spectral signal. However, the situation is quite different for

multi-spectral band filterings, the overall output noise would be sub-

stantially supressed, due to the incoherent addition of different spectral

band filtered signals.

Several plots of $\overline{SNR}_n^{(3)}$ as a function of spectral bandwidth $\Delta\lambda_n$,

for various values of normalized input spatial frequency Ω, are given

in Fig. 20. The plot for low frequency case (i.e., $\Omega = 0.1$) was evaluated

by using the Eq. (92) while for $\Omega = 0.4$ the plot for $\Omega = 0.4$ is obtained

by using Eq. (88). From this figure we conclude that the $\overline{SNR}_n^{(3)}$, due to

phase-noise at the Fourier plane can be noticeably improved by using a

broadband temporally partial coherent illumination, which is similar to

the effect due to the phase-noise at the input plane, as shown in Fig. 4.

The higher the spatial frequency of the input signal, $\overline{SNR}_n^{(3)}$ can be

improved to several tens of orders, as compared with low spatial frequency

case. We note that the improvement of $\overline{SNR}_n^{(3)}$ is several orders higher

than $\overline{SNR}_n^{(1)}$ due to the phase-noise at input plane, for higher spatial

frequency case. Similar to the input phase-noise effect, the $\overline{SNR}_n^{(3)}$

can also be improved for shorter lower wavelength limit $\lambda_{\ell n}$. The

variation of $\overline{SNR}_n^{(3)}$ as a function of spectral bandwidth $\Delta\lambda_n$, for

various values of $\lambda_{\ell n}$, are plotted in Fig. 21. From these results, we

see that the output $\overline{SNR}_n^{(3)}$ is approximately exponential increasing as a

function of $\Delta\lambda_n$. As similar to the effect due to phase-noise at input

Figure 20. Plots of normalized signal-to-noise ratio $\overline{SNR}_n^{(3)}$, due to phase-noise at Fourier plane, as a function of spectral bandwidth $\Delta\lambda_n$, for various normalized spatial frequency Ω.
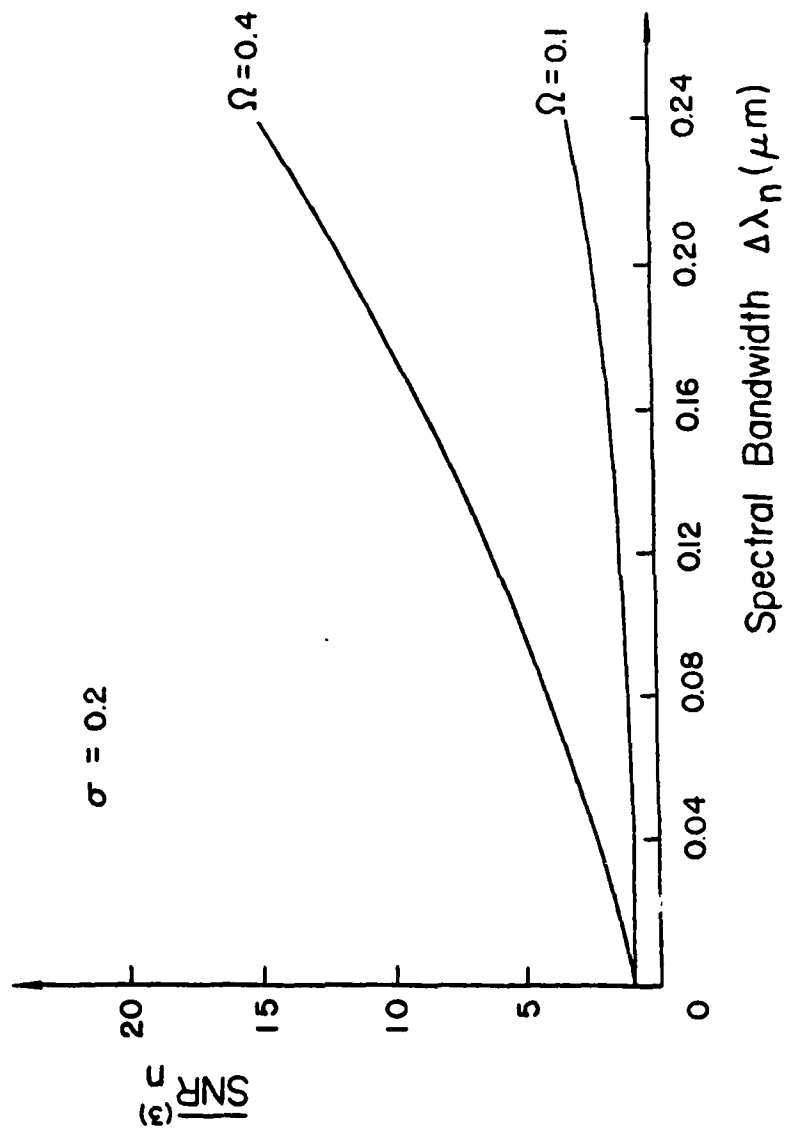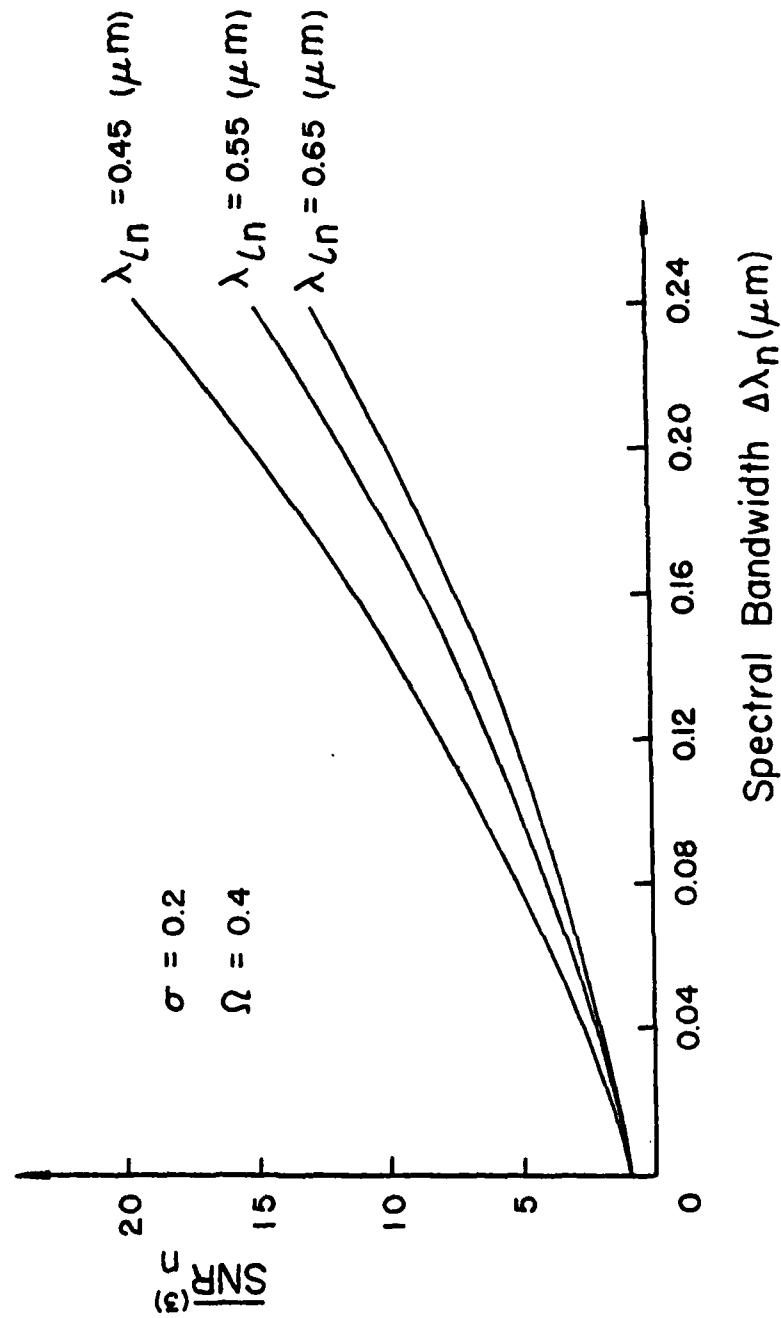
Figure 21. Plots of normalized signal-to-noise ratio $\overline{SNR}_n^{(3)}$, due to phase-noise at Fourier plane, as a function of spectral bandwidth $\Delta\lambda_n$, for various $\lambda_{\ell n}$.

plane, the improvement is somewhat higher for shorter wavelength temporally partial coherent illumination.

4.3.2 Grain-Noise

In the evaluation of the noise performance due to grain-noise at the Fourier plane, we shall handle the problem somewhat differently. Since the scale of the signal spectrum is proportional to the illuminating wavelength of the light source, the diffraction due to each of the spectral band filters behave quite differently with different wavelength illumination. The grain-noise at the filter plane can be substantially smoothed out with a broader band temporally partial coherent illumination. Thus, we would expect a higher output signal-to-noise ratio for a broadband illumination (e.g., white-light). We shall now provide a quantitative analysis of the effect due to grain-noise at the Fourier plane. Here we utilize a narrow spectral band filter with an additive film-grain noise, as described in the following:

$$H_n(\beta) = \left[1 + G(\beta) \right] \, \text{rect}\left(\frac{\beta}{\nu f \lambda} \right) . \tag{93}$$

By substituting this filter function into Eq. (39), and employing the same analysis as we did for the phase-noise case, the mean value of the output intensity distribution can be determined by the following integration:

$$E\left[I_n(y') \right] = E\left[\int_{\lambda_{\mathit{an}}}^{\lambda_{\mathit{an}}} \iiiint_{-\infty}^{\infty} S(\alpha_1 - \nu_0 f \lambda, \beta_1) S^*(\alpha_2 - \nu_0 f \lambda, \beta_2) \right.$$

$$\times \left[1 + G(\beta_1) \right] \left[1 + G(\beta_2) \right] \text{rect}\left(\frac{\beta_1}{f \nu \lambda} \right) \text{rect}\left(\frac{\beta_2}{f \nu \lambda} \right)$$

$$\times \exp\left\{ -i \frac{2\pi}{\lambda f} \left[(\alpha_1 - \alpha_2) x' + (\beta_1 - \beta_2) y' \right] \right\}$$

$$\times d\alpha_1 \, d\beta_1 \, d\alpha_2 \, d\beta_2 \, d\lambda . \tag{94}$$

With reference to Eqs. (81), (49), and (50), the above equation can be written as:

$$E[I_n(y')] = \int_{\lambda_{\ell n}}^{\lambda_{hn}} \int\int_{-\infty}^{\infty} \{\delta(\beta_1)\,\delta(\beta_2) + \tfrac{1}{2}\delta(\beta_1)\,\delta(\beta_2 - \nu f \lambda)$$
$$+ \tfrac{1}{2}\delta(\beta_1)\,\delta(\beta_2 + \nu f \lambda) + \tfrac{1}{2}\delta(\beta_2)\,\delta(\beta_1 - \nu f \lambda)$$
$$+ \tfrac{1}{2}\delta(\beta_2)\,\delta(\beta_1 + \nu f \lambda) + \tfrac{1}{4}\delta(\beta_1 - \nu f \lambda)\,\delta(\beta_2 - \nu f \lambda)$$
$$+ \tfrac{1}{4}\delta(\beta_1 + \nu f \lambda)\,\delta(\beta_2 + \nu f \lambda) + \tfrac{1}{4}\delta(\beta_1 + \nu f \lambda)$$
$$\times \delta(\beta_2 - \nu f \lambda) + \tfrac{1}{4}\delta(\beta_1 + \nu f \lambda)\,\delta(\beta_2 + \nu f \lambda)\}$$
$$\times \{[1 + 2C_A + C_A^2[\exp(2.3D) - 1]\exp[-|\beta_1 - \beta_2|/a]$$
$$+ C_A^2\}\exp[-i\tfrac{2\pi}{\lambda f}(\beta_1 - \beta_2)y']\,d\beta_1\,d\beta_2\,d\lambda \quad , \quad (95)$$

which is equal to

$$E[I_n(y')] = \Delta\lambda_n(1 + C_A)^2(1 + \cos 2\pi\nu y')^2 + \tfrac{1}{2}C_A^2[\exp(2.3D)$$
$$-1][3\Delta\lambda_n + \tfrac{a}{f\nu}8K_0(\Delta\lambda_n)\cos 2\pi\nu y'$$
$$+ K_0'(\Delta\lambda_n)\cos 4\pi\nu y')] \quad , \quad (96)$$

where

$$K_0(\Delta\lambda_n) \overset{\Delta}{=} \exp(-\lambda_{\ell n}f\nu/2a)[1 - \exp(-\Delta\lambda_n f\nu/2a)] \quad , \quad (96a)$$

and

$$K_0'(\Delta\lambda_n) \overset{\Delta}{=} \exp(-\lambda_{\ell n}f\nu/a)[1 - \exp(-\Delta\lambda_n f\nu/a)] \quad . \quad (96b)$$

For the ensemble average of the square irradiance, we have

$$E[I_n^2(y')] = E[\int\int_{\lambda_{\ell n}}^{\lambda_{hn}} \int\int\int\int_{-\infty}^{\infty} [\delta(\beta_1) + \tfrac{1}{2}\delta(\beta_1 - \nu f \lambda_1) + \tfrac{1}{2}\delta(\beta_1 + \nu f \lambda_1)]$$
$$\times [\delta(\beta_2) + \tfrac{1}{2}\delta(\beta_2 - \nu f \lambda_1) + \tfrac{1}{2}\delta(\beta_2 + \nu f \lambda_1)]$$
$$\times [\delta(\bar{\beta}_1) + \tfrac{1}{2}\delta(\bar{\beta}_1 - \nu f \lambda_2) + \tfrac{1}{2}\delta(\bar{\beta}_1 + \nu f \lambda_2)]$$

$$\times \left[\delta(\bar{\beta}_2) + \frac{1}{2}\delta(\bar{\beta}_2 - \nu f \lambda_2) + \frac{1}{2}\delta(\bar{\beta}_2 + \nu f \lambda_2) \right]$$

$$\times \left[1 + G(\beta_1) + G(\beta_2) + G(\bar{\beta}_1) + G(\bar{\beta}_2) + G(\bar{\beta}_1)G(\beta_2) \right.$$

$$+ G(\beta_1)G(\bar{\beta}_1) + G(\beta_1)G(\bar{\beta}_2) + G(\beta_2)G(\bar{\beta}_1) + G(\beta_2)G(\bar{\beta}_2)$$

$$\left. + G(\beta_1)G(\bar{\beta}_2) \right] \exp\left\{ -i\frac{2\pi}{\lambda_1 f}(\beta_1 - \beta_2)y' - i\frac{2\pi}{\lambda_2 f}(\bar{\beta}_1 - \bar{\beta}_2)y' \right\}$$

$$\times d\beta_1 d\beta_2 d\bar{\beta}_1 d\bar{\beta}_2 d\lambda_1 d\lambda_2 \bigg] \; . \tag{97}$$

By substituting the mean value and the autocorrelation function of the film granularity (same as Eqs. (49) and (50) into Eq. (97) the ensemble of the square irradiance would be

$$\begin{aligned}
E\left[I_n^2(y') \right] = {}& \Delta\lambda_n^2 (1 + 4C_A + 6C_A^2)(1 + \cos 2\pi\nu y')^4 \\
& + 2C_A^2 \left[\exp(2.3D) - 1 \right](1 + \cos 2\pi\nu y')^2 \\
& \times \left\{ 11 + \frac{10a}{f\nu\Delta\lambda_n} K_0(\Delta\lambda_n) \cos 2\pi\nu\cdot y \right. \\
& \left. + \frac{a^2}{f^2\nu^2\Delta\lambda_n^2} K_7(\Delta\lambda_n)\cos 4\pi\nu y' \right\} ,
\end{aligned} \tag{98}$$

where

$$\begin{aligned}
K_7(\Delta\lambda_n) \stackrel{\Delta}{=} {}& \exp(\Delta\lambda_n f\nu/2a) + \exp(-\Delta\lambda_n f\nu/2a) \\
& - 2 + \exp(\lambda_{en} f\nu/a)\left[1 - \exp(-\Delta\lambda_n f\nu/a) \right] \\
& - 2\exp\left[-(2\lambda_{en} + \Delta\lambda_n)/2a \right] .
\end{aligned} \tag{98a}$$

From the results of Eqs. (96) and (98), the output SNR, due to nth spectral band filter, for a temporally partial coherent illumination can be obtained such as

$$\begin{aligned}
SNR_n^{(4)}(y') = {}& \left\{ (1+C_A)^2(1+\cos 2\pi\nu y')^2 + \frac{1}{2}C_A^2\left[\exp(2.3D)-1\right] \right. \\
& \times \left[3 + \frac{a}{f\nu\Delta\lambda_n}\left(8K_0(\Delta\lambda_n)\cos 2\pi\nu y' + K_0'(\Delta\lambda_n) \right) \right.
\end{aligned}$$

$$\times \cos 4\pi\nu y')]\} / \{C_A^2 (1+\cos 2\pi\nu y')^2 [\exp(2.3D)-1]$$

$$\times [4 + \frac{12a}{f\nu\Delta\lambda} K_0(\Delta\lambda n)\cos 2\pi\nu y' + \frac{a}{2f\nu\Delta\lambda_n}$$

$$\times (\frac{4}{f\nu\Delta\lambda_n} K_7(\Delta\lambda n) - K_0'(\Delta\lambda_n))\cos 4\pi\nu y']\}^{1/2}, \qquad (99)$$

where the superscript (4) denotes the effect due to grain-noise at the Fourier plane. It is also interesting to note that, by letting $\Delta\lambda_n$ equals to zero, we obtain the following output SNR for strictly temporal coherent illumination, i.e.,

$$SNR_n^{(4)}(y')_{coherent} = \{(1+C_A)^2 (1+\cos 2\pi\nu y')^2 + \frac{1}{2}C_A^2$$

$$\times [\exp(2.3D)-1][3+4\exp(-\lambda_{\ell n}f\nu/2a)\cos 2\pi\nu y'$$

$$+ \exp(-\lambda_{\ell n}f\nu/a)\cos 4\pi\nu y']\} / \{C_A^2 (1+\cos 2\pi\nu y')^2$$

$$\times [\exp(2.3D)-1][4+6\exp(-\lambda_{\ell n}f\nu/2a)\cos 2\pi\nu y'$$

$$- \frac{1}{2}\exp(-\lambda_{\ell n}f\nu/a)\cos 4\pi\nu y']\}^{1/2}, \quad \text{for } \Delta\lambda_n=0. \quad (100)$$

From Eqs. (99) and (100), the normalized SNR, due to nth spectral band filter, can be obtained, such as

$$\overline{SNR}_n^{(4)} = \frac{1}{M}\sum_{m=1}^{M} \{(1+C_A)^2 (1+\cos 2\pi\nu y_m')^2 + \frac{1}{2}C_A^2 [\exp(2.3D)$$

$$-1][3+\frac{a}{f\nu\Delta\lambda_n}(8K_0(\Delta\lambda n)\cos 2\pi\nu y_m' + K_0'(\Delta\lambda n)$$

$$\times \cos 4\pi\nu y_m')][4+6\exp(-\lambda_{\ell n}f\nu/2a)\cos 2\pi\nu y_m'$$

$$- \frac{1}{2} \exp(-\lambda_{en} f \nu / a) \cos 4\pi \nu y'_m] \}^{1/2} /$$

$$\{ [4 + \frac{12a}{f\nu \Delta \lambda n} K_0(\Delta \lambda n) \cos 2\pi \nu y'_m + \frac{a}{2f\nu \Delta \lambda n}$$

$$\times (\frac{4}{f\nu \Delta \lambda n} K_7(\Delta \lambda n) - K'_0(\Delta \lambda n)) \cos 4\pi \nu y'_m]^{1/2}$$

$$\times [(1 + C_A)^2 (1 + \cos 2\pi \nu y'_m)^2 + \frac{1}{2} C_A^2 [\exp(2.3D)$$

$$- 1] [3 + 2 \exp(-\lambda_{en} f \nu / 2a) \cos 2\pi \nu y'_m$$

$$+ \exp(-\lambda_{en} f \nu / a) \cos 4\pi \nu y'_m] \} \quad , \tag{101}$$

where we note that

$$\lim_{\Delta \lambda n \to 0} K_0(\Delta \lambda n) / \Delta \lambda n = \frac{f\nu}{2a} \exp(-\lambda_{en} f \nu / 2a) \quad , \tag{101a}$$

$$\lim_{\Delta \lambda n \to 0} K'_0(\Delta \lambda n) / \Delta \lambda n = \frac{f\nu}{a} \exp(-\lambda_{en} f \nu / a) \quad , \tag{101b}$$

$$\lim_{\Delta \lambda n \to 0} K_7(\Delta \lambda n) / \Delta \lambda n = 0 \quad . \tag{101c}$$

We stress that, for all practical cases, the mean value of the grain-noise is much smaller than unity, (i.e, $C_A^2 \ll C_A$). Thus Eq. (101) can be reduced to a simpler form, such as

$$\overline{SNR}_n^{(4)} = \frac{1}{M} \sum_{m=1}^{M} \{ 4 + 6 \exp(-\lambda_{en} f \nu / 2a) \cos 2\pi \nu y'_m$$

$$- \frac{1}{2} \exp(-\lambda_{en} f \nu / a) \cos 4\pi \nu y'_m \} / \{ 4 + \frac{12a}{f\nu \Delta \lambda n}$$

$$\times K_0(\Delta \lambda n) \cos 2\pi \nu y'_m + \frac{a}{2f\nu \Delta \lambda n} (\frac{4}{f\nu \Delta \lambda n} K_7(\Delta \lambda n)$$

$$- K'_0(\Delta \lambda n) \cos 4\pi \nu y'_m) \} \quad . \tag{102}$$

For low frequency signal [i.e., Eq. (87) , Eq. (102) can be further reduced to,

$$\overline{SNR}_n^{(4)} = (4 - \frac{2f\nu}{a} \lambda_{en})^{1/2} / [4 - \frac{f\nu}{a} (2\lambda_{en} + \Delta \lambda n)]^{1/2} \quad . \tag{103}$$

From the results of Eqs.(102) and (103),we see that the $\overline{SNR}_n^{(4)}$ increases as the spectral bandwidth $\Delta\lambda_n$ increases. This means that a higher $\overline{SNR}_n^{(4)}$ is achievable with a broader band temporally partial coherent illumination, as predicted. Several curves of the $\overline{SNR}_n^{(4)}$ as a function of spectral bandwidth $\Delta\lambda_n$, for various normalized signal frequencies $(\Omega = \nu/\nu_c)$,are plotted in Fig. 22. From this figure, again we see that, the $\overline{SNR}_n^{(4)}$ increases exponentially as a function of spectral bandwidth $\Delta\lambda_n$ of the filter, for higher spatial frequency of the input object. On the other hand, if the spatial frequency of the input signal is low (e.g., $\nu \sim 0$), the $\overline{SNR}_n^{(4)}$ would be independent of the spectral band-width $\Delta\lambda_n$. That is, the output SNR would not be improved by using a broader band temporally partial coherentillumination. We stress that this behavior is quite different from the effect due to phase-noise at the Fourier plane for which a higher $\overline{SNR}_n^{(3)}$ can always be obtained by increasing $\Delta\lambda_n$, even for zero spatial frequency at the input object (i.e., $\Omega = 0$), that is,

$$\overline{SNR}_n^{(3)}\Big|_{\nu=0} = \frac{8}{\frac{2\lambda_{\ell n}(1+\Delta\lambda_n/\lambda_{\ell n})}{\Delta\lambda_n} + \frac{3(2\lambda_{\ell n}+\Delta\lambda_n)}{\lambda_{\ell n}+\Delta\lambda_n}} \quad . \tag{104}$$

It is also worthwhile to show the asymptotic results of $\overline{SNR}_n^{(3)}$, due to phase-noise at Fourier plane for low frequency signal, i.e.,

$$\overline{SNR}_n^{(3)}\Big|_{\substack{\nu=0 \\ \Delta\lambda_n=0}} = 1 \quad , \tag{105}$$

which is for strictly temporal coherence illumination, and

$$\overline{SNR}_n^{(3)}\Big|_{\substack{\nu=0 \\ \Delta\lambda_n=\infty}} = \frac{8}{3} \quad , \tag{106}$$

which is for strictly temporal incoherent illumination. While for the case of film-grain noise, the $\overline{SNR}_n^{(4)}$ is

$$\overline{SNR}_n^{(4)}\Big|_{\substack{\nu=0 \\ \Delta\lambda_n=\infty}} = 1 \quad . \tag{107}$$

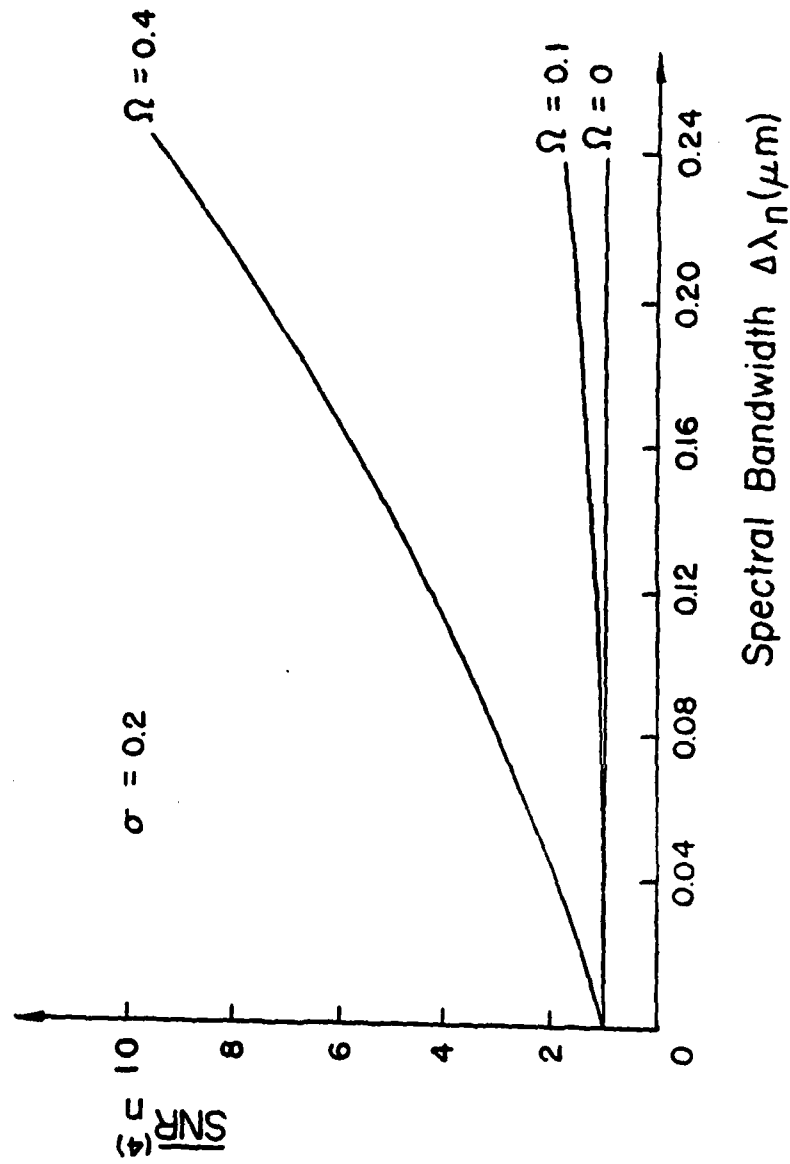Figure 22. Plots of normalized signal-to-noise ratio $\overline{SNR}$ (4), due to grain-noise at Fourier plane, as a function of spectral band-width $\Delta\lambda_n$, for various normalized spatial frequency Ω.

From these asymptotic results of Eqs. (105) to (109), we confirm our conclusion stated previously; nam ly the $\overline{SNR}_n^{(3)}$ can always be improved for phase-noise at the Fourier plane for a broader band temporally partial coherent illumination, while for grain-noise at the Fourier plane, the $\overline{SNR}_n^{(3)}$ can not be improved for $\nu = 0$. However, for high frequency case (e.g., $\Omega = 0.4$), the $\overline{SNR}_n^{(3)}$ increases quite noticeable as $\Delta\lambda_n$ increases as shown in Fig. 22.

Although $\overline{SNR}_n^{(3)}$, due to grain-noise at input plane, is monotonically decreasing function of the mean value C_A of grain-noise, as shown in Fig. 8, however the $\overline{SNR}_n^{(4)}$ is independent of C_A, i.e.,

$$\overline{SNR}_n^{(4)} = \frac{1 + C_A}{C_A \left(\left| 4\frac{\xi\nu}{a}(2\lambda_{\ell n} + \Delta\lambda_n) \right| \right)^{1/2}}, \quad \text{for } \Omega = 0, \quad (108)$$

which is obtained from Eq. (67).

We shall again note that, the overall normalized output signal-to-noise ratio $\overline{SNR}^{(4)}$ can be obtained by

$$\overline{SNR}^{(4)} = \frac{1}{N} \sum_{n=1}^{N} \overline{SNR}_n^{(4)},$$

where N is the total number of the spectral band filters, at the Fourier plane. Thus a higher $\overline{SNR}^{(4)}$ can always be obtained for larger N, particularly for higher input spatial frequency case (i.e., $\Omega \gg 0$). We further note that, although $\overline{SNR}_n^{(4)}$ is independent of $\Delta\lambda_n$ as shown in Fig. 22, however $\overline{SNR}^{(4)}$ would have significant improvement since the output noise distributions (i.e., grain-noise at Fourier plane) due to each spectral wavelength λ, are mutually incoherent. In other words, the signals diffracted from the spectral band filter, would be precisely superimposed at the output image plane to form a higher intensity signal, while the noise diffracted from the filter plane would be randomly added to form a smoother noise background. Thus, a higher overall output ..R can always be obtained due to grain-noise, as well as phase noise, at the

Fourier plane. Nevertheless, the number of the spectral band filters is generally limited by the spatial frequency v_o of the phase grating. However, the higher v_o, the larger the size of the achromatic transform lenses are required. But larger achromatic transform lens is generally expensive and more elaborate to construct in practice.

4.4 Summary

In summary, we would point out that, the effects due to temporal coherence on the noise performance of a white-light optical signal processor have been quantitatively evaluated from partial coherence theory stand point. Both the phase-noise and the grain-noise at the input and Fourier planes are treated in the evaluation. We have shown that these noises have significant effects on the system noise performances with temporally partial coherent illumination, as summarized in the following:

1) There are significant effects on output noise reduction, due to phase-noise at the input and Fourier planes and grain-noise at the Fourier plane, by a broadband temporally partial coherent illumination.

2) There is however no significant effect on noise reduction due to grain-noise at the input plane by a broad-band temporally partial coherent illumination.

3) Except due to the grain-noise at the input plane, the output normalized signal-to-noise ratio $\overline{SNR}_n$ are generally monotonically increasing functions of $\Delta\lambda_n$, the spectral bandwidth of nth spatial filter.

4) The output normalized signal-to-noise ratio $\overline{SNR}_n$ increases (except due to grain-noise at input plane) as the input spatial frequency increases. However, increases the input spatial frequency would

also increase the spectral bandwidth of the filter. Thus

it reduces the number of the processing spectral band

filters at the Fourier plane, for a fixed ν_o.

5) The normalized signal-to-noise ratio $\overline{SNR}_n$ also increases

(except due to grain-noise at the input plane) as the

lower wavelength limit (i.e., $\lambda_{\ell n}$) of the spectral band

filter decreases. In otherwords, the $\overline{SNR}_n$ improves for

shorter wavelength temporally partial coherent illumination.

6) The normalized signal-to-noise ratio $\overline{SNR}_n^{(2)}$ is a mono-

tonically decreasing function of the mean value C_A of grain-

noise at the input plane. But the $\overline{SNR}_n^{(4)}$, due to the

grain-noise at Fourier plane, is independent of C_A.

7) The overall normalized signal-to-noise ratio $\overline{SNR}$ is equal to

the sum of $\overline{SNR}_n$, except for the grain-noise at the input

plane which is independent of n. $\overline{SNR}$ improves as N number

of spectral band filters increases, as shown in Fig. 16.

Finally, we conclude that, the proposed optical signal processor

is capable of improving the noise performance, with a broadband temporally

incoherent (i.e., white-light) source. Except the grain-noise at the

input plane, the technique is capable of suppressing the noise effects

at the input and Fourier planes, as an incoherent processor, although the

processing is carried out by a temporally partial coherence mode.

V. Polychromatic Matched Filtering

5.1 Polychromatic Correlation Detection

We shall demonstrate a grating based polychromatic coherent signal

correlation detection. We shall show that this polychromatic correlation

detection technique is simple and flexible to operate and this technique

offers the advantage of multicolor signal detections, which is a step

closer to the actual human visual recognition.

Let us insert a color signal transparency in contact with a sinu-

soidal diffraction grating at the input plane P_1 of a polychromatic

coherent optical processor, as shown in Fig. 23. The complex

light amplitude distribution behind the input plane can be described as

$$s(x,y;\lambda)T(x,y) = [s_r(x,y;\lambda_r) + s_g(x,y;\lambda_g) + s_b(x,y;\lambda_b)]T(x,y), \qquad (109)$$

where s_r, s_g, and s_b are the red, green, and blue amplitude transmittances

of the color signal transparency, λ_r, λ_g, and λ_b are the red, green, and

blue wavelengths of the coherent sources, and $T(x,y)$ is a sinusoidal

grating which can be described as,

$$T(x,y) = K[1 + \cos(p_0 x)],$$

where K is a proportionality constant, and p_0 is the angular spatial

frequency of the grating.

Since the input plane is illuminated by a collimated polychromatic

coherent plane waves of red, green, and blue wavelengths, the complex

light distributions at the back focal plane of the achromatic transform

lens are

$$S(\alpha,\beta;\lambda) = S_r(\alpha,\beta;\lambda_r) + S_g(\alpha,\beta;\lambda_g) + S_b(\alpha,\beta;\lambda_b) + S_r(\alpha \pm \frac{f\lambda_r}{2\pi} p_0, \beta)$$

$$+ S_g(\alpha \pm \frac{f\lambda_g}{2\pi} p_0, \beta) + S_b(\alpha \pm \frac{f\lambda_b}{2\pi} p_0, \beta), \qquad (110)$$

where we have ignored the proportionality constant for simplicity,

(α,β) denotes the spatial coordinate system of the Fourier plane, f is

the focal length of the achromatic transform lens, and $S_r(\alpha,\beta)$, $S_g(\alpha,\beta)$,

and $S_b(\alpha,\beta)$ are the corresponding color Fourier spectra of $s_r(x,y)$,

$s_g(x,y)$ and $s_b(x,y)$. From this equation, we see that the red, green,

and blue color spectra are centered at $\alpha = \pm \frac{f\lambda_r}{2\pi} p_0$, $\alpha = \pm \frac{f\lambda_g}{2\pi} p_0$, and

$\alpha = \pm \frac{f\lambda_b}{2\pi} p_0$ locations along the α axis, respectively. Since, in practice,

the all color signal transparencies are spatial frequency limited, it

is possible to calculate the appropriate spatial carrier's frequency

p_0 of the grating so that the primary color Fourier spectra would be
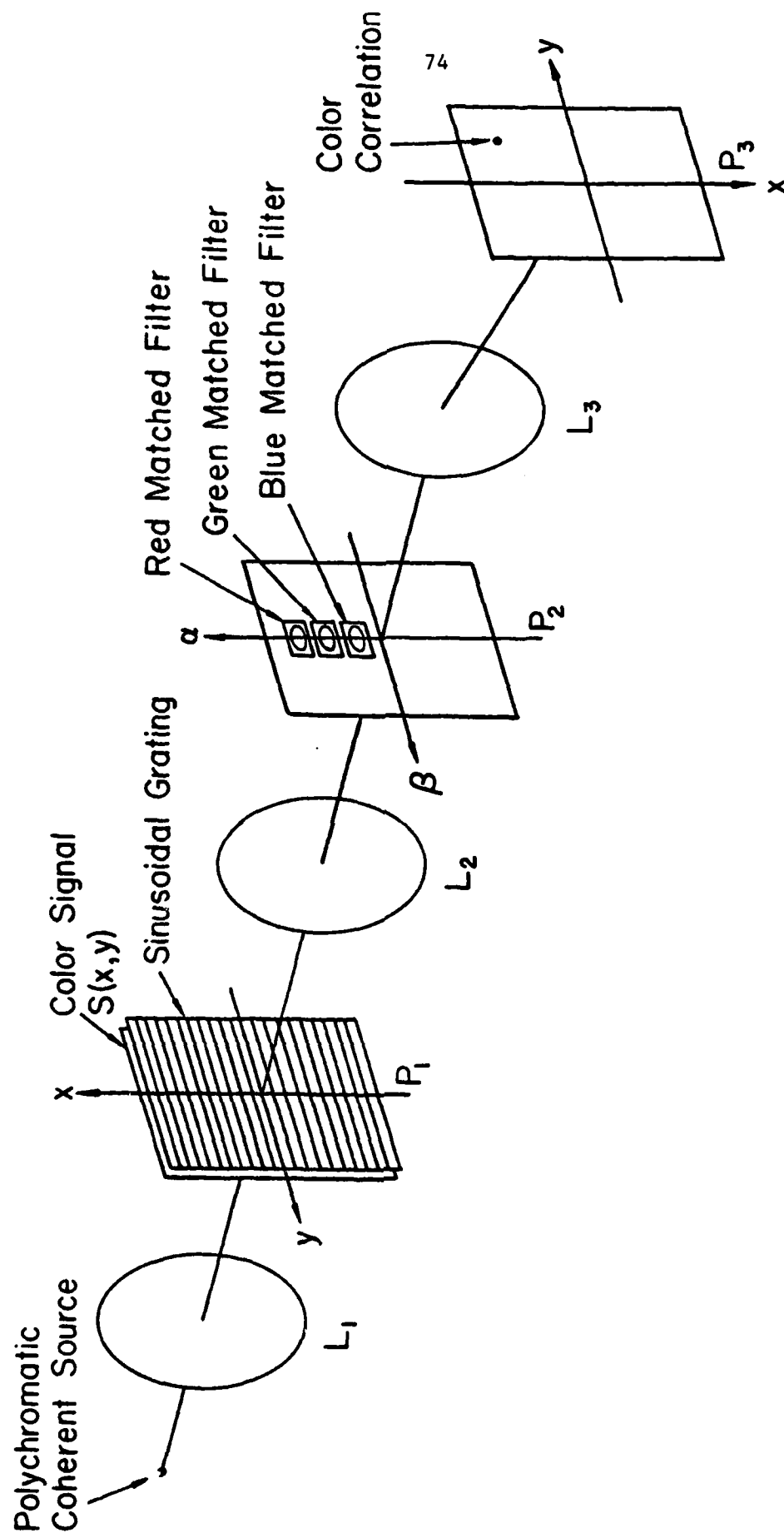
spatially separated in the Fourier plane.

Figure 23. A polychromatic coherent correlator. L; achromatic transform lens.

In color signal detection, we assume that a set of color sensitive matched spatial filters are constructed. The corresponding amplitude transmittances are

$$H_r(\alpha,\beta) = K_1 + K\left|S_r(\alpha - \frac{f\lambda_r}{2\pi}\,p_o,\beta)\right|\cos[\frac{f\lambda_r}{2\pi}\,\alpha x_o + \phi_r(\alpha - \frac{f\lambda_r}{2\pi}\,p_o,\beta)],$$

$$H_g(\alpha,\beta) = K_1 + K\left|S_g(\alpha - \frac{f\lambda_g}{2\pi}\,p_o,\beta)\right|\cos[\frac{f\lambda_g}{2\pi}\,\alpha x_o + \phi_g(\alpha - \frac{f\lambda_g}{2\pi}\,p_o,\beta)],$$

$$H_b(\alpha,\beta) = K_1 + K\left|S_b(\alpha - \frac{f\lambda_b}{2\pi}\,p_o,\beta)\right|\cos[\frac{f\lambda_b}{2\pi}\,\alpha x_o + \phi_b(\alpha - \frac{f\lambda_b}{2\pi}\,p_o,\beta)] \qquad (111)$$

where x_o is an arbitrary carrier spatial frequency, Ks are the appropriate proportionality constants, and

$$S_r(\alpha,\beta) = |S_r(\alpha,\beta)|\exp[i\,\phi_r(\alpha,\beta)],$$

$$S_g(\alpha,\beta) = |S_g(\alpha,\beta)|\exp[i\,\phi_g(\alpha,\beta)],$$

$$\text{and}\quad S_b(\alpha,\beta) = |S_b(\alpha,\beta)|\exp[i\,\phi_b(\alpha,\beta)], \qquad (112)$$

are the primary color detecting signal spectra.

If we properly insert these color sensitive matched spatial filters in the Fourier plane p_2 of the polychromatic coherent processor, as illustrated in Fig.24, the complex light distribution at the output plane p_3 of the processor would be

$$g(x,y) = \Sigma[s_n(x,y)\exp(ip_o x)$$

$$+ s_n(x,y)\exp(ip_o x) * s_n(x - x_o,y)\exp(ip_o x)$$

$$+ s_n(x,y)\exp(ip_o x) * S_n(-x + x_o,y)\exp(ip_o x)], \text{ for } n=r,g, \text{ and } b, \qquad (113)$$

where * denotes the convolution operation, and we have ignored the proportionality constants for convenience.

From the above equation, we see that the first summation terms are the zero-order terms which are diffracted in the neighborhood of the optical axis at the output plane, and the second and third
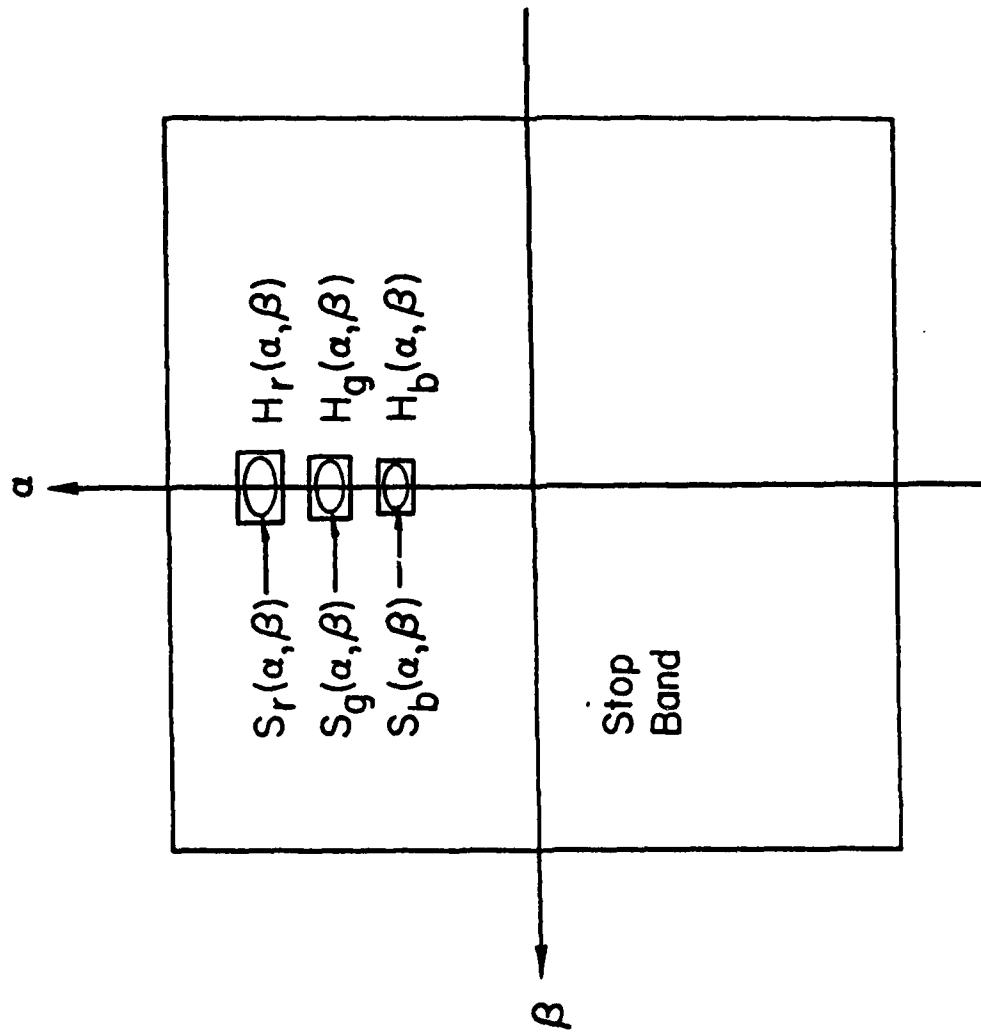
Figure 24. Multicolor complex spatial filtering. H_r, H_g, and H_b are red, green, and blue color sensitive matched spatial filters.

summation terms are the primary color convolution and correlation terms,

which are diffracted in the neighborhood of $(-x_o, 0)$ and $(x_o, 0)$ at the

output plane of the polychromatic coherent processor, as sketched in

Fig. 25. From this result, we see that this proposed polychromatic pro-

cessing technique is capable of performing color signal correlation

detection and the technique is rather simple and flexible to operate.

One should also note that this polychromatic process technique is

also capable of performing multicolor signals detections, if the

conjugate orders of color Fourier spectra are utilized, as depicted

in Fig. 26. Where the subscripts of 1 and 2 represent two different

sets of matched spatial filters for color signals no. 1 and no. 2,

respectively. We would also note that, if each of the color signals to be

detected contain only one primary color, then it is possible to

synthesize a total of six matched color sensitive spatial filters

for simultaneous signal detection. Needless to say that, by

utilizing a multigrating technique, as described in a previous paper[19],

this technique is capable of performing N number of color signal corre-

lation detections, with relative ease of physical operation, as illus-

trated in Fig. 27.

5.2 Color Sensitive Spatial Filter

We shall now describe a technique of generating a set of spatially

multiplexed color sensitive matched filters for color signal correlation

detection, as illustrated in Fig. 28. This set of color sensitive matched

filters can be generated sequentially with respect to the color wavelengths

of the coherent sources. For example, the red color sensitive matched

filter is generated when the shutter of red coherent source is open and the

recording aperture of the encoding mask MS is located at the position

where the red color Fourier spectrum is exposed. And, similarly for the
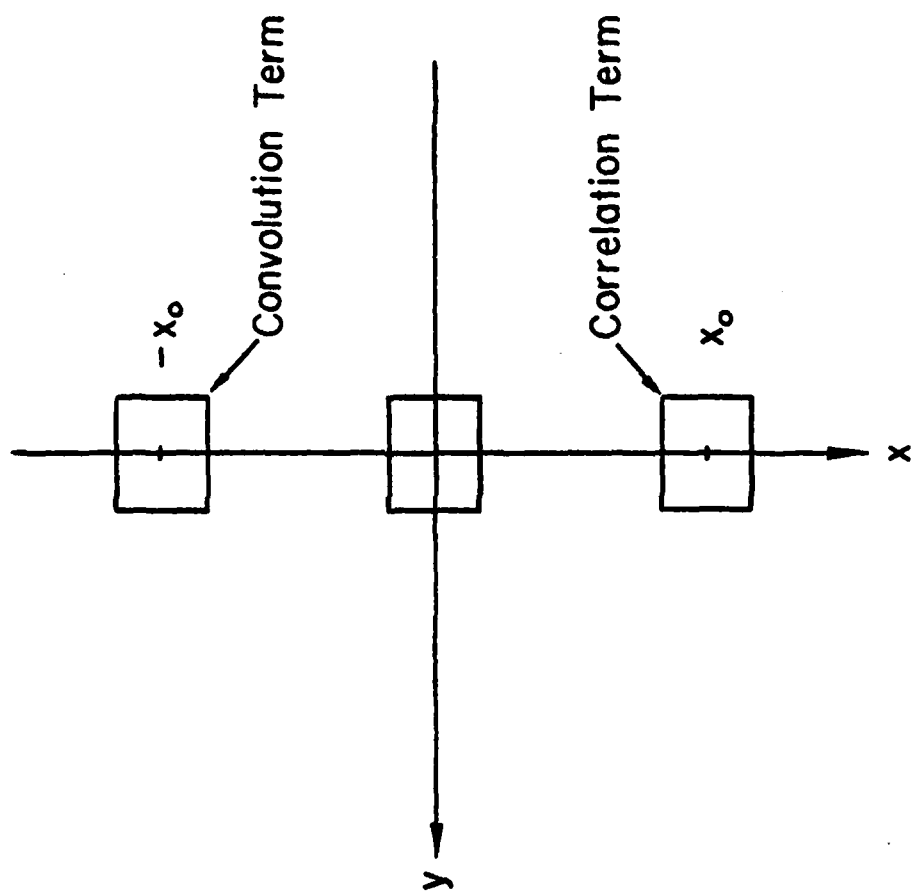
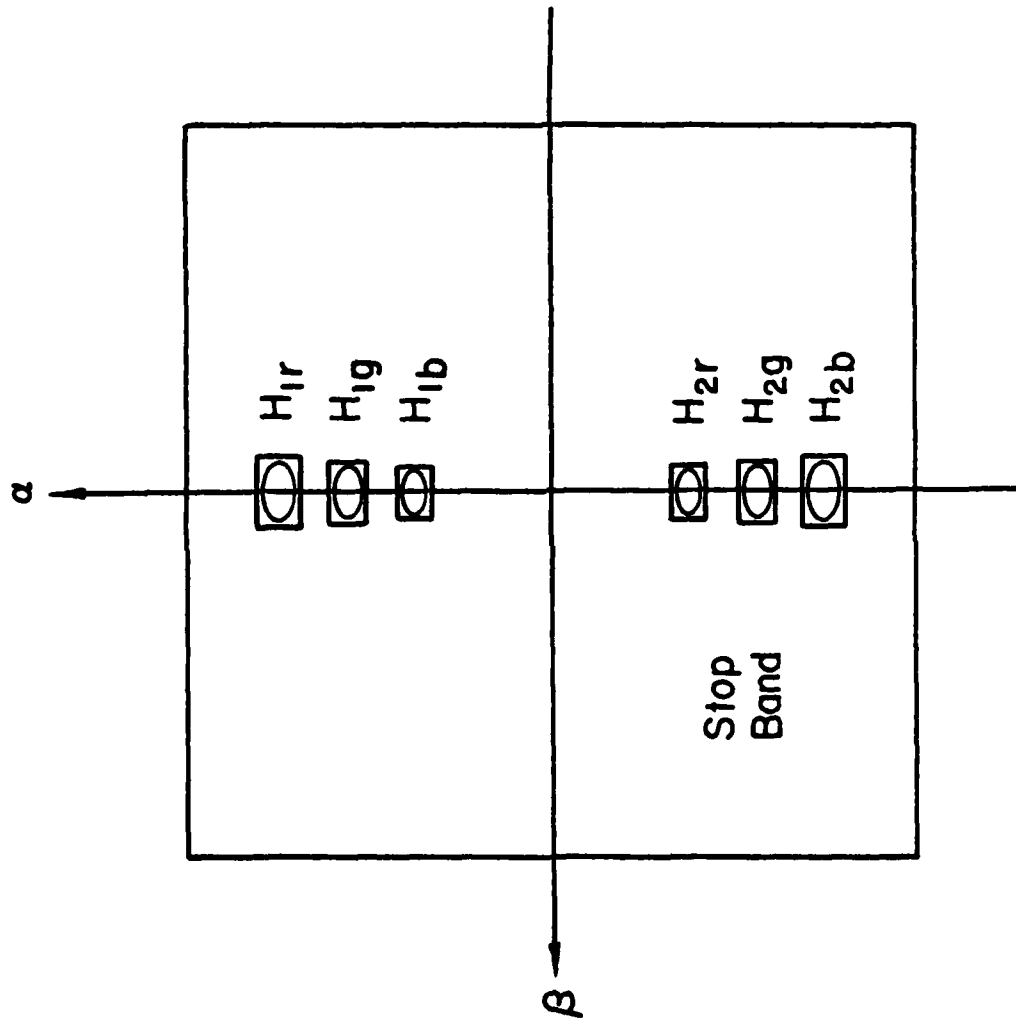Figure 25.   Sketched of the output diffraction.

Figure 26.   Multicolor signals aptial filterings.

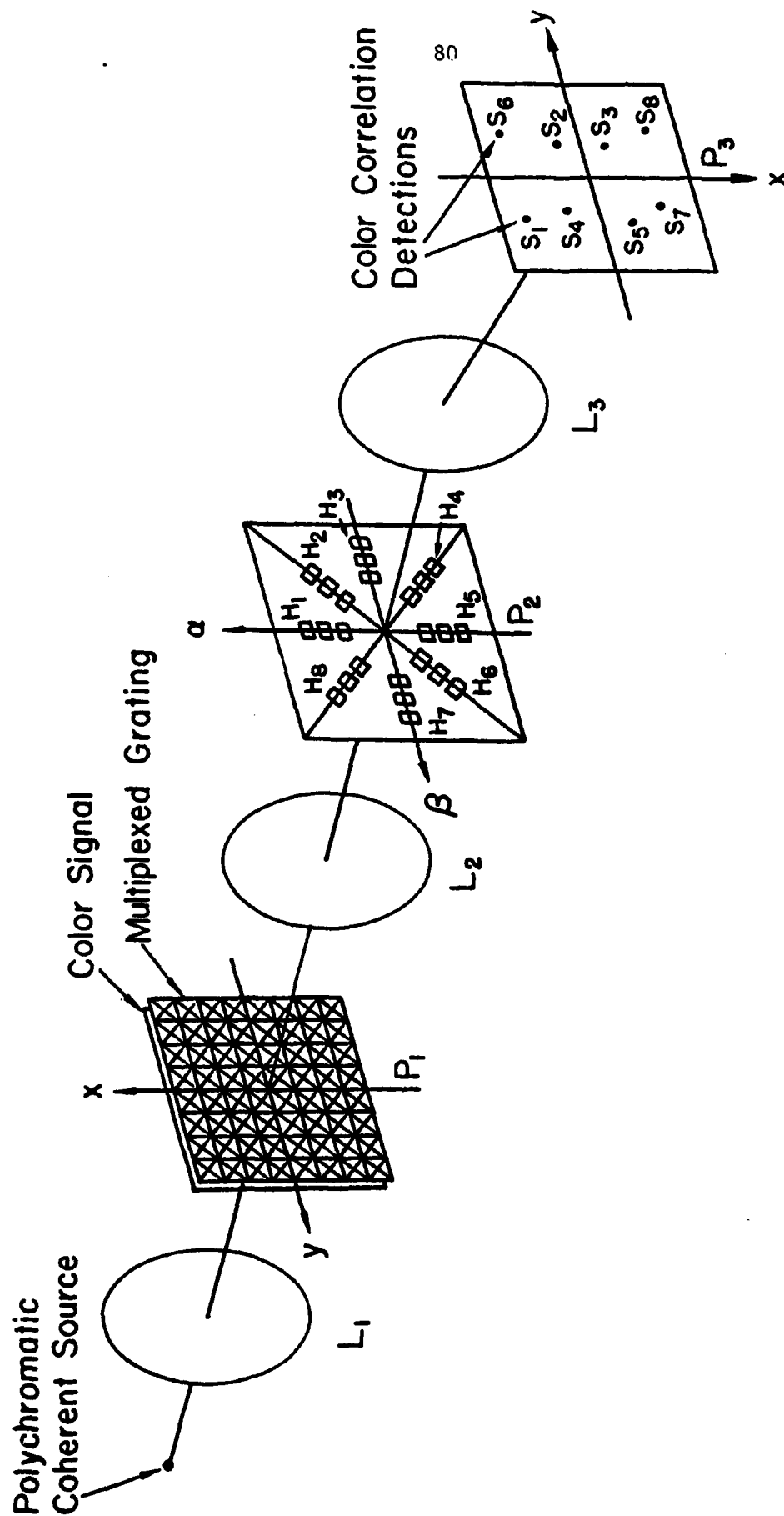Figure 27. A polychromatic coherent correlator for multisignals
correlation detections. L; achromatic transform lens.

Figure 28.   Synthesis of spatially multiplexed color sensitive
             matched filters. BS; beam splitters, M; mirror, SF;
             spatial filter, MS; recording mask, H; holographic
             plane, AP; recording aperture, L; achromatic transform
             lens.

generation of the green color sensitive matched filter and the blue

color sensitive matched filter, with the same color detecting signal

transparency. In this manner, we see that, a set of color signal

matched filters can be sequentially synthesized, without physically

overlapping in the Fourier plane. Similarly, if one takes advantage

of the conjugate orders of the Fourier spectra, another set of the

color sensitive matched filters for a different color detecting

signal can be generated, in the lower half of the spatial frequency

plane. Unlike the wavelenght-multiplexing techniques[20,21], higher

diffraction efficient color sensitive matched filters can be synthe-

sized. There in another advantage of this technique, a large number

of multiple color sensitive matched filters can be generated as

illustrated in Fig. 27. This large capacity multi-signal matched

filtering program is currently under investigation.

## VI.   Experimental Demonstrations

6.1   Character Recognition

We shall illustrate an experimental result obtained with the

incoherent signal detection. Figure 29(a) shows a set of alphanumerics

as an input object transparency. Figure 29(b) represents the character

G to be detected, for which a complex spatial filter was constructed

with the interferometric technique. Figure 29(c) shows the correlation

detection obtained with the incoherent correlation detection technique,

where a narrow band mercury arc lamp was used as the incoherent light

source. Figure 29(d) shows the electronic scanned of the correlation

peak obtained from the result of Fig. 29(c). For comparison we also

provide the correlation detection peak obtained with coherent tech-

nique as shown in Fig. 30(a). Fig. 30(b) shows the corresponding

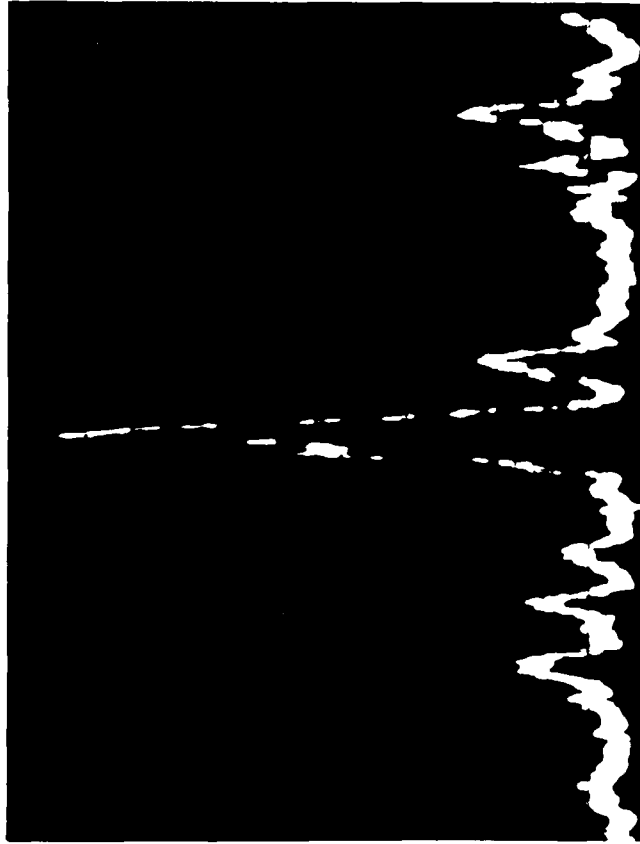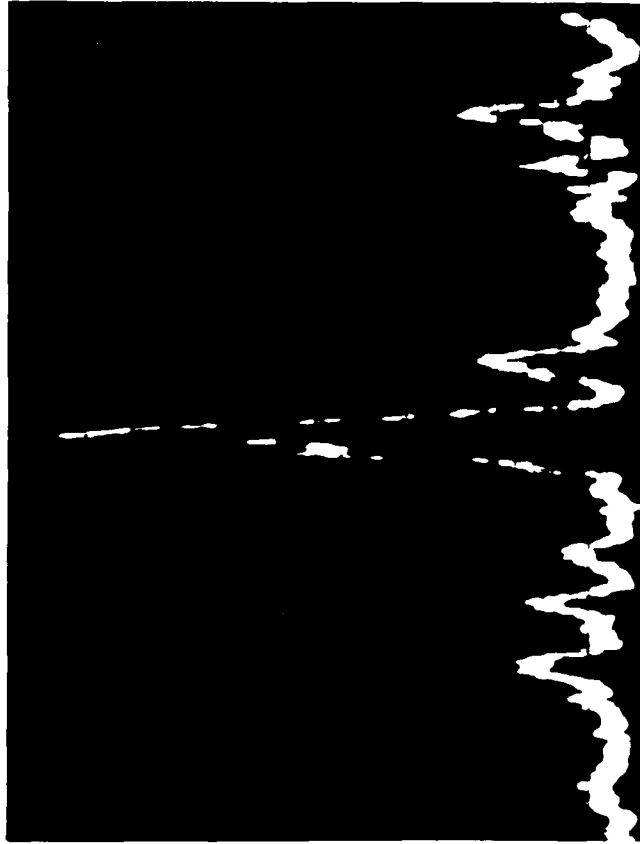electronic scanned result of Fig. 30(a). With reference to the
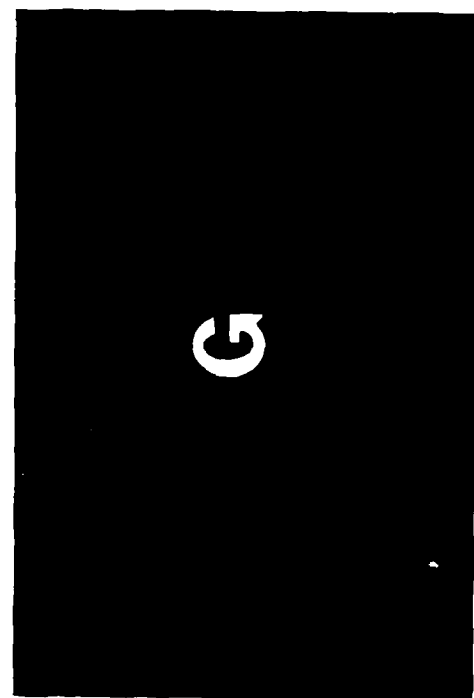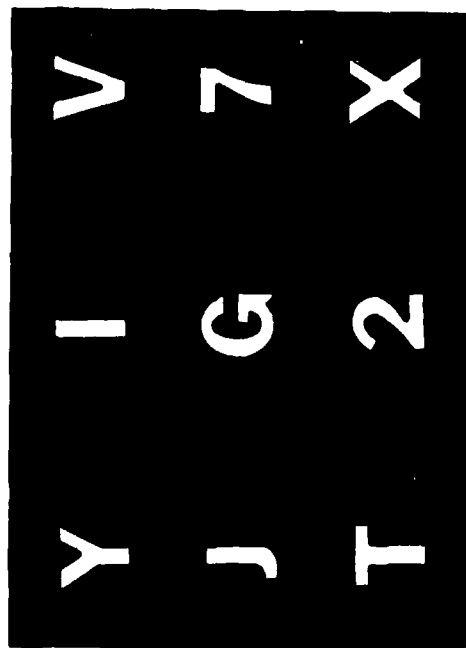
Figure 29. Character recognition with incoherent light.
(a) Input alphanumeric;
(b) Alphabet G to be detected;
(c) Correlation detection of G;
(d) Electronic scanned correlation peak.

(b)

(a)

Figure 30.   Character recognition with coherent source.
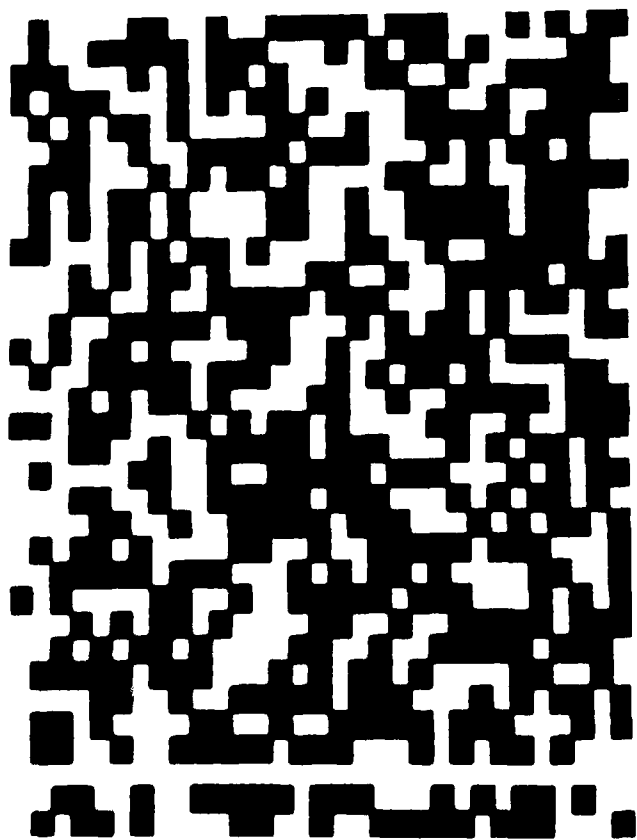(a) Correlation peak obtained with coherence
source.
(b) The corresponding electronic scanned.

results obtained with the incoherent source as shown in Fig. 29(d),
we note that higher signal-to-noise correlation peak can be achieved
with the incoherent correlation technique.

6.2 Detection of Pseudorandom (PN) Code

The basic idea of using pseudorandom (PN) code for the spread
spectrum communication is to encode the informational signal (either
with direct sequence modulation or frequency hopping or the combination
of both), so that the signal is capable of anti-jamming or interference
during the transmission. Since the spread spectrum communication
is a large time-bandwidth signal, the optical correlator is particularly
suitable to decode the broad spectrum signal. We shall have to demon-
strate an experimental result that an incoherent optical correlator is
suitable for such applications. Figure 31(a) shows a pseudorandom
(PN) code as an input object transparency. Fig. 31(b) represents a
code work that we would wish to detect. A complex spatial filter of
this code word was constructed with the interferometric technique.
Figure 31(c) shows the corresponding correlation peak obtained with
the incoherent processing technique. The light source utilized was
a 75W mercury arc lamp with a green interference filter wavelength
5461$\overset{\circ}{A}$ and 100$\overset{\circ}{A}$ bandwidth. Figure 31(d) shows the profile of the
corresponding correlation peak as obtained by electronic densitometry
scanned.

In comparison, we also provide the correlation peak obtained with
the coherent processing technique, as shown in Fig. 32(a) Figure 32(b)
shows the electronic scanned correlation profile obtained with the
coherent method. By comparing the results obtained with the incoherent
processing technique of Fig. 31, we note that the result obtained by
the incoherent technique offers a high correlated signal-to-noise ratio.
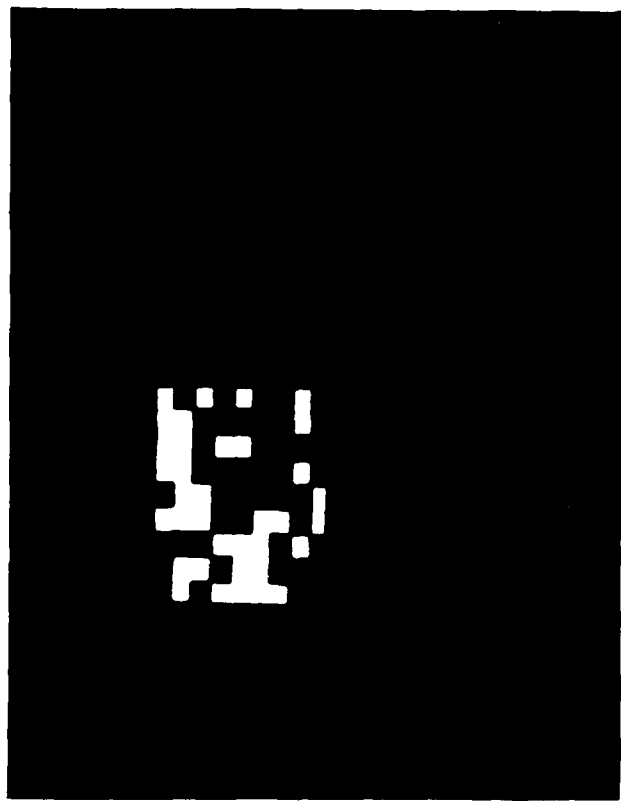
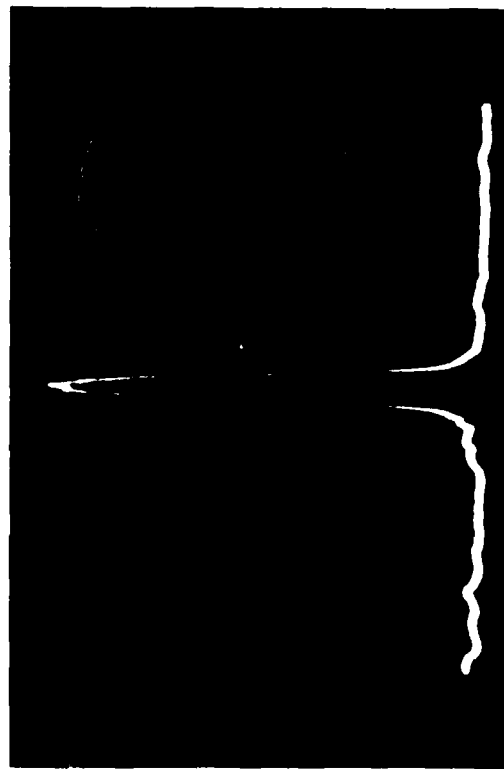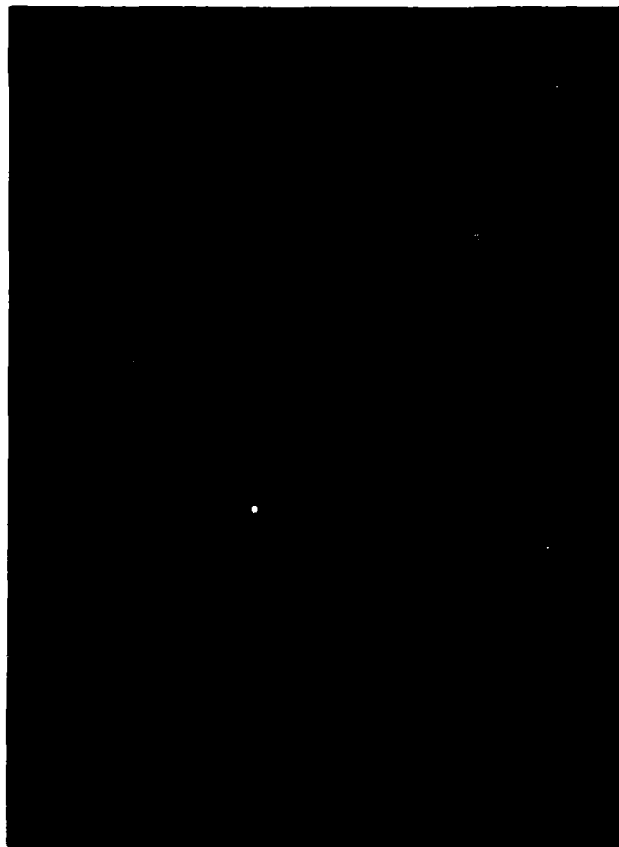Figure 31. Detection of pseudorandom code
(a) A pseudorandom code.
(b) A code word.
(c) Detection with incoherent source.
(d) Electronic scanned correlation peak.

(b)

(a)

Figure 32. Pseudorandom code detection with coherence source.
(a) Correlation detection with coherence source.
(b) An electronic scanned correlation peak of (a).
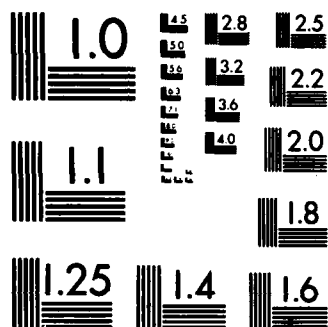
MICROCOPY RESOLUTION TEST CHART

NATIONAL BUREAU OF STANDARDS-1963-A

We would stress that, this incoherent correlation detection technique can be extended with white-light source, for which a research program is under consideration.

6.3   Polychromatic Signal Detection

We shall now illustrate that the proposed optical correlator is suitable for color signal correlation detection. The significance of color signal detection is a step closer to the actual human recognition process. We note that the proposed grating based correlation technique could either utilize coherent or incoherent source. For simplicity, our experimental demonstration would utilize a polychromatic coherent source. In principle, the correlation detection can be utilized by the entire spectral band of a white-light source, where a research program in under investigation.

Strictly speaking, coherent light sources emitting red, green, and blue color wavelengths should be used for the color signal correlation detection. For simplicity, we shall use only two of the primary colors of light sources in our experiments. In the first experimental demonstration, a set of color English alphabets, as shown in Fig. 33(a), is used as input color object transparency whereas the upper row of these alphabets is in green, middle row is in yellow, and lower row is in red. A red and a green color sensitive matched spatial filters for detecting the color alphabet A are generated in the Fourier plane, as described in previous sections. A HeNe laser emitting a 6238$\overset{\circ}{\text{A}}$ red light on an argon laser emitting a 5145$\overset{\circ}{\text{A}}$ green light are used in the proposed polychromatic optical processor, as shown in Fig. 23. Figure 33(b) shows the color signal correlation detection peaks of the color alphabet A. In this figure, the left hand corner correlation peak is in green, the middle correlation peak is in yellow,
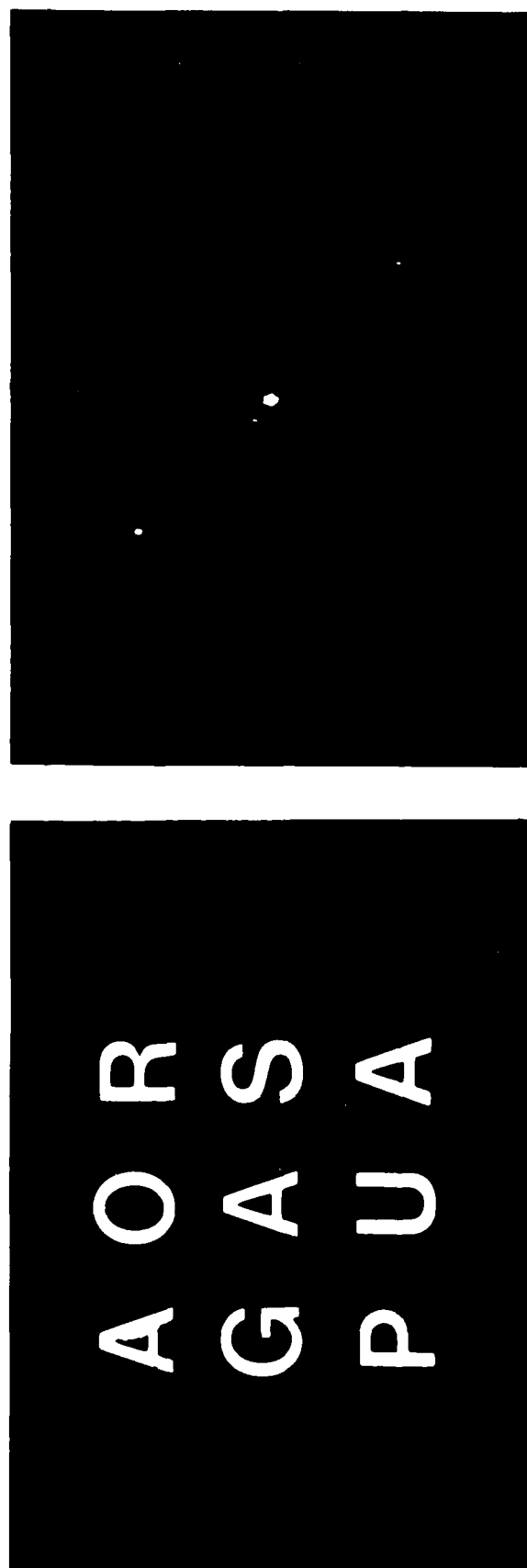
(a)

(b)

Figure 33. Color character recognition.
(a) An input color object transparency of a set of color English alphabets.
(b) Color correlation detections of character A.

and the right hand corner correlation peak is in red. From this result

we see that, the color sensitive matched spatial filters possess a

high degree of color correlation detection selectivity.

In the second experimental demonstration, a continuous tone

color aerial photographic image transparency, as shown in Fig. 34(a)

is used as input object. The color of the ground terrain is generally

yellowish with scattered spots of light green. The forest and some

scattered trees apperas to be redish brown and yellow. The lakes and

ocean are in dark green. Figure 34(b) shows a section of terrain

is used as a color detecting signal. A red and a green color sensitive

matched filters for detecting the color terrain of Fig. 34(b), are

generated. Again a HeNe laser for red light and an argon laser for

green light are used for the color signal correlation detection.

Figure 34(c) shows the correlation detection peak. In reality this

correlation peak is in yellow color.

For our third experimental demonstration, a continuous tone color

image transparency of a campus street scene in The Pennsylvania State

University, as shown i- Fig. 35(a), is used in the input object.

Figure 35(b) shows the color objects (i.e., a blue van and a red stop

sign) used as color detecting signals. Since the stop sign is

primarily in red and the van is in blue, therefore, a red color sensitive

matched filter for the stop sign and a blue color matched filter for

the van are independently constructed in spatial frequency plane. In

this experiment, a HeNe laser emitting a 6328$\overset{\circ}{\text{A}}$ red light and an argon

laser emitting a 4880$\overset{\circ}{\text{A}}$ blue light are used for the color signal

correlation detections. Figure 35(c) shows the color signal correlation

detection result. The left hand correlation peak is in blue, which

(b)

(a)

(c)

Figure 34. Color signal detection of an aerial photographic
transparency.
(a) An aerial color photograph.
(b) Color terrain to be detected.
(c) The corresponding correlation peak is primarily
yellow.

92

(b)

(a)

(c)

Figure 35. Multisignal correlation detections.

(a) A color object transparency; the stop sign is red and the van is blue.

(b) Two color detecting signals; the blue van and red stop sign.

(c) The corresponding correlation detections; the correlation peak for the van is blue and the correlation peak for stop sign is red.

represents the correlation detection of the blue van, whereas the right

hand correlation peak is in red, which represents the correlation

detection of the red stop sign.

In concluding this demonstration we note that, the polychromatic

correlation detection is suitable for color coded signal detection,

which would be usable for color coded pseudorandom code application.

VII. Conclusion

This study has led to certain definite conclusions. In

particular:

1. Incoherent optical correlator offers a higher signal-

    to-noise ratio as compared with a coherent correlator.

2. The incoherent correlator is very suitable for decoding

    the pseudorandom PN code as applied in spread spectrum

    communication.

3. Optimum matched filtering is a useful decoding tool

    for burst-error-correlating PN code.

4. The technique is very suitable for color signal correlation

    detection, which is one step closer to the actual human

    recognition.

5. The polychromatic correlation technique is suitable for

    color coded pseudorandom code decoding.

6. It is feasible of utilzing this incoherent correlator

    in a real-time mode, a research program is currently

    pursuing.

7. The incoherent optical correlator has a superb noise

    suppression effect as compared with the coherent system,

    particular with the utilization of a broad spectral

    band light source.

The net effect of these conclusions is to emphasize the truth of our initial assumption of the incoherent optical correlator can be an essential part of the spread spectrum communication signal decoding.

VIII. <u>References</u>

1. R. C. Dixon, <u>Spread Spectrum Systems</u>, Wiley-Interscience, New York, NY, 1976.

2. F. T. S. Yu, Optics. Comm., <u>27</u>, 23(1978).

3. F. T. S. Yu, Appl. Opt., <u>17</u>, 3571(1978).

4. F. T. S. Yu and A. Tai, Appl. Opt., <u>18</u>, 2705(1979).

5. S. K. Case and R. Alferness, Appl. Phys., <u>10</u>, 41(1976).

6. H. J. Caulfield, private communications.

7. G. M. Morris and N. George, Appl. Opt., <u>19</u>, 3843(1980).

8. B. Watrasiewicz, Opt. Acta., <u>16</u>, 321(1969).

9. F. T. S. Yu, S. L. Zhuang and S. T. Wu, Appl. Phys., <u>B27</u>, 99(1982).

10. M. Borne and E. Wolf, <u>Principles of Optics</u>, 2nd rev. ed., Pergamon Press, New York, NY, 1964.

11. B. Saleh, <u>Photoelectron Statistics</u>, Springer-Verlag, New York, NY, 1978.

12. E. N. Leith and J. Roth, "Noise Performance of an Achromatic Optical System," Appl. Opt., <u>16</u>, 2803-2811(1979).

13. S. L. Zhuang and F. T. S. Yu, "Coherence Requirement for Partially Coherent Optical Processing," Appl. Opt., <u>21</u>, 2587-2595(1982).

14. E. L. O'Neill, "Introduction to Statistical Optics," Addison-Wesley Press, Reading, MA(1963).

15. F. T. S. Yu, "Markov Photographic Noise," J. Opt. Soc. Am., 5, 342-344(1969).

16. B. J. Uscinski, <u>The Elements of Wave Propagation in Random Media</u>, McGraw-Hill, New York, NY, (1977).

17. H. T. Chao, S. L. Zhuang, S. Z Mao and F. T. S. Yu, "Broad Spectral Band Color Image Deblurring," Appl. Opt. to be published.

18. P. Chavel and S. Lowenthal, "Noise and Coherence in Optical Image Processing. 11. Noise Fluctuations," J. Opt. Soc. Am., <u>68</u>, 721-732(1978).

19. F. T. S. Yu and M. S. Dymek, Appl. Opt. <u>20</u>, 1450(1981).

20. S. K. Case, Appl. Opt., <u>18</u>, 1890 (1979).

21. Y. Ishii and K. Murata, Opt. Lett., <u>7</u>, 230 (1982).

IX. <u>Personal</u>

Francis T. S. Yu	Principal Investigator
S. L. Zhuang	Research Assistant
T. H. Chao	Research Assistant
B. Javidi	Research Assistant

X. <u>List of Publications</u>

1. F. T. S. Yu, S. L. Zhuang and Q. Zheng, "Source Encoding for Partially Coherent Optical Processing," J. Opt. Soc. Am., Vol. 72, p. 1600A, December 1981.

2. T. H. Chao and F. T. S. Yu, "Grating Generation with an Encoded Extended Incoherent Source," Opt. Lett., Vol. 7, pp. 251-252, June 1982.

3. F. T. S. Yu, Y. W. Zhang and S. L. Zhuang, "Coherence Requirement for Partially Coherent Correlation Detection," Appl. Phys., Vol. B-30, pp. 23-27, January 1983.

4. F. T. S. Yu and T. H. Chao, "Color Signal Correlation Detection by Matched Spatial Filtering," submitted to Appl. Phys.

5. S. L. Zhuang, "Coherence Requirement, Transfer Function and Noise Performance of a Partially Coherent Optical Processor," A Ph.D. Dissertation, The Pennsylvania State University, November 1982.

6. F. T. S. Yu and T. H. Chao, "Polychromatic Signal Detection by Complex Spatial Filtering," to present to the SPIE Proceedings on "Advances in Optical Information Processing," Los Angeles, January 17-21, 1983.

7. S. L. Zhuang and F. T. S. Yu, "Noise Performance of a White-Light Optical Signal Processor; Part I, Temporal Partially Coherent Processing," in preparation.

MISSION
of
Rome Air Development Center

RADC plans and executes research, development, test and selected acquisition programs in support of Command, Control Communications and Intelligence (C^3I) activities. Technical and engineering support within areas of technical competence is provided to ESD Program Offices (POs) and other ESD elements. The principal technical mission areas are communications, electromagnetic guidance and control, surveillance of ground and aerospace objects, intelligence data collection and handling, information system technology, ionospheric propagation, solid state sciences, microwave physics and electronic reliability, maintainability and compatibility.

END

FILMED

9-83

DTIC